Title
Systems Biology of Bioenergetic Shifts in Alzheimer's Disease and Aging

Author
Dong, Yue

Publication Date
2019

Peer reviewed|Thesis/dissertation

UNIVERSITY OF CALIFORNIA,

IRVINE

SYSTEMS BIOLOGY OF BIOENERGETIC SHIFTS IN ALZHEIMER'S DISEASE AND AGING

DISSERTATION

submitted in partial satisfaction of the requirements
for the degree of

DOCTOR OF PHILOSOPHY

in Biomedical Engineering

by

Yue Dong

Dissertation Committee:
Professor Gregory J. Brewer, Co-Chair
Professor Frithjof Kruggel, Co-Chair
Professor Michelle A. Digman
Professor Kim N. Green
Professor Carl W. Cotman

2019

DEDICATION

To my family and friends for their love, encouragement and support.

TABLE OF CONTENTS

LIST OF FIGURES

LIST OF TABLES

ACKNOWLEDGEMENTS

This research project would not have been possible without the support and guidance that I received from many people. I would like to express my deepest appreciation to my supervisor Dr. Gregory J. Brewer for all the support and guidance, during my study in the field of Alzheimer's Disease and aging as well as the time I spent at University of California at Irvine. On the academic level, Dr. Brewer taught me fundamentals of conducting scientific research. Under his supervision, I learned how to define a research problem, find a solution to it, and finally publish the results. On a personal level, Dr. Gregory J. Brewer inspired me by his hardworking and passionate attitude.

My deepest gratitude to Dr. Michelle A. Digman for her continuous support, invaluable advice and providing me the great opportunity to work on fluorescence lifetime imaging microscopy (FLIM). I appreciate Dr. Enrico Gratton for his inspirational discussions. I am very thankful to Dr. Frithjof Kruggel for his valuable input, help and encouragement. Many thanks to my rest of my dissertation committee members, Dr. Kim Green and Dr. Carl W. Cotman for their great support and valuable advice.

Many thanks to the help of Rachel Cinco-Hedde, Ning Ma, and Sara Sameni at Laboratory for Fluorescence Dynamics, UC Irvine for the FLIM technique support and training.

Finally, I would like to thank my family and friends for their consistent support, love and encouragement throughout this journey.

CURRICULUM VITAE

Yue Dong

EDUCATION

Ph.D. Biomedical Engineering June 2019
University of California, Irvine
Doctoral Advisor: Dr. Gregory J. Brewer (BME)

Bachelor of Medicine July 2011
Hebei Medical University, China

RESEARCH EXPERIENCE

Graduate Student Researcher June 2014 – June 2019

Biomedical Engineering Department, University of California, Irvine
Research on Alzheimer's Disease, at Professor Gregory Brewer's Lab

- **Develop** hypotheses and **design** experiments
- **Consult** experimental designs with PI and collaborators and **set** goals
- **Plan** weekly, monthly schedules to ensure completion of experimental tasks
- **Conduct experiments in neuronal biology** such as collection of mouse brain and blood samples, separation of hippocampus, primary neuron culture and NADH measurements on live neurons
- **Perform** experiments using **techniques** such as fluorescent lifetime imaging microscopy (FLIM), mass spectrometry and computational modeling
- **Collect** and **interpret** data to quantitatively **verify** hypotheses
- **Update** results to PI and collaborators and **adjust** on experimental strategies
- **Supply** several solutions to a problem and **select** the most practicable one
- **Present** results to groups up to 100 students of various knowledge and professors
- **Help** PI **investigate** companies for quote requests, product information and technical supports and **provide** with **integrated information**
- **Assist** PI on **cost budget** and **help determine** the optimal company
- **Train** students on basic experimental skills, operation on instruments and management of mouse colonies
- **Write** or **edit** wide range of materials including course assignments, grant/fellowship application and research papers
- **Help laboratory maintenance** such as ordering laboratory supplies

Graduate Student Researcher September 2012 – June 2014

Biomedical Engineering Department, University of California, Irvine
Laboratory Rotation

- **Communicated** with team members on experimental designs, short- and long-term goals of the projects and potential **applications or patents** in **medical care market**
- **Applied 3-Dimensional cultures** of endothelial cells (ECs), mesenchymal stem cells (MSC) and hematopoietic stem cells (HSC) to mimic bone marrow niche for drug screening
- **Seeded** breast cancer cells in **3-dimensional collagen matrix** to track immigration of cancer cell
- **Encapsulated islets** using **alginate capsules** to prevent immune response

Research Assistant September 2007 – August 2009

Hebei Medical University, Shijiazhuang, China

- **Extracted** vascular disease as a model and **transferred** into a research model
- **Induced** mesenchymal stem cells (MSC) into endothelial cells (ECs) and fibroblasts of ischemia myocardium (FIMs) into cardiomyocyte-like cells (CLCs)
- **Seeded** ECs **on scaffolds** (acellular dermal matrix) and **implanted** into skeletal muscles of SD rats
- **Seeded** FIMs **on scaffolds** (acellular colon muscle film and Bio-Gide) and cultured *in vitro*
- **Published** 2 articles relative to cardiovascular tissue engineering as first author

CLINICAL EXPERIENCE

Clinical Medical Intern September 2009 – July 2011

The Third Hospital of Hebei Medical University, China

- **Participated** and **assisted** surgeries including cardiovascular, gynaecologic, obstetric and gastrointestinal surgeries
- **Gathered information** from patients and patient families and performed physical examinations
- Suggested auxiliary examinations and tests
- **Integrated information** and results of examinations and **consulted** diagnosis with doctors
- **Established** comprehensive case records and documents of examinations and diagnosis

- **Interpreted** results of examinations, diagnosis and **discussed** treatment options with patients and patient families
- **Coordinated communications** among doctors, patients and patient families
- **Monitored** vital signs and conditions for patients in intensive care unit (ICU)
- **Recorded** and **tracked** daily health conditions for patients
- **Assisted** patients on blood tests, Chest X-ray, CT scan, ultrasonic test, endoscopy and medical care such as pericardial and pleural effusion drainage
- **Operated** electrocardiograph (ECG), blood pressure measurement and cardiopulmonary resuscitation (CPR) for patients
- **Educated** more than 50 patients on medication and administration
- **Evaluated** therapeutic effects with doctors after surgeries and treatments and **helped** make schedules on treatments for next stage
- **Scheduled** regular clinical review for discharged patients

SKILLS

- **Software:** Microsoft Word, Excel, PowerPoint, Matlab, R Statistical Software, SPSS Statistics, Waters MassLynx, QuanLynx, MetaboAnalyst, KEGG, SimFCS, ZEN, MetaMorph, VersaDoc, KC4^{TM}, ImageJ
- **Languages:** Fluent in Chinese (Mandarin), English
- **Laboratory:** mass spectrometry, tissue culture and engineering (in scaffolds and extracellular matrix such as fibrin and collagen), cell culture (primary, cell line and stem cells, 3D and 2D), SDS-PAGE electrophoresis, Coomassie Blue staining, immunofluorescence, animal experiments, intrinsic NADH imaging
- **Instruments:** LC-Mass Spectrometry, ESI LC-TOF, Fluorescence-lifetime imaging microscopy (FLIM), Confocal microscope, Mastercycler, VersaDoc Imager, Sonicator, Plate reader

PUBLICATIONS

- **Dong, Y.**, Digman, M. A. & Brewer, G. J. Age- and AD-related redox state of NADH in subcellular compartments by fluorescence lifetime imaging microscopy. *Geroscience*, doi:10.1007/s11357-019-00052-8 (2019).
- **Dong, Y.**, Sameni, S., Digman, M.A., & Brewer, G. J. (2019) Reversibility of age-related oxidized free NADH redox states in Alzheimer's Disease neurons by imposed external Cys/CySS redox shifts (in revision).
- **Dong, Y.** and Brewer, G. J. (2019) Global metabolic shifts in age and Alzheimer's mouse brains pivot at NAD^+/NADH redox sites (submitted).
- **Dong, Y.**, Zhang, L., Shao, S. X., Yin, Q., Chen, W., & Zhao, C. F. (2010). The study of myocardial-like tissue engineering constructed by fibroblasts of ischemia myocardium. Chinese Journal of Cell Biology, 3.
- **Dong, Y.**, Zhang, L., Shao, S. X., Yin, Q., Chen, W., & Zhao, C. F. (2009). Phenotypical Stability of Endothelial Cells Differentiated from Bone Marrow Mesenchymal Stem Cell in Vitro and in Vivo [J]. Chinese Journal of Cell Biology, 6.

HONORS

- Excellent Student Award, Hebei Medical University, China 2007 - 2009
- First-class Scholarship, Hebei Medical University, China 2007 - 2009

ABSTRACT OF THE DISSERTATION

Systems Biology of Bioenergetic Shifts in Alzheimer's Disease and Aging

By

Yue Dong

Doctor of Philosophy in Biomedical Engineering

University of California, Irvine, 2019

Professor Gregory J. Brewer, Co-Chair

Professor Frithjof Kruggel, Co-Chair

Aging increases the risk of neurodegenerative diseases including Alzheimer's disease (AD) and Parkinson's Disease. AD is a progressive neurodegeneration with loss of cognitive memory, leading to dementia. The goal of this work is to systematically trace an upstream metabolic or energetic shift in aging and AD to identify targets to delay or even reverse the course of aging and pathologies in AD. Based on the epigenetic oxidative redox shift (EORS) theory of aging, we developed the hypothesis that age- and AD-related oxidative shifts deplete NADH levels in hippocampal neurons, which further trigger the downstream energetic and metabolic shifts sensed at NAD^+/NADH redox sensitive sites. Regulated by redox-sensitive transcription factors, metabolic shifts are enforced epigenetically, which initiate a vicious cycle and exacerbate the course of aging and AD. This work investigates upstream oxidative shifts in NADH redox states and verifies causative links to systematic downstream metabolic and energetic networks. As nicotinamide adenine dinucleotide (NAD and NADH) plays critical roles in metabolic

oxidation-reduction reactions in energetic pathways as well as redox detoxification systems, we further examined if these age-related oxidized free NADH redox states and depletion of NADH are reversible and restored with external redox modification in primary cultures by manipulating different redox potentials of Cysteine/Cystine (Cys/CySS). NADH measurements were performed on live neurons of primary hippocampal cultures of non-transgenic (NTg) and triple-transgenic AD mouse model (3xTg-AD) across the age-span, by using the fluorescence lifetime imaging microscopy (FLIM) technique. This FLIM technique is a non-invasive approach of the intrinsic fluorescence in NADH. After transformation of pixels of FLIM images by Fast Fourier Transform (FFT), we were able to distinguish different NADH lifetimes, analyze and quantify free and enzyme-bound NADH in subcellular compartments in the phasor plot. We found a strong age effect that diminished the free NADH levels in mitochondria, cytoplasm and nuclei with further depletion with AD genetic load. With an imposed oxidized Cys/CySS state of 0 mV in neuron culture, we found a lower capacity for maintaining free NADH in old age versus young age neurons of both NTg and 3xTg-AD mouse neurons. Remarkably, under an external imposed Cys/CySS reductive state, the mitochondrial free NADH levels were rejuvenated to the levels of young age neurons in both NTg and 3xTg-AD mouse neurons. Our findings suggest a potential reductive treatment to reverse the loss of free NADH in old and AD neurons. To test our hypothesis of an age-related metabolic shift triggered by oxidation in NADH redox states, we applied untargeted Ultrahigh Performance Liquid Chromatography-Tandem Mass Spectroscopy (UPLC-MS/MS) to globally detect and measure the metabolite levels from NTg and 3xTg-AD mouse hippocampal brains across the age-span. We observed strong age-related global elevations up to 2-3-fold in energy

metabolism including glycolytic ATP-produced steps, fatty acid β-oxidation and branched chain amino acid metabolism. The direction of metabolic changes with age pivoted at NAD^+/NADH redox sensitive dehydrogenases. We found for the first-time age-related decreases in the upstream metabolites of dehydrogenases and increases in the downstream metabolites of glycolysis and the TCA cycle. Our results support the hypothesis and provide a potential reductive treatment to possibly counter AD and extend healthy lifespan, by reversal of low free NADH levels in old and Alzheimer's neurons via a series of NADH-sensor mechanisms.

CHAPTER 1

INTRODUCTION

Alzheimer's disease (AD) is an age-related progressive complex neurodegenerative disease affecting 5.8 million Americans in 2018 and this number is growing (Gaugler et al., 2019). Aging increases the risk for neurodegenerative diseases. Questions remain on whether AD is a consequence of aging brains by reaching above a threshold of metabolic shift, pathological load or memory loss. Clinical trials indicate the mechanism of AD is still unclear, which impedes the development of effective therapies for AD. Evidence abounds of oxidized shifts or alteration in metabolomics in aging or AD. However, the causative links between oxidative shifts and systematic metabolomics and energy production in aging and AD brains has also not been well established. Further, how and if age-related changes in systemic redox-state promotes the development of aging brain metabolic shift and AD cognitive deficits remains unclear (Hajjar et al., 2018). In this dissertation, we provide evidence that an age- and AD-related oxidative shift in NADH redox state is an upstream event that triggers systematically downstream shifts in metabolic and energetic networks, pivoting at NAD^+/NADH redox sensitive sites. Further, benefiting from the mature neuronal culture technology developed by Dr. Brewer, by imposed extracellular reductive states of Cysteine/Cystine (Cys/CySS) in primary neuronal cultures, we successfully rejuvenated and restored the intracellular oxidized NADH redox states in old age neurons from both non-transgenic (NTg) and triple-transgenic (3xTg-AD) mouse hippocampal neurons.

1.1 Aging and Alzheimer's Disease (AD)

Aging is defined as a progressive loss in function and increase in morbidity and mortality with time (Squier, 2001). Aging is characterized by features such as memory loss, oxidative shifts and metabolic disturbances (Brewer, 1998; Hajjar et al., 2018; Dong and Brewer, 2019 submitted). Aging increases the risk for neurodegenerative diseases, including Alzheimer's disease (AD). The projected number of people above 65 years of age with AD will grow from 5.8 million to 13.8 million by 2050 (Gaugler et al., 2019). AD is characterized by cognitive deficits or dementia with hypothesized mechanistic associations with extracellular β-amyloid plaque accumulation, intracellular neurofibrillary tangles (NFTs) (Hardy and Selkoe, 2002), metabolic disturbances (Bubber et al., 2005), oxidative stress (Zhu et al., 2007), calcium dysregulation (Stutzmann et al., 2006) and bioenergetic deficits (Parihar and Brewer, 2007). The Mini-Mental State Examination (MMSE) score is widely used to evaluate the cognitive function among the elderly including orientation, attention, memory, language and visual-spatial skills to rapidly assess the degree of dementia or mild cognitive impairments (MCI). 32% of the subjects with mild cognitive impairment (MCI) will transit to AD in 5 years (Ward et al., 2013). The conventional cutoff score of MMSE less than 24 is considered as a sign of MCI, compared to a 30 for unimpaired subjects. Yet an MMSE score of 26 or 27 may be a cutoff in symptomatic populations with similar educational and socioeconomic background (Kukull et al., 1994).

1.1.1 AD Biomarkers for Diagnosis

Identification of AD biomarkers offers information on brain changes for early diagnosis before the dementia stage (Alzheimer's Association, 2018). Different categories of biomarkers provide different aspects of information relative to the AD pathologies. The largest genetic factor for AD is APOE ε4 allele, which increases the risk 1.5-fold with one copy of ε4 and 12-fold with two copies of ε4 (Shi and Holtzman, 2018). The ε4 promotes a 5-11 year earlier onset of AD (Davidson et al., 2018). Biomarkers in cerebrospinal fluid (CSF) validated for AD and MCI include increased total tau (T-tau), elevated phosphorylated tau (p-tau181, p-tau231), decreased β-amyloid peptide (Aβ42, Aβ40) (Herukka et al., 2015) and oxidatively modified CSF protein (Di Domenico, 2016), which are beginning to be evaluated for MCI. Proposed biomarkers for MCI in plasma include β-Amyloid levels (Yaffe et al., 2011), inflammatory cytokines (Teunissen et al., 2003), neurofilament (Mattsson et al., 2017), fatty acids and exosomes (Winston et al., 2016). Aβ may be considered as an "upstream" AD biomarker whereas other biomarkers such as increased CSF phospho-tau and decreased glucose utilization may be viewed as biomarkers for "downstream" pathological changes (Sperling et al., 2011), since CSF Aβ presents consistently low even at earliest stages of cognitive impairments (Swerdlow, 2011). Aβ protein in the CSF appears to reflect increased entrapment of cerebral Aβ deposition that fails to reach the CSF. The Alzheimer's Disease Neuroimaging initiative (ADNI) recently reports a 92.7% sensitivity and 85% specificity in immunoassay of CSF Aβ42 in distinguishing controls and AD subjects (Weiner et al., 2017). Additionally, combinations of CSF biomarkers improved the accuracy in prediction on early-stage AD, such as increased ratios of p-tau181/ Aβ42 (Harari et al., 2014), reduced ratio of Aβ42/

Aβ40 in AD are more marked than Aβ42 alone (Hampel et al., 2010). Blood-based lipidomic biomarkers may be useful for preclinical AD detection among cognitively normal older adults (Mapstone et al., 2014). Genetic biomarkers other than ApoE show low penetrance (Lutz et al., 2016). Neuroimaging techniques (Shaw et al., 2009) are now frequent adjuncts to diagnosis (Petersen et al., 2010). Imaging biomarkers such as magnetic resonance imaging (MRI) are applied clinically to detect the conversion/ transition of mild cognitive impairment (MCI) to AD using the structural abnormality index scores, which reflect the degree of volume loss in the parenchyma and ventricular enlargement (Vemuri et al., 2009). Additionally, the use of [18F]-fluorodeoxyglucose (FDG)-Positron emission tomography (PET) in clinical trials provides an approach to study the cerebral glucose uptake and glucose utilization prior to the onset of dementia (Reiman et al., 2004). As the FDG-PET mainly measures the synaptic activities, it therefore serves as an early biomarker of AD (Foster et al., 2008). However again, less-invasive evaluation of plasma or CSF biomarkers for diagnosis and prognosis after treatment lack a clinically verifiable mechanism and largely ignore the complexity of metabolic changes with age. Our working hypothesizes that the largest risk factor, age, imposes an oxidative redox shift, which triggers downstream metabolic shifts. Here we provide evidence for this mechanism and suggest how it could be used as a biomarker of at-risk subjects as well as a blood-based mechanistic biomarker of druggable target engagement and treatment efficacy.

1.1.2 AD Therapies

Effective pharmacological therapy for cognitive impairment involved in the prodromal AD and mild AD dementia currently remains an unmet need. Only four drugs are approved for the treatment of AD-associated dementia with limited utility, in which three of drugs work on central nervous system (CNS) cholinergic pathways (Graham et al., 2017). Memantine was approved to target the N-methyl-D-aspartate (NMDA) receptor and glutaminergic pathways for AD treatment (Winblad and Poritis, 1999). Mounting phase 3 clinical trial failures after positive phase 2 indicated the need for new guidelines in clinical drug development with validated biomarkers (Mangialasche et al., 2010). Clinical trials to modify the course of the disease have targeted β-amyloid production and clearance, largely by immunization or using secretase inhibitors to lower Aβ production (Godyń et al., 2016). No anti-amyloid therapy has been effective partially because of the complexity of γ-secretase (Graham et al., 2017). Moreover, the long-term safety and efficacy of the drugs for AD treatments are not clear (Graham et al., 2017).

1.1.3 AD Mouse Models

The well-defined pathologies in AD include extracellular plaques comprising the β-amyloid peptide and intracellular neurofibrillary tangles (NFTs) aggregated by the hyperphosphorylated tau (p-tau) protein. Overexpression of these proteins provides a genetic basis to generate transgenic mouse models of AD (St George-Hyslop, 2000). Transgenic AD mice that develop one or both of the brain AD pathologies provide a preclinical model for studying the effects of lesion severity and cognitive deficits. They also have enabled the search for therapeutic drugs to reduce pathology. Genetic causes

of early-onset AD involve mutations in the amyloid precursor protein (*βAPP*) gene (on chromosome 21), the presenilin 1 (*PS1*) gene (on chromosome 14) and the presenilin 2 (*PS2*) gene (on chromosome 1) that code for proteins that process the large APP into Aβ (Brouwers et al., 2008). The ε4 allele of apolipoprotein E (*APOE*) increases the risk for late-onset AD (Cruts and vanBroeckhoven, 1998). In the transgenic mouse models, promoters drive overexpression of Aβ or/ and tau pathologies. Examples of commonly used AD transgenic mouse models include PDAPP mice, Tg2576 mice and 3xTg-AD mice (Elder et al., 2010). In PDAPP mice, a platelet derived growth factor (PDGF) promoter drives a human APP transgene, which contains a familial Alzheimer's disease (FAD) associated mutation (V717F, with valine at residue 717 substituted by phenylalanine) (Games et al., 1995). This results in an approximately 10-fold rise in human APP protein compared to the endogenous mouse APP levels, which promote age-dependent amyloid plaque deposition starting at 6 months with marked accumulated by 12 to 15 months (Elder et al., 2010; Reilly et al., 2003). PDAPP mice develop numerous pathological hallmarks including thioflavin S-positive Aβ deposits, neuritic plaques, synaptic loss, astrocytosis and microgliosis (Games et al., 1995). With similar methods, the Tg2576 AD mouse, uses a hamster prion protein promoter (PrP)), to drive overexpression of a human APP transgene containing the Swedish FAD mutation (K670N/M671L) (Hsiao et al., 1996). This Tg2576 mouse model expressed human APP more than 5-fold higher than the levels of endogenous mouse APP and exhibited age-related amyloid plaque deposition first seen at 11-13 months. In Tg2576 mice, spatial memory was impaired in 9 to 10-month mice (Hsiao et al., 1996). Both PDAPP and Tg2576 mice are characterized by elevated level of Aβ, amyloid plaques, dystrophic

neurites and gliosis as well as learning and memory impairments (Ashe, 2001; Elder et al., 2010). The triple-transgenic mouse model (3xTg-AD) harbors $PS1_{M146V}$, APP_{Swe} and tau_{p301L} transgenes (Oddo et al., 2003). Human APP_{Swe} and tau_{p301L} are under control of the mouse Thy1.2 regulatory promoter. Tau_{p301L} was co-injected onto a homozygous $PS1_{M146V}$ knock-in background. 3xTg-AD mice display both parenchymal plaques at 6 month and tangle pathology by 12 months. Moreover, age-dependent synaptic dysfunction and long-term potential (LTP) deficits were reported to occur before plaque and tangle pathology (Odd et al., 2003). Compared to the age-matched non-transgenic (NTg) mice, the 3xTg-AD mice showed increased levels of lipid peroxidation and antioxidant enzymes (Resende et al., 2008). Mitochondrial dysfunction includes structural abnormalities (Monteiro-Cardoso, 2015) and decrements in axonal motility (Manczak and Reddy, 2012). Synaptic decrements were also found in the 3xTg-AD mouse model (Baglietto-Vargas et al., 2015; 2018). In our studies, we used the 3xTg-AD mouse model to investigate the age- and AD-related shifts in redox-energy metabolism and determine if the oxidative and energetic shifts were reversible with external redox modifications, which may potentially rescue the loss of synapses in AD.

1.1.4 How Age Contributes to AD

Though AD is not a normal part of aging and those who age remain resistant to dementia (Robinson et al., 2018) advanced age is the greatest risk factor for AD. Yet little is known about the mechanisms implicated. Different perspectives view AD as either an inevitable consequence of brain aging by surpassing a threshold of pathology or largely ignore the co-morbidities of brain aging. Aging and AD brains share some common phenomena

such as hippocampal atrophy, some degree of plaque and tangle pathology in individuals above 85 years old and mitochondrial oxidative damage (Swerdlow, 2011). Possible mechanisms include mitochondrial dysfunction (Hauptmann et al., 2009), inflammation (Ravaglia et al., 2007), hypometabolism (Mosconi et al., 2008) and systemic oxidative shift that could promote increased processing pathologies of tau and Aβ, alter metabolism to reduce energetic capacity (Mariani et al., 2005; Sultana and Butterfield, 2010; Hajjar et al., 2018). Benefiting from the mature protocol for hippocampal neuronal isolation and culture developed by Brewer and Torricelli (2007), we were able to study changes in redox-energy states across the age-span in cultured adult neurons from NTg and 3xTg-AD mouse hippocampal brains. Further, this neuronal culture technique facilitated on the manipulation of the redox environment in culture medium to examine the reversibility of age- and AD-related oxidative shifts. Studying redox-energy on NTg and 3xTg-AD hippocampal mouse brains with either cultured neurons or tissue provides insights on if and how age may contribute to the development of AD from the possible upstream perspective of redox-bioenergetics.

1.2 Systems Biology of Bioenergetics and Metabolism in Aging and AD

The major energy source for neurons is glucose, which is oxidized for the energetic production of ATP. Energy is generated through a series of biological reactions dependent on oxidation by NAD^+ of the reducing sugar inputs, from glycolysis through the TCA cycle, coupled to the electron transport chain (ETC). Alternatively, glucose can be directed to the PPP that produces NADPH and pentose sugars for biosynthesis. Among these metabolic pathways, several sugar-phosphate intermediates are critically

dependent on NAD^+ and $NADP^+$ for the generation of NAD(P)H to power the pathway and maintain the balance of reductive and oxidative power *in vivo*. These vital sugar-phosphate intermediates comprise glucose 6-phosphate (g6p), dihydroxyacetone phosphate (dhap) and glyceraldehyde 3-phosphate (gly3p) upstream of NAD+/NADH-dependent glyceraldehyde phosphate dehydrogenase (GAPDH). Downstream of the GAPDH redox-reaction in glycolysis are 1,3-bisphosphoglycerate, 3-phosphoglycerate and phosphoenolpyruvate. Upstream of the α-ketoglutarate dehydrogenase (KGDHC) rate-limiting step in the TCA cycle and other TCA cycle dehydrogenases are isocitrate (IDH), succinate (SDH) and malate (MDH). Metabolites downstream of each NAD+/NADH dependent dehydrogenase listed above are α-ketoglutarate, succinyl-CoA, fumarate and oxaloacetate (oxa). Other upstream metabolites such as glutamine, fatty acids and branched chain amino acids (BCAAs) also feed into the TCA cycle at the sites of α-ketoglutarate, acetyl-CoA and succinyl-CoA. In the PPP, glucose-6-phophate is upstream of the first $NADP^+$/NADPH-dependent glucose-6-phosphate (G6P) dehydrogenase and 6-phosphogluconate (6pg) and ribulose 5-phosphate (r5p) are downstream (Magistretti and Allaman, 2013). We propose an age-dependent upstream-downstream shift in metabolites, triggered by oxidative shifts and sensed at the NAD^+/NADH redox-sensitive sites in the metabolic networks, especially implicating the energy-producing pathways, possibly related to AD pathologies.

1.2.1 Metabolic and Bioenergetic Disturbances in Aging

Ralser *et al.* (2007) demonstrated that carbohydrate flux is dynamically rerouted from glycolysis to the PPP under oxidative stress in yeast cells through reduced activity in

glycolytic enzymes, including TPI (triose phosphate isomerase) and GAPDH (glyceraldehyde-3-phosphate dehydrogenase) and increased concentrations of PPP metabolites under oxidative stress Krüger also provided solid evidence to affirm the roles of PPP during the antioxidant response in yeast cells as a metabolic redox sensor (Krüger et al., 2011). The brain depends largely on glucose for energy supply. Glucose uptake and transporter expression declined significantly in female mouse brains at early stage of aging in both NTg and 3xTg-AD genotypes (Ding et al., 2013). Studies on mitochondrial metabolism in elderly human brains indicated 30% lower in glutamate-glutamine cycle flux and reduced neuronal mitochondrial metabolism (Boumezbeur et al., 2010). In the aged mouse samples, mitochondrial dysfunction in the brains drove a metabolic shift from OXPHOS to glycolysis, leading to increased expression of lactate dehydrogenase genes and increased brain lactate levels (Ross et al., 2010). Increasing number of "-omics" studies screen the age-dependent alterations in perspectives of global metabolome (Jové et al., 2014), genome (Lipinski et al., 2010) and proteome (Manavalan et al., 2013). Another approach relies on the platform of computation to systematically model the metabolome and bio-energy in the network. Computational modeling is commonly applied to dynamically simulate the changes of metabolic fluxes with its advantages of quantitation, dynamic and systematic mapping. Ralser's group modeled enzymatic reactions of glycolysis and PPP by using the CellDesigner software to detect the changes of metabolite concentrations under normal and reduced activities of TPI and GAPDH (Ralser et al., 2007). In Ralser's model, the sum of cellular $NAD(P)^+$ and NAD(P)H (NAD pool) was set to be constant and the ratio of NAD(P)H/$NAD(P)^+$ drove the reactions, rather than the absolute concentrations (Ralser et al., 2007). Cortassa's group translated

the metabolite profiles of glycolysis, PPP (NADPH-generating), glycogenolysis and polyols (NADPH-consuming) into metabolic fluxes by using MATLAB (Cortassa, 2014), in which the pool of NAD(P)H+NAD(P)$^{+}$ was also considered as a constant. Berndt integrated a kinetic metabolic-energetic network from glycolysis, PPP, TCA cycle, ECT and OXPHOS in a computational model (Berndt et al., 2012; 2015, **Fig. 1.1**). Given that in AD, KGDHC activity declines 25-75% (Mastrogiacomo et al., 1993), Berndt's modeling stimulated depletions in mitochondrial NADH levels together with inhibitions of KGDHC activity ranging from 0-70% in activity. At the inhibition of 60% KGDHC activity, ATP production dropped 50% compared to the non-inhibition (Berndt et al., 2012).

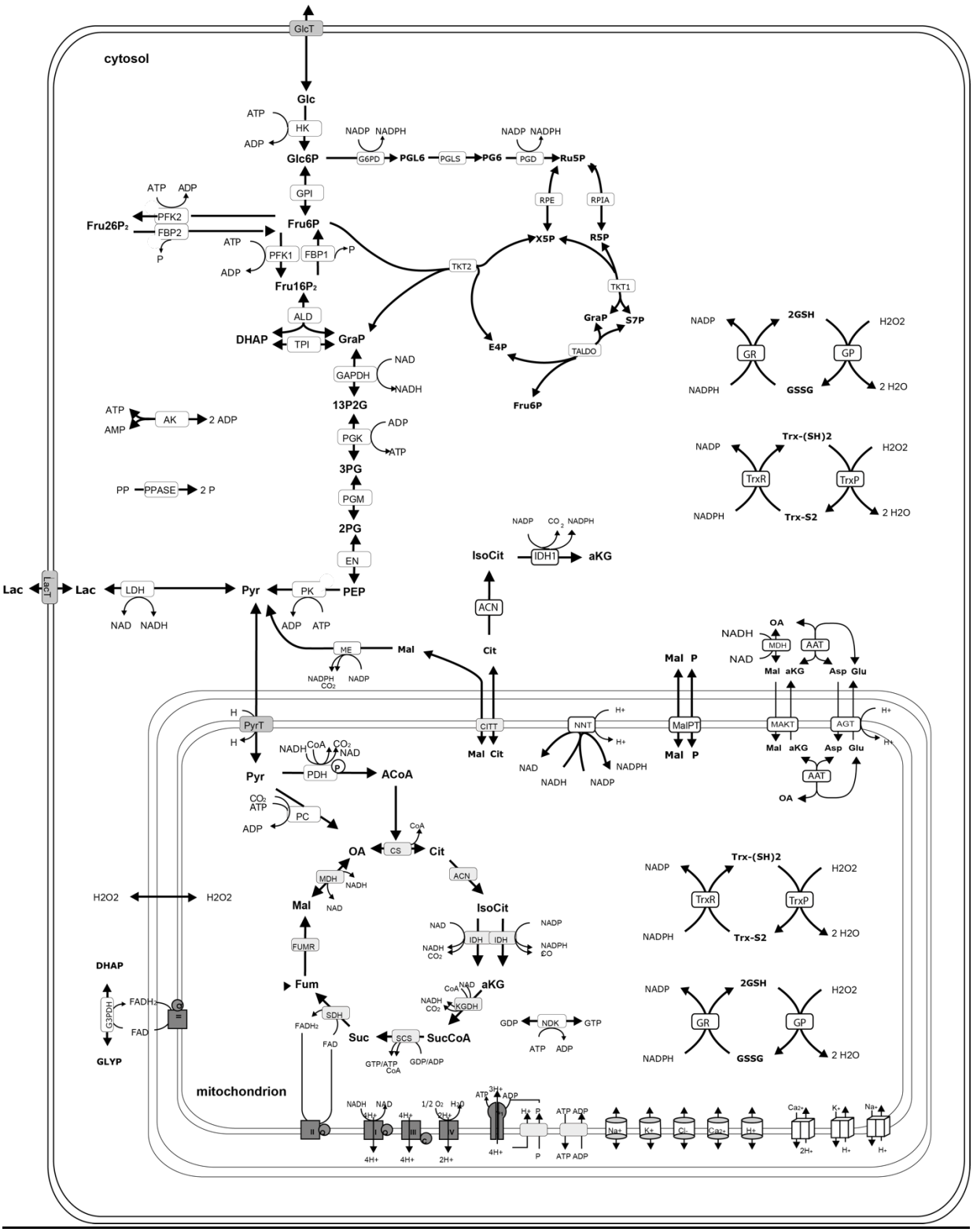

Figure 1.1 Schematic representation of central neuronal energy metabolism. This computational metabolic system includes glycolysis, pentose phosphate pathway, TCA cycle, respiratory chain (RC) and oxidative phosphorylation (OXPHOS) (Berndt et al., 2015).

However, most metabolic modeling neglects how metabolic flux would be dynamically changed under different NAD(P)H/NAD(P)$^+$ ratios and oxidative states, even diurnally (Eckel-Mahan et al., 2013; Aguilar-Arnal et al., 2016). Given that age-associated oxidative shifts in hippocampal/cortical neurons include lower levels of NAD(P)H and GSH (Ghosh et al., 2012) and depolarization in the mitochondrial membrane potential (Δψ) (Sullivan and Brown, 2005; Parihar et al., 2008), but these changes have not been associated with a metabolic shift and not studied in an Alzheimer mouse model as a function of age. In chapter 3, we experimentally altered the NADH levels across the age-span for proof of concept that intracellular low free NADH levels can be externally boosted. Furthermore, we systematically measured metabolite shifts in global metabolic pathways in NTg and 3xTg-AD mouse brains across the age-span. We especially investigated if and how age- and AD-associated oxidative shifts in NADH redox states interfered with the metabolic networks sensed at NAD$^+$/NADH redox sites.

1.2.2 Metabolic and Bioenergetic Disturbances in AD

An age-associated sedentary low-energy state is implicated in AD morbidity and is coincident with observations of metabolic shifts and decline in glucose uptake with aging (Ding et al., 2013; Gage et al., 1984; Gumbiner et al., 1992). Deficiencies of GLUT1 and GLUT3 in AD brains impaired brain glucose uptake and metabolism, which contribute to neurodegeneration and hyperphosphorylation of tau in AD (Liu et al., 2008). The glucose and insulin intolerance were found in 6-month-old APP/PS1 AD mouse brains, accompanied by significant memory loss and impaired cognitive ability (Pedrós et al., 2014). A study of 20 patients with early-onset dementia of Alzheimer type (DAT) revealed

a 50% reduced metabolic rate of glucose in brain and significant elevation of lactate production compared to non-demented subjects (Hoyer, 1998). Lactate is an alternative energy supply for neurons during hypoglycemia (Aubert et al., 2005). Ding and colleagues demonstrated the utilization of ketone bodies and lactate as alternative energy supplies during early glucose insufficiencies (Ding et al., 2013). The decrease in enzyme activities of dehydrogenases in the first half of the TCA cycle (KGDH, SDH) correlated with cognitive deficit ($r = -0.65$), whereas the enzyme activities in the second half were upregulated ($r = +0.53$) as a possible compensatory response in AD patients (Bubber et al., 2005). Since these bioenergetic correlations with cognitive impairment are stronger than those with beta-amyloid plaques ($r=0.52$) and as strong as those with synapse loss ($r=0.73$; Terry et al., 1991), we are encouraged to evaluate the redox role of bioenergetic changes with aging and AD. Yao group demonstrated that during AD, the metabolic profile shifts from glucose-driven bioenergetics to a less efficient compensatory ketogenic pathway, which contributes to white matter degeneration (Yao et al., 2011). The Fluoro-2-deoxy-D-glucose positron emission tomography (FDG-PET) image revealed glucose metabolic reductions in the parieto-temporal, frontal and posterior cingulate cortices in AD brains (Mosconi, 2005). Typical FDG-PET findings indicate lower glucose metabolism in brain regions of temporal association cortex, precuneus, and posterior cingulate. Importantly, this FDG-PET is used as a biomarker for early diagnosis of AD, at MCI or preclinical AD stage (Inui et al., 2017). Metabolic signatures relatively to AD progression have mainly implicated hypoxia, oxidative stress and membrane lipid remodeling (Orešič et al., 2011). Moreover, pathway analysis of metabolomic results suggested that only the pentose phosphate pathway (PPP) shifted significantly behind the progression to AD

(Orešič et al., 2011). Alterations in ceramides and sphingomyelins promotes Aβ pathology, inflammation in AD and further neuronal apoptosis (Alessenko et al., 2004). CSF choline, arginine, valine, proline, serine, histidine, creatine and carnitine were viewed as potential biomarkers to evaluate AD progression (Wang et al., 2013). By high-resolution mass spectrometry, the post-mortem human brain metabolome from AD and age-matched controls revealed a 94-97% correct prediction of AD based on a predictive model for AD progression and strikingly 100% diagnostic accuracy in a blind test of 60 samples (Ibáñez et al., 2012). Among those AD-related global metabolic signatures, answers to how many were caused directly from the AD pathologies separately from the normal aging may possibly reveal the mechanism of underlying AD pathology and dementia.

1.3 Age- and AD-Related Oxidative Shifts

1.3.1 Redox Couples with Aging

The balance between oxidant production and antioxidant defense is critical for normal cell survival (Aon et al., 2010). Biological redox energy spans the scale from highly reduced energy levels of NADPH, GSH and NADH around -400 mV to most oxidized oxygen at 800 mV (Brewer, 2010). The maintenance of intracellular redox states is mainly dependent on reductive/ oxidative couples *in vivo*, such as glutathione/ oxidized glutathione (GSH/GSSG), reduced/oxidized nicotinamide adenine dinucleotide phosphate ($NADPH/NADP^+$) and reduced/oxidized nicotinamide adenine dinucleotide ($NADH/NAD^+$) (Sohal and Orr, 2012). The extracellular redox state in plasma is largely maintained by the reductive/ oxidative couple of cysteine/ cystine (Cys/CySS) (Jones and

Go, 2010). Sufficient amounts of NADPH are necessary to keep the intracellular ratio of GSH/GSSG at high levels and maintain cellular redox states (Seila et al., 2012). About 60% of NADPH *in vivo* is produced by the PPP in humans. Ghosh *et al.* (Ghosh et al., 2014b) showed that NAD(P)H levels were upstream of GSH and an oxidative shift. The steady-state thiol/disulphide redox potentials are highly compartmentalized in cells (Hansen et al., 2006). Based on a limited number of studies in cell culture, the cytoplasmic steady-state redox potential of Cys/CySS (E_h= -160 mV) is far more oxidized compared to that of GSH/GSSG (E_h= -220 to -260 mV) and Trx-1 (E_h= -280 mV), indicating a function of a sulphur switch in the extracellular Cys/CySS redox couple to an intracellular GSH/GSSG (Jones et al., 2004). In Ghosh and Brewer's previous studies, adding excess extracellular Cys relative to CySS to the culture medium was able to improve the intracellular reductive state (increase NADH) of aged neurons and this imposed reductive shift could decrease the death of aged neurons in culture (Ghosh and Brewer, 2014a). Early studies on steady-state redox potential in human plasma with age demonstrated reductive/ oxidative couples of Cys/CySS and GSH/GSSG significantly shifted towards more oxidized after middle age (Go and Jones, 2017). According to the redox theory of aging, the oxidative stress encompasses two aspects: one with macromolecule damage disruption of redox signaling and leading to age-related diseases; the other one termed 'eustress' within the controlled redox signaling, contributing to healthy longevity (Go and Jones, 2017). Age-related oxidative shifts correlate to a series of downstream alterations, dysfunctions and epigenetic changes, which would further cause alterations of receptor expression, signaling molecules, transcription factors and enzyme functions (Brewer, 2010; Sohal et al., 2012). However, numerous animal studies and human trials with anti-

oxidants have failed to improve animal lifespan or human morbidities, possibly because the NADH redox state is upstream of ROS production (Ghosh et al., 2014b).

1.3.2 NADPH-Coupled Detoxification System

The reduced form of nicotinamide adenine dinucleotide phosphate (NADPH) provides reducing equivalents for antioxidant defense (Bradshaw, 2019). NADPH is mainly produced in the pentose phosphate pathway (PPP) or converted from NADH by nicotinamide nucleotide transhydrogenase (NNT) located in the inner mitochondrial membrane (Ronchi et al., 2016). Most descriptions of metabolism treat the generation of NAD(P)H and $NAD(P)^+$ as necessary contributors to metabolism and maintenance of redox states within physiological ranges. However, external events as common as feeding and sleeping shift the levels of NAD(P)H and $NAD(P)^+$ (Aguilar-Arnal et al., 2016; Jones, 2012) raising the possibility that these redox states control the metabolic pathways as a pivot to redirect anabolic and catabolic pathways when an oxidative shift occurs (Ralser et al., 2007; Krüger et al., 2011; Schubert, 2005). Another mechanism of redox balance includes NADPH oxidase (NOX). NOX cytosolic subunit proteins were remarkably increased in the progression of AD. Moreover, the NOX in frontal and temporal cortex were found to be dramatically upregulated, implicating elevated NOX levels in the progression of AD pathogenesis by more superoxide production (Ansari and Scheff, 2011). Thus, suppression of phagocyte NADPH oxidase (PHOX) activity diminished neuronal impairment in neurodegenerative disease models, providing a novel therapeutic target (Gao et al., 2012). NADPH ameliorates neurodegeneration by inhibiting p38 mitogen-activated protein kinases (p38MAPK) activation (Zhou et al., 2018), which

implicated in a wide range of cellular stress and inflammatory responses. Though physiological levels of ROS are critical to mediate cell signaling, pathological levels of ROS result in irreversible oxidative damages and cell death pathways (Dai et al., 2014). The ROS levels are determined by the balance between rate of ROS scavenging systems and rate of ROS production by respiratory complexes and ROS emission (Cortassa et al., 2014). The endogenous antioxidant system includes superoxide dismutase (SOD), catalase, NADPH-linked redox system such as glutathione peroxidases, glutathione reductase (GR) and thiol-disulphide oxidoreductase systems including thioredoxin (Trx) and glutaredoxin (Grx) (Dai et al., 2014; Bradshaw, 2019). Other NADPH-dependent enzymes such as malic enzyme (ME) and isocitrate dehydrogenase 1 and 2 (IDH1 and 2) are critical in role of converting $NADP^+$ into NADPH. Communication of NADPH between mitochondria and cytoplasm is achieved by mitochondrial NADPH shuttles (Lewis et al., 2014) and transhydrogenase (Ronchi et al., 2016). Age- and AD-related declines in NADPH due to losses in the NAD pool and oxidative shifts in NADPH/ $NADP^+$ ratios largely lessen the capacity for oxidant detoxification (Bradshaw, 2019). At an initial stage, an oxidative shift can be counterbalanced by metabolic redirections for more NAD(P)H production. However, as the deterioration beyond the ability of compensation, the accumulating oxidative shifts and depletion of NAD(P)H may hinder the energetic generation in mitochondria. These relationships have not been determined in brain neurons to establish their importance to brain aging and AD.

1.3.3 Mitochondrial Impairment

Age-related oxidative stress and depolarization of mitochondrial membrane potential (Δψ) with increased ROS levels correlated with mitochondrial impairment and toxicity in hippocampal neurons (Parihar and Brewer, 2007). The mitochondrial dysfunction was earlier than the development of AD pathologies in the mouse model (Yao et al., 2011; Chou et al., 2011). Wiley et al. (2016). demonstrated that the senescence state (MiDAS) from mitochondrial dysfunction can be rescued with pyruvate and depletion of SIRT3 and SIRT5 induced senescence. The mitochondrial dysfunction is considered a common final pathway in aging and AD brains (Müller et al., 2010). The age- and AD-related energetic deficits in turn hamper mitochondrial fission and promote the formation of mitochondria-on-a-string (MOAS) (Zhang et al., 2016). Martins et al. (2017) also found decreased mitochondrial number with age in the hippocampus along with abnormal mitochondrial morphology with elongation, swelling and disorganized cristae. In the 3xTg-AD model, mitochondrial motility decrements were due to increased dynamin-related protein 1 (Drp1) levels that raises fission (Manczak and Reddy, 2012). The overproduction of Aβ in AD is associated with the increased expression of dynamin-related protein 1 (Drp 1), increased number of fragmented mitochondria, loss of Δψ and loss of ATP production (Onyango et al., 2016; Wang et al., 2008). As mitochondrial DNA (mtDNA) encodes essential components in OXPHOS, the age- and AD-related oxidative damage induces mutations of mtDNA (Cui et al., 2012). Activities and expression of enzymes in the TCA cycle, ETC and OXPHOS, such as complex IV (cytochrome oxidase; COX) and complex I (NADH: ubiquinone oxidoreductase), declined in the aging and AD phenotypes (Aksenov et al., 1999; Reddy, 2007). In the ETC, complex I and IV are partially encoded by mitochondrial

DNA (mtDNA) while complex II (succinate dehydrogenase) is entirely encoded by nuclear genes. Accumulating evidence suggests age-related increases of mtDNA COX genes and mtDNA content (Barrientos et al., 1997; Hirai et al., 2001) and mitochondrial mass (Hirai et al., 2001). As mtDNA is particularly sensitive to oxidative damage, age- and AD-related oxidative stress in turn promote the susceptibility of mtDNA mutation (Lin and Beal, 2006). Numerous mitochondrial alterations resulted from mitochondrial dysfunctions, however to trace the most upstream that triggers downstream changes appear to be critical to uncover the mechanism of AD pathologies and more importantly to develop an effective therapy for AD.

1.3.4 EORS Theory

Multiple theories have been propounded to explain aging, including Harman's free radical theory (Harraan, 1955), the insulin resistance theory (Watson and Craft, 2003), and the Epigenetic oxidative redox shift (EORS) theory (Brewer, 2010). The EORS theory of aging, unifying the free radical theory and insulin resistance theory, proposes that sedentary low-energy states with aging trigger an oxidative shift and mitochondrial dysfunction. To satisfy the demand of resting energy, metabolic pathways reroute, which are epigenetically enforced and regulated by redox-sensitive transcription factors, such as up-regulation of glycolysis (Brewer, 2010); whereas the low mitochondrial capacitance and insulin resistance would exacerbate the sedentary low energy state and aging, forming a vicious cycle (Brewer, 2010). According to the EORS theory of aging, AD would be initiated by an oxidative shift and followed by metabolic shifts, which are regulated by redox-sensitive transcription factors. The metabolic shifts are proposed to be divided into

two stages in response to an oxidative shift. At an early stage, mitochondrial impairment and low energetic capacity leads to down-regulation of the tricarboxylic acid cycle (TCA or citric acid cycle) and up-regulation of the glycolytic pathway for energy supply. As oxidative shifts become more serious with aging, metabolic fluxes redirect from glycolysis to the pentose phosphate pathway (PPP) to generate more NAD(P)H and to counterbalance oxidative shifts at the following stage. Numerous reports associate oxidative shifts and metabolic alterations with aging and in AD (Humphries et al., 2006; Ross et al., 2010; Kuhla et al., 2011; Ghosh et al., 2012; Ding et al., 2013). However, which pathways, enzymes and metabolites are more prominent and sensitive in response to the oxidized shifts remain unclear, indicating opportunities for therapeutic interventions.

1.4 NADH Bridges Redox Systems, Metabolic and Energetic Networks

1.4.1 NADH Synthesis and Consumption

The reduced form of nicotinamide adenine dinucleotide (NADH) as the major intracellular redox currency, is produced from several metabolic pathways including glycolysis, the tricarboxylic acid (TCA) cycle and the reversed direction of mitochondrial transhydrogenase (NNT). NADH generates the proton gradient to power ATP generation in OXPHOS. Thus, NADH importantly bridges redox states, metabolic pathways and energy generation. The NADH pool consists of two forms of free in solution and bound to protein. Since enzymes can only use free NADH in biofunctions, distinguishing free from bound NADH to facilitate studies of age- and AD-associated capacities in free NADH regeneration and energetic states. Here, we employed two-photon lifetime imaging fluorescence microscopy to resolve label-free signals from free and bound NADH in sub-

regions of live neurons with age and AD-genotype (all in chapter 2). Moreover, during energetic shortage, the reaction direction of NNT reversed to more free NADH production at the cost of NADPH (Ronchi et al., 2016). As the NADH transfers its proton (H^+ and electron) during oxidative phosphorylation, the concentration of NADH limits the synthesis of ATP by affecting the generation of the proton gradient (Cooper, 2000). The consumption of NADH under oxidative stress or oxidative shifts, together with a decline of other reductive compounds in redox couples, impair the generation of ATP and lead to energetic deficits in neurons.

1.4.2 NAD Pool Size Maintained by the Balance of Biosynthesis and Consumption

The NAD pool is defined as the total of NADH and NAD^+ but levels are highly compartmentalized (Xiao et al., 2018). NAD^+ levels are maintained via three biosynthetic pathways: the Preiss-Handler, de novo biosynthesis and salvage pathways (Verdin, 2015). The precursors of NAD^+ including nicotinic acid, tryptophan, nicotinamide (NAM) and nicotinamide riboside (NR) are available from food to feed into NAD^+ biosynthesis pathways. The Preiss-Handler pathway and de novo biosynthesis pathway converge at the point of nicotinic acid mononucleotide (NAMN). NAMN is finally transformed to NAD^+. In the salvage pathway, the precursor nicotinamide is replenished either from diet or from degradation of NAD^+ by NAD-consuming enzymes, including Sirtuins (SIRTs), the adenosine diphosphate (ADP)-ribose transferases (ARTs) and poly (ADP-ribose) polymerase (PARPs), and the cyclic ADP-ribose (cADPR) synthases (CD38 and CD157) (Canto et al., 2015; Bai and Canto, 2012). Nicotinamide is recycled into nicotinamide mononucleotide (NMN) by nicotinamide phosphoribosyltransferase (NAMPT) to generate

NAD^+ (Verdin, 2015). Here, we looked for an age- and AD-related shift in the balance between the synthesis and consumption of NADH in neurons. Reaction kinetics control the levels of NADH product at about 7-8-fold lower than NAD^+ in mitochondria limited by the NADH levels (Williamson et al., 1967). Here we addressed the question of whether these NADH levels are sensitive measures of metabolic shifts with age and AD-like genotype, since a decline in free NADH levels would decrease capacity for ATP synthesis via oxidative phosphorylation. Either the redox shift or the energy shortage with demand could cause many downstream dysfunctions associated with aging and AD including altered amyloid and tau processing, LTP (Walsh et al., 2002), calcium handling (LaFerla, 2002), mitochondrial function and motility (Gibson & Blass, 1976; Manczak and Reddy, 2012), DNA repair (Imam et al., 2006) and autophagy (Nixon, 2013). With aging, the activity of NAD-biosynthesis decreases while the activities of NAD^+-consuming enzymes increase such as CD38 (Camacho-Pereira et al., 2016), which together contribute to the age-associated decline in the NAD pool size. In liver and muscle of aged mice, age-related DNA damage activated PARP activity (global PARylation) along with other DNA repair proteins which decreased NAD^+ levels as a consequence (Mouchiroud et al., 2013). In parallel with the decline of NAD^+ levels, the activity of SIRT1 decreased (Braidy et al., 2011). Further, the drop of NAD pool diminishes NADH production, which depletes ATP stores leading to the release of apoptosis inducing factors (AIF) and induction of cell apoptosis under stress (Yu et al., 2002). Paradoxically, the activity and mRNA expression of NADase CD38 increased with aging in multiple tissues to further deplete NAD^+ levels (Camacho-Pereira et al., 2016). Interestingly, studies in CD38 knockout mice indicate that CD38 plays an important role in regulating hippocampus-dependent learning and memory

tasks including the Morris water maze and the object recognition test (Kim et al., 2016). Additionally, NAMPT expression drops steadily with aging in both NTg and 3xTg-AD mouse neurons (Ghosh et al., 2014b), leading to declines in NAD^+-synthesis from nicotinamide via the salvage pathway and consequent declines in NADH. Increasing evidence shows neuroprotective effects of SIRT1 activation in age-related neurodegeneration, possibly as a feedback mechanism to activate protective effects despite the consumption of NAD^+ (Kim et al., 2007; Khan et al., 2012). PARP inhibitors together with NAD^+ precursors boost ATP levels and increased gene expression of enzymes in the TCA cycle and glycolysis, such as citrate synthase and kexokinase (Mouchiroud et al., 2013). Answers to the following questions may provide insight on which mechanisms are upstream to initiate shifts in redox-metabolomics-energy networks in aging and AD brains: 1) How much do NADH levels shift in old and AD brains when the NAD pool size diminishes with aging? 2) Can these intracellular NADH levels be manipulated? 3) What are the impacts of shifts in NADH on metabolic and energetic pathways in aging and AD brains?

1.4.3 NADH/NAD^+ in Aging and AD Brains

Though both NADH and NAD^+ levels diminished in aging and AD brains, accumulating evidences demonstrated that the NADH/NAD^+ ratios were shifted to an oxidized state (more NADH loss than NAD^+ loss) in the mouse or rat brain tissue with age and AD (Zhu et al., 2015; Parihar et al., 2008; Ghosh et al., 2012). Normal NADH/NAD^+ redox potentials are maintained by the malate-aspartate and glutamate-aspartate shuttles (Pittelli et al., 2011). NADH/NAD^+ ratios not only reflect the redox states of the redox

signaling systems (Ying, 2008), but also sever as a metabolic readout to indicate metabolic shifts between glycolysis with more free NADH production and OXPHOS for more NADH consumption (Stringari et al., 2015). We therefore proposed that the age- and AD-associated oxidative shifts in NADH redox states triggered shifts in metabolomics and energy networks as downstream pivoted at the redox sensitive sits of NADH/NAD^+.

1.5 Summary

Brewer's epigenetic oxidative redox shift (EORS) theory proposed that age-associated sedentary behavior triggers an oxidative shift and impaired mitochondrial function, which causes epigenetically enforced metabolic shifts that lead to energetic deficits (Brewer, 2010). We hypothesized that an age- and AD-related oxidative shift is upstream of shifts in energy-producing metabolic pathways and energetic deficits as well as changes in amyloid processing. In chapter 2, we provide new insight into the age-related basis of Alzheimer's disease as an upstream shift in free NADH levels at the segregated subcellular compartment in live neurons. As free NADH critically sets the redox state, energetic supply to oxidative phosphorylation and metabolic states, we further determined the mitochondrial free NADH concentrations across the age-span. These studies were enabled by using two-photon excitation fluorescence lifetime imaging microscopy. This non-invasive, sensitive method utilizes auto-fluorescent NADH as a natural probe to quantify free NADH concentrations and fractions in subcellular compartments of live primary neurons across the age-span of young, middle and old ages in adult wild-type and AD-model mouse hippocampal neurons. In chapter 3, to examine if the age- and AD-related oxidative shifts and depletion in free NADH can be rescued by external

modification of the redox state, we manipulated the intracellular free NADH by imposed external oxidative or reductive Cys/CySS redox shifts in neuronal culture. We determined the mitochondrial free NADH concentrations and total NADH pool size with each redox state across the age-span in adult wild-type and AD-model mouse neurons. In chapter 4, to support our hypothesis, we investigated global metabolomic shifts downstream pivot at NAD^+/NADH redox sites as a function of age and AD genotypes by using untargeted mass spectrometry from mouse hippocampal tissue. The following details further rationale and significance for a biosystems approach to aging and Alzheimer's disease.

CHAPTER 2

AGE- AND AD-RELATED REDOX STATE OF NADH IN SUBCELLULAR COMPARTMENTS BY FLUORESCENCE LIFETIME IMAGING MICROSCOPY (PUBLISHED IN GEROSCIENCE, 2019)

Yue Dong[1], Michelle A. Digman[1,2] and Gregory J. Brewer[1,3]

[1]Department of Biomedical Engineering, University of California Irvine, Irvine, California, United States of America,

[2]Laboratory of Fluorescence Dynamics, Department of Biomedical Engineering, University of California Irvine, Irvine, California, United States of America,

[3]MIND Institute, Center for Neurobiology of Learning and Memory, University of California, Irvine, CA, United States of America

Keywords NADH • Aging brain • Alzheimer's disease • FLIM • Mitochondria • Redox States

2.1 Abstract

Nicotinamide adenine dinucleotide (reduced form: NADH) serves as a vital redox-energy currency for reduction-oxidation homeostasis and fulfilling energetic demands. While NADH exists as free and bound forms, only free NADH is utilized for complex I to power oxidative phosphorylation, especially important in neurons. Here we studied how much

free NADH remains available for energy production in mitochondria of old living neurons. We hypothesize that free NADH in neurons from old mice is lower than the levels in young mice and even lower in neurons from the 3xTg-AD Alzheimer's disease (AD) mouse model. To assess free NADH, we used lifetime imaging of NADH autofluorescence with 2-photon excitation to be able to resolve the pool of NADH in mitochondria, cytoplasm and nuclei. Primary neurons from old mice were characterized by a lower free/bound NADH ratio than young neurons from both non-transgenic (NTg) and more so in 3xTg-AD mice. Mitochondrial compartments maintained 26% to 41% more reducing NADH redox state than cytoplasm for each age, genotype and sex. Aging diminished the mitochondrial free NADH concentration in NTg neurons by 43% and in 3xTg-AD by 50% The lower free NADH with age suggests a decline in capacity to regenerate free NADH for energetic supply to power oxidative phosphorylation which further worsens in AD. Applying this non-invasive approach, we showed the most explicit measures yet of bioenergetic deficits in free NADH with aging at the subcellular level in live neurons from in-bred mice and an AD-model.

2.2 Introduction

Aging is generally accompanied by progressive loss in cognitive function (Squier, 2001). The Epigenetic Oxidative Redox Shift (EORS) theory of aging proposes that a sedentary low-energy state with aging triggers an oxidative shift and mitochondrial dysfunction and further causes metabolic disturbances (Brewer, 2010). Indeed, aging increases the risk for neurodegenerative diseases, including Alzheimer's disease (AD). A 2016 report projects that by 2050, the number of people above 65 years of age with AD will grow from

5.4 million to 13.8 million (Alzheimer's Association, 2016). Aging and AD share some common characteristics such as oxidative stress (Zhu et al., 2015), mitochondrial impairment (Lin and Beal, 2006) and bioenergetic deficits (Parihar et al., 2008), which are associated with cognitive deficits or dementia. In the 3xTg-AD mouse model that we used, Fattoretti et al. (2010) reported decreased mitochondrial numeric density (number of mitochondria/μm^3 of cytoplasm) in CA1 in 10-month-old mice, but the volume and average length increased. Martins et al. (2017) also found decreased mitochondrial number with age in the hippocampus along with abnormal mitochondrial morphology with elongation, swelling and disorganized cristae. Manczak & Reddy (2012) found decrements in the motility of mitochondria in the 3xTg-AD model due to changes in Drp1 levels for fission. We propose that these mitochondrial structural changes reflect functional deficits of free NADH as a bioenergetic substrate for oxidative phosphorylation (OXPHOS) that initiates a vicious cycle involving redox imbalance, energetic shortage and mitochondrial dysfunction.

The brain consumes large amounts of energy to fire action potentials (Attwell and Laughlin, 2001). Neurons primarily depend on the energy-transducing capacity of mitochondria to meet redox and phosphorylation demands. Since the reduced form of nicotinamide adenine dinucleotide (NADH) is the major intracellular redox currency and the substrate for generation of ATP as the energy currency via oxidative phosphorylation (OXPHOS) in mitochondria, mitochondrial NADH availability to the electron transport chain (ETC) becomes a critical issue (Brewer, 2010). NADH functions as a pivotal metabolite that bridges redox states, metabolic pathways and energy (ATP). Neurons

respond to higher energy demands by increasing free NADH production in the TCA cycle as electron donors to feed the electron transport chain (ETC) for ATP generation. We hypothesized that aging brain neurons exhibit an oxidized NADH redox state with decreased free NADH and these free NADH levels are further decremented by the genetic burden of AD-like mutations in 3xTg-AD mouse neurons. Antioxidant defenses also depend on NADH and its reductive conversion to NADPH and GSH. For instance, the forward reaction of nicotinamide nucleotide transhydrogenase (NNT) oxidizes NADH and reduces $NADP^+$ to generate NADPH (Ronchi et al., 2016). However, during oxidative shifts, the backward reaction of NNT drives NADH production at the expense of NADPH (Ronchi et al., 2016). NADPH also donates electrons to GSSG for regeneration of GSH. Evidence for which of these is upstream comes from titrated inhibition of enzymes for their synthesis and supplementation of precursors (Ghosh et al., 2014b). From these studies in neurons, NAD(P)H appears upstream of GSH, since decreasing NAD(P)H lowers GSH levels more than the reverse and neuron survival was more dependent on NAD(P)H, especially in neurons from old mice and those from an Alzheimer model mouse brain (Ghosh et al., 2014b). Therefore, determination of the availability of free NAD(P)H in mitochondria was evaluated to provide a possible mechanism of age-related and Alzheimer's associated decrements in energy supply and oxidative redox shifts.

Although NADH and NAD^+ are reduced and oxidized forms of nicotinamide adenine dinucleotide, only NADH has intrinsic fluorescence (Chance and Thorell, 1959). Different excited state lifetimes of free and bound NADH enable determination of the free NADH available from that bound to enzymes (Lakowicz et al.,1992). The long intrinsic

fluorescent lifetime of NADH is due to the protein-bound state (Yu and Heikal, 2009; Stringari et al., 2012). The ratio of free to protein-bound NADH correlates with the NADH/NAD^+ ratio (Bird et al., 2005). Our previous work measured steady-state levels of NAD(P)H without discriminating between free and bound forms (Ghosh et al., 2012; 2014). These studies found age-related and AD-associated declines in NAD(P)H concentrations, NADH regenerating capacity, NAMPT and NNT gene expression for regeneration in neurons from non-transgenic (NTg) and an age-matched triple transgenic Alzheimer's mouse (3xTg-AD). We can do this because of techniques for isolating neurons from any age animal and culturing them in a common serum-free environment (Brewer et al., 1998, 2007). These neurons are thus removed from an aging immune system, age-related changes in hormones and the vasculature. *In vitro*, we demonstrated the age-related increased susceptibility to biochemical stressors as a critical mechanism in aging (Brewer, 1998; 2010). Based on measures in aged rat neurons challenged with glutamate, steady state NADH and glutathione decline with age before declines in ATP (Parihar et al., 2008). Flux control experiments indicated that the often-reported declines in mitochondrial function with age are caused by lower supplies of NADH substrate, rather than problems with the complex I enzyme that uses the NADH to generate a proton gradient across the mitochondrial membrane to power generation of ATP (Jones and Brewer 2010). In mitochondria isolated from 3xTg-AD brains, respiratory capacity was shown to be impaired (Yao et al., 2009). Conventional biochemical approaches performed on the cell lysates as a snapshot of redox states to measure NADH concentrations in cells introduces errors as the NADH is oxidized when exposed to air (Uppal and Gupta, 2003; Klaidman et al., 1995) and rapidly consumed by mitochondrial demand for ATP.

Further, these studies could not discriminate neuronal from glial mitochondria and did not examine the age-dependence or how the proportion of free to bound NADH dynamically changes in living neurons during aging and AD. Since the distribution of NADH and NAD^+ are highly compartmentalized within cells (Xiao et al., 2018), here we determine how aging and AD affects the re-distribution of free to bound NADH ratios. Though intrinsic fluorescence does not discriminate between NADH and NADPH due to identical photophysical properties (Yu and Heikal, 2009), the autofluorescence of intracellular NADH levels contributes the majority of the NAD(P)H intensity (et al., 1989). Here, we applied a non-invasive, sensitive method that utilizes the intrinsic NADH fluorescence lifetimes as a natural probe to identify the shifts in free NADH levels, free to bound NADH ratios (Van Munster and Gadella, 2005) and re-distribution of NADH among subcellular compartments in NTg and age-matched 3xTg-AD mouse neurons from young to old ages.

2.3 Materials and Methods

Mouse Model

We used LaFerla's triple transgenic mouse model of AD (3xTg-AD) with human transgenes *βAPP* (SWE), *PS1* (M146V), and *Tau* (P301L) to mimic the neuropathological features of AD (Oddo et al., 2003). Nontransgenic (NTg) C57BL/6 mice (Charles River) were used as controls. All mice underwent genotyping before using in experiments.

Primary Neuron Culture

Adult hippocampal neurons were isolated from NTg and 3xTg-AD age-matched mouse brains at young (3-4 months old), middle ages (9-10 months old) and old ages (18, 21,

22, 23 months old) (Brewer and Torricelli, 2007). Briefly, hippocampus of each hemisphere was sliced at 0.5 mm and combined in Hibernate A (BrainBits LLC, Springfield, IL), 2% B27 supplement (Invitrogen), and 0.5 mM Glutamax (Invitrogen) for 8 min at 30° C. The slices were transferred and digested with 2 mg/mL papain (Worthington) in Hibernate without B27 for 25 min at 30° C. After trituration, neurons were separated from debris and microglia on an Optiprep (Sigma-Aldrich) density gradient. The neuron-enriched fraction was collected and viable neurons counted by exclusion of trypan blue. Neurons were plated at 50,000 cells/cm^2 on 15 mm glass coverslips (Assistent; Brand, Carolina Biologicals). Slip were precoated overnight with poly-D-lysine, 100 µg/mL in 18 MΩ deionized water. Neurons were cultured in NbActiv1 (BrainBits) with 5 ng/mL mouse FGF2 and 5 ng/mL mouse PDGFbb (Invitrogen) for trophic support for 9-12 days at 37°C in 5% CO_2, 9% O_2 at saturated humidity. Viability in our neuronal cultures was similar to previous studies of neurons from young, middle and old ages of both genotypes (Ghosh et al., 2012). The neuronal densities of all ages and genotypes in culture were similar without fragmented axons or dendrites. Further, the strong TMRE intensity of mitochondria indicated negative membrane potentials, without perinuclear fragmentation for no obvious age- or AD- related differences or qualitative changes in number of stained mitochondria per neuron. Furthermore, in follow-up experiments, the intracellular NADH levels of old neurons of both genotypes were remarkably responsive to an external imposed reductive and oxidative stress in cultures (Dong and Brewer, in revision).

TMRE Staining of Mitochondria

To label mitochondria with minimal interference in their membrane potential (Ward et al., 2000), tetramethylrhodamine ethyl ester (TMRE; Molecular Probes) stock solution was made in DMSO at 5 mM. After series dilutions with culture medium (NbActiv1), neurons were incubated with 10 nM TMRE in NbActiv1 for 20 min under 5% CO_2 at 37°C. After incubation, the coverslip was rinsed twice gently with warm NbActiv1. The cell slip was mounted in a slip-holder (Warner Instruments). Experiments were conducted on at least three coverslips from independent cultures with 10-20 neurons for young, middle and old ages.

FLIM Imaging

Fluorescence lifetime images were acquired on a Zeiss LSM 710 microscope (Carl Zeiss, Jena, Germany) using a 63x oil immersion objective, 1.2 N.A. (Carl Zeiss, Oberkochen, Germany). The environment was controlled at 5% CO_2 and 37°C at saturated humidity while collecting FLIM images. The 2-Photon excitation Titanium:Sapphire MaiTai laser (Spectra-Physics, Mountain View, CA) was modelocked at 740 nm generating ~120 fs pulses with a repetition rate of 80 MHz. Image scan speed was 25.21 µs/pixel and images were collected at 256 x 256 pixels. The emission from the excited native NADH in the cultured neurons was filtered with a bandpass at 460/80 nm. FLIM data was acquired using SimFCS32/64 FLIMBox (ISS, Champaign, IL). FLIM lifetime calibration of the system used a Coumarin 6 solution (at 100 µM) with a known lifetime as 2.5 ns. One hundred counts per pixel were collected for one FLIM image of the same field of view.

FLIM Phasor Data Analysis

As described previously (Stringari et al., 2012; 2015), every pixel of the FLIM image is transformed in one pixel in a phasor plot by performing a Fast Fourier Transform (FFT) of the intensity decay I(t). The coordinates g and s in the phasor plot are the real and imaginary part of the FFT as follows (Stringari et al., 2015):

$$g_{i,j}(\omega) = \frac{\int_0^t I_{i,j}(t)cos(\omega t)dt}{\int_0^t I_{i,j}(t)dt}$$

$$s_{i,j}(\omega) = \frac{\int_0^t I_{i,j}(t)sin(\omega t)dt}{\int_0^t I_{i,j}(t)dt}$$

Where the intensity signal (I) at indices *i* and *j* identify a pixel of the image and ω frequency ($\omega=2\pi f$), with f the laser repetition rate (80 MHz) and t is the period of the laser, 12.5 ns. Based on the linearity of the phasor coordinates, the g and s position of each pixel represents the fraction of free to bound NADH in the image (Stringari et al., 2015).

We examined regions of interest (ROI) for mitochondrial, cytoplasmic and nuclear subcellular compartments segmentation using circles. We conducted measurements of g, s, and NADH bound fraction from five ROIs on each compartment of each neuron. We then calculated the average of five ROIs in each compartment per cell and further averaged the values of g, s and bound fraction of 10 neurons from each mouse (n=20

neurons/age/genotype for female and n=10 neurons/age/genotype for male). Free NADH fraction was given by one minus the bound NADH fraction.

Free NADH Calibration

β-Nicotinamide adenine dinucleotide (NADH, Sigma-Aldrich, Inc) was prepared fresh at 450 μM in a 0.2 mM Tris-HCl buffer, pH 7.5 and stored at 4°C for use. As the free NADH solution gradually oxidizes in air, the absolute concentration of the prepared free NADH solution for calibration was determined in a NanoDrop 2000 UV-Vis Spectrophotometer (Thermo Fisher Scientific Inc). After blanking with 100 mM Tris-HCl pH 7.4, the absorbance of the free NADH was measured at 340 nm wavelength. Calculated the actual free NADH concentration for calibration based on the Beer-Lambert law: $\boldsymbol{A = \varepsilon bc}$ **,** where ***A*** is the readout absorbance value from nanodrop; ε is the extinction coefficient of NADH (6.22 at 340 nm); **b** is the length of light path (1 mm for NanoDrop) and **c** refers to concentration of NADH in the solution. Each time after imaging neurons, with the laser power and exposure parameters unchanged, we loaded the free NADH solution in the microscope system for absolute free NADH calibration measurements.

Measurements of Absolute NADH Concentrations in Mitochondria (Ma et al., 2016)

Before calibration with free NADH for absolute NADH quantification, we calibrated the instrument response function with a known standard,100 μM Coumarin 6 with lifetime at 2.5 ns. In the phasor plot, the pure free NADH lifetime is short of 0.4 ns (green cursor in **Fig. 2.1**). Whereas, the NADH bound to LDH (lactate dehydrogenase) has a longer lifetime of 3.4 ns (red cursor in **Fig. 2.1**). The lifetime distribution of the NADH signal from

the cells represents the fractional combination of free and bound NADH along the line between the pure free NADH and bound NADH (green line in **Fig. 2.1**). To measure the total NADH in the neurons, we first acquired a FLIM image of a known concentration of free NADH calibrated using the absorbance spectrophotometer. We then corrected for the difference between a lower quantum yield of the free and higher quantum yield of the bound form of NADH as described by Ma et al. (2016). To determine the mitochondrial free NADH concentration, we multiplied the measured total NADH by the corresponding free NADH fraction in mitochondria. Masks of mitochondrial, nuclear and cytoplasmic regions were made individually.

Statistics

Data are presented as means and S.E. One-way or Two-way ANOVA was used to assess the difference of means and variances in Excel. The number of replicates is indicated in the legends. The level of significance was set at $p < 0.05$ to reject the null hypothesis. Multiple comparison ANOVAs were analyzed by ProStat software (Poly Software, Pearl River, NY) using Fisher's LSD method.

2.4 Results

2.4.1 Distribution of Free and Bound NADH in Neuronal Mitochondria, Cytoplasm and Nucleus

We isolated and cultured neurons in a uniform medium from mice at young, middle and old ages, removed from a complicated aging context *in vivo* including age-related inflammation, hormones and vasculature. Prior studies showed no significant age-related

differences in neuronal viability (Patel et al., 2003; Ghosh et al., 2012), basal respiration, complex I activity with excess substrate (Jones and Brewer, 2010), resting ATP levels (Parihar et al., 2008) or mitochondrial number per cell (Ghosh et al., 2012), but significant age-associated oxidative shifts of steady state NADH/FAD redox ratio after middle age (Ghosh et al., 2012). Better than steady state fluorescence measures of NADH, two-photon lifetime imaging of NADH discriminates between free and bound NADH portions of the total NADH as well as neuronal subcellular distributions in live cells. Mitochondria were localized within neurons by fluorescent staining with tetramethyl rhodamine ethyl ester (TMRE), which partitions into mitochondria by their negative membrane potential (**Fig. 2.1a, f;** Ward et al., 2000). In the same field of view, we investigated the distribution of intrinsic NADH of individual neurons by two-photon fluorescence lifetime imaging microscopy (FLIM) (**Fig. 2.1b, g**), which show the distribution of two-photon intensities within neuronal sub-regions segregated into mitochondria (red circle ROIs), nuclei with their central circular appearance (yellow circles) and elsewhere in regions lacking mitochondria as cytoplasmic compartments (pink circles). Each pixel in the FLIM intensity image was transformed into phasor space by a Fast Fourier Transform (FFT) to determine the distribution of bound and free forms of NADH within each compartment of middle age neurons from NTg (**Fig. 2.1c-e)** and 3xTg-AD mice **(Fig. 2.1h-j)** (Stringari et al., 2015). The real and the imaginary parts of the FFT transformation are represented as G and S coordinates in the phasor plots. Each compartmental NADH cluster presented in the phasor plot (**Fig. 2.1 c-e, h-j**) is composed of a combination of free and bound NADH with lifetimes of 0.4 ns (green circle in the phasor plot) and 3.4 ns (red circle) respectively (Datta et al., 2015). Cellular pixels are distributed along the line joining the pure free and

protein-bound NADH (green line). The free/bound NADH ratio serves as an indicator of NADH redox state. A lower free/bound NADH fraction indicates a more oxidized NADH state and a higher free/bound NADH ratio implies a more reduced NADH redox state. Mitochondria distributed closest to the free NADH lifetimes (green cursor) compared to nuclei and cytoplasm, indicating the highest free/bound NADH ratio, highest free NADH fraction and more reductive NADH redox state in the mitochondria. Conversely, the cytoplasm showed the highest fraction of bound NADH with less free NADH, consistent with a more oxidized redox state. A smaller genotype effect was suggested by a small shift toward more bound NADH (red circle) in 3xTg-AD age-matched neurons for each compartment as indicated by the vertical yellow lines, centered on the NTg mitochondria at G= 0.71 (**Fig. 2.1**).

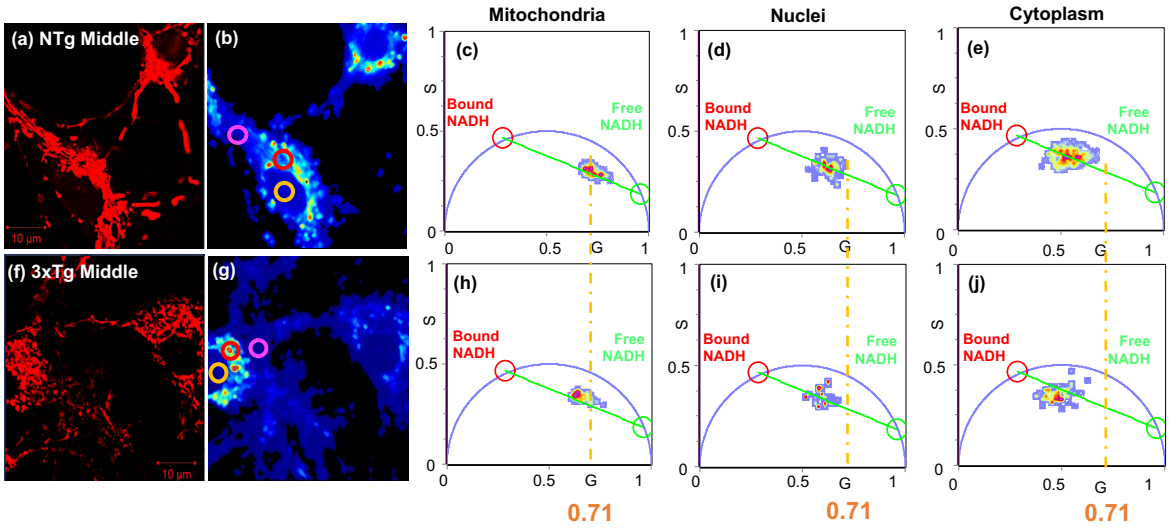

Figure 2.1. Highest free NADH fraction in mitochondria compared to nuclei and cytoplasm in each genotype. AD genotype shows lower free NADH fraction than the corresponding compartment levels of NTg neurons. (a, f) TMRE stain for mitochondrial localization of neurons from **(a)** NTg and **(f)** 3xTg-AD 9-month (middle- age) female mouse. **(b, g)** NADH-FLIM intensity images of the corresponding neurons. To determine the proportion of free and bound NADH in each compartment, ROIs were chosen relative to the TMRE image for analysis on mitochondrial (red circle), nuclear (yellow) and cytoplasmic (pink) compartments. **(c-e, h-j)** Phasor plots present compartment-specific differences in the ratios of free to bound NADH redox states from the corresponding NTg and 3xTg middle age neurons. Pure, free NADH with lifetime of 0.4 ns is shown by green circle and bound NADH with lifetime of 3.4 ns with a red circle on the semicircle. All the NADH compartmental clusters fall along the lines between pure free NADH (green cursor) and protein-bound NADH (red cursor). The vertical orange lines are centered on the NTg young mitochondrial distribution for reference at G=0.71.

2.4.2 Age- and Ad- Related Oxidative Shifts from Free to More Bound NADH

With aging, NADH regenerating capacity declines (Ghosh et al., 2012) which could promote oxidative and energetic shifts. *In vivo*, NADH exists as either bound to enzymes or free in solution. The free/bound NADH ratio is altered by the cellular redox, metabolic and energetic states. Normally, the free NADH levels maintain balanced between the activity of glycolysis for producing more free NADH and more reliance on oxidative phosphorylation (OXPHOS) for consuming free NADH (Yu and Heikal, 2009). To determine whether aging or the 3xTg-AD genotype affects the NADH redox states, we compared free/bound NADH ratios from different age neurons of both genotypes (**Fig. 2.2**). To illustrate the distribution of free/bound NADH in FLIM images of neurons, we present NADH color maps of neurons with different ages for NTg (**Fig. 2.2 a-c**) and 3xTg-AD mouse neurons (**Fig. 2.2 e-g**) respectively. In these color maps, cyan-green color reflects more free NADH and pink-purple color indicates more bound NADH. With aging, in both NTg (**Fig. 2 a-c**) and 3xTg-AD (**Fig. 2 e-g**) neurons, the higher cyan-green free NADH shifted toward more pink-purple bound NADH, indicating depletion of free NADH and shift toward a more oxidized NADH redox state with age. Furthermore, 3xTg-AD neurons presented comparatively a more pink-purple bound NADH distribution than the age-matched NTg neurons, meaning an even lower free NADH in 3xTg-AD neurons. The free/bound NADH distribution of whole neurons at ages of young, middle and old were quantitatively transformed into one phasor plot for NTg (**Fig. 2.2d**) and 3xTg-AD neurons (**Fig. 2.2h**). In genotypes, age drives substantial shifts from free to more bound NADH along the free-bound trajectory. The cluster of young age neuron presents much closer to the free NADH form (green cursor) whereas the cluster of old age neuron displays a

shift toward bound NADH (red cursor). This indicates that young age neurons contained the highest free NADH fractions and old aged neurons contained the most bound NADH with depletion in free NADH. Compared to the clusters of NTg neurons (**Fig. 2.2d**), those of the age-matched 3xTg-AD neurons were shifted toward more bound NADH, implying the AD genotype accelerated the age-related shifts toward more bound NADH and depletion of free NADH.

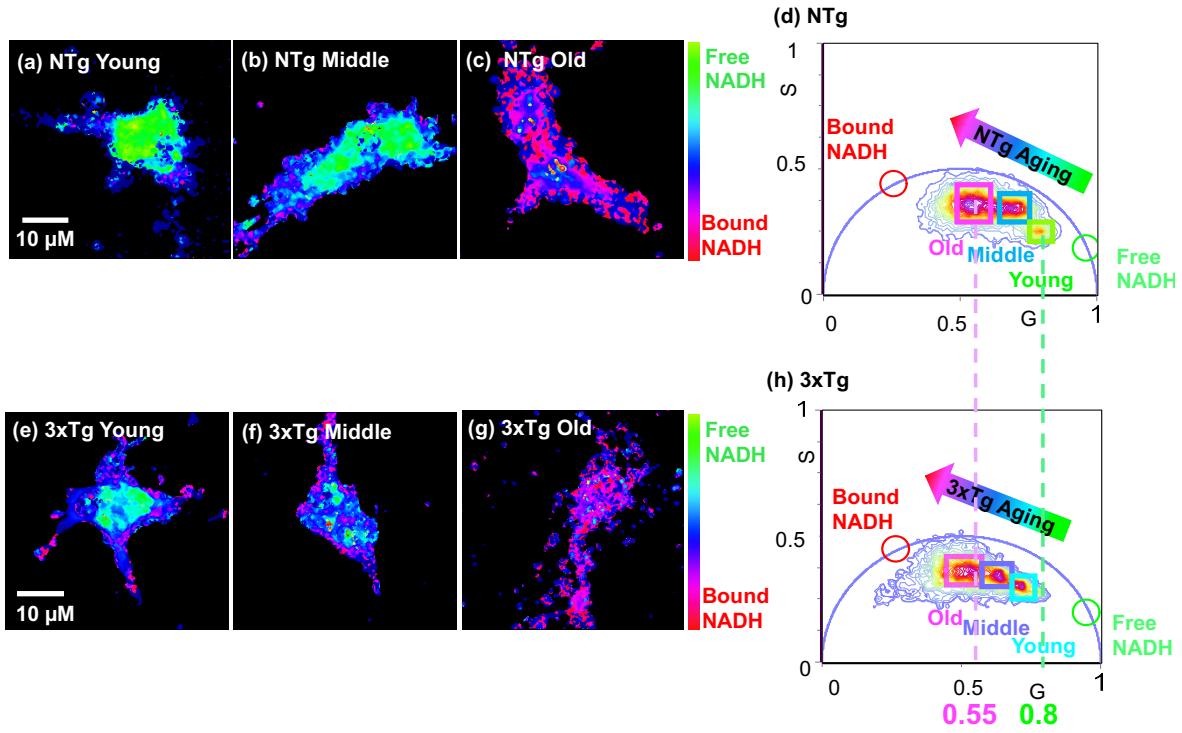

Figure 2.2. Aging promotes shifts toward more bound and less free NADH in NTg and 3xTg-AD neurons. FLIM color maps of young, middle and old age neurons from NTg **(a-c)** and 3xTg-AD **(e-g)** mice illustrate a dramatically age-dependent depletion in free NADH level of both genotypes shown as the color shifts from more green-cyan (free NADH) to more pink-purple (bound NADH) with aging. Comparatively, the 3xTg-AD neurons present more bound NADH than the age-matched NTg neurons seen as a more pink-purple color in the age-matched 3xTg-AD neuron. **(d, h)** Phasor plots show the shift in distribution from free to bound NADH in neurons from young, middle and old age neurons of NTg and 3xTg-AD brains, respectively**.** Each cluster that falls along the free-bound NADH trajectory (line between free and bound NADH) represents the combination of free and bound NADH from the corresponding single neuron in the colormap.

2.4.3 Mitochondria Show the Most Reduced State with Highest Free NADH Fraction among Subcellular Compartments

To statistically validate these results, we selected five regions of interest for each compartment of 10-20 neurons in separate cultures of each age and genotype and sex. We expected compartmental differences in neurons because compartments of HeLa cells measured by thiol/disulfide redox states showed that mitochondria were the most reduced followed by nuclei and cytoplasm, which was comparatively the most oxidized (Hansen et al., 2006). In addition, as the distribution of NADH is highly compartmentalized (Xiao et al., 2018), we further investigated how the free/bound NADH ratios change in mitochondria, cytoplasm and nuclei with aging of both NTg and 3xTg-AD neurons.

Age Effect

Aging strongly drove a decline in the free NADH fractions in all subcellular compartments, $p< 0.001$, in both genotypes and both genders. In male NTg mouse neurons (**Fig. 2.3a**), from young to old age, mitochondrial free NADH fractions declined 23%, nuclear free NADH fractions decreased 12% and cytoplasmic free NADH levels dropped 23%. Similarly, in female neurons (**Fig. 2.3b**), aging drove least decline in nuclear free NADH fractions of NTg female neurons with only 18%, but a 26% drop in mitochondrial free NADH fraction (**Fig. 2.3b)**. In male and female 3xTg-AD neurons, the slopes of age-associated declines in free NADH fractions present similar changes in percentages to that of gender-matched NTg neurons in each compartment, but further drops in the AD-genotype neurons in response to aging. The age-related depletion of free NADH levels in all compartments suggests an impaired capacity for free NADH regeneration and lower

capacity for energetic supplement in old aged neurons of both NTg and 3xTg-AD mouse brains. With aging, the nuclear compartment declined the least compared to that of mitochondria and cytoplasm in both NTg and 3xTg-AD of both genders, indicating a better buffering capacity and protective mechanism in nuclei against age-related oxidative shifts and depletion in free NADH levels.

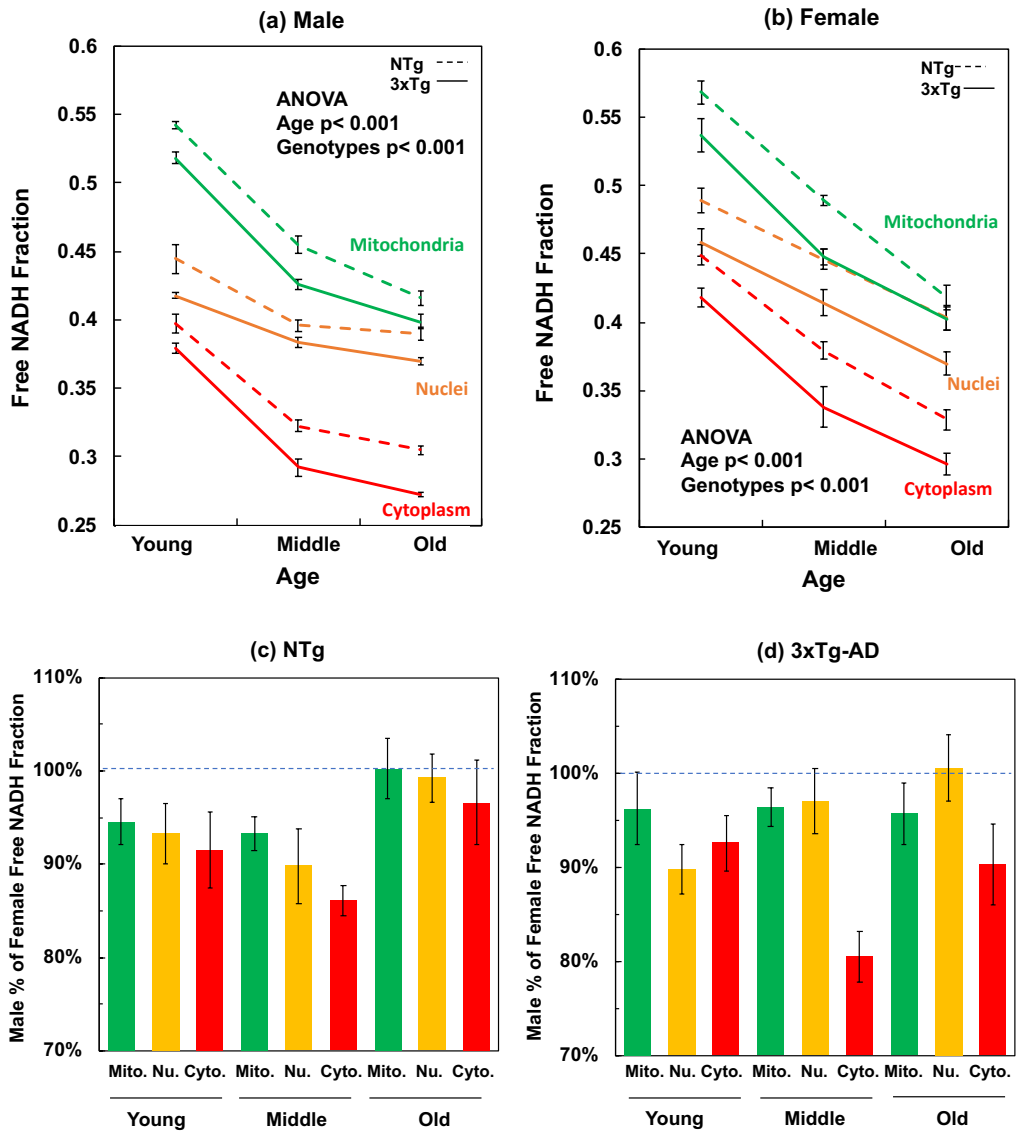

Figure 2.3. Mitochondrial, nuclear and cytoplasmic free NADH fractions decline with age are further depleted with AD-genotype of both (a) male and (b) female mouse neurons. For the compartment effect, mitochondria were the most reduced with the highest free NADH fractions and cytoplasm presents the most oxidized NADH state with the lowest free NADH levels (ANOVA for the compartment-differences, in male, NTg $F(2, 89)= 397$, $p< 0.001$, 3xTg-AD $F(2, 89)= 927$, $p< 0.001$; in female, NTg $F(2, 179)=154$, $p< 0.001$, 3xTg-AD $F(2, 179)=106$, $p< 0.001$). Aging depleted free NADH levels in all compartments of both genotypes. ANOVA for male, mitochondria $F(2, 59)= 338$, $p< 0.001$, nuclei $F(2, 59)= 56$, $p< 0.001$, cytoplasm $F(2, 59)= 262$, $p< 0.001$; For female, mitochondria $F(2,119)= 161$, $p< 0.001$, nuclei $F(2, 119)= 51$, $p< 0.001$, cytoplasm $F(2, 119)= 96$, $p< 0.001$). The 3xTg-AD genotype demonstrated significantly more bound NADH and more oxidized NADH redox state than the age-matched NTg neurons in each compartment. By gender **(Fig. 3c, d),** male neurons were lower in free NADH fraction than the female neurons at young and middle ages, but the multiple comparison results indicated no significant differences in old ages between female and male neurons. Two way ANOVA for gender effect on compartments, mitochondria $F(1, 59)= 13$, $p< 0.001$; nuclei $F(1, 59)= 13$, $p< 0.001$; cytoplasm $F(1, 59)= 25$, $p< 0.001$) In 3xTg-AD neurons, male NADH fraction was lower than that in female neuron of each compartment (mitochondria $F(1, 59)= 7$, $p< 0.01$; nuclei $F(1, 59)= 8$, $p< 0.01$; cytoplasm $F(1, 59)= 51$, $p< 0.001$) and each age (young $F(1, 59)=18$, $p< 0.001$; middle $F(1, 59)=26$, $p< 0.001$; old $F(1, 59)= 8$, $p< 0.01$).

Compartment Effects

Fig. 2.3a and 2.3b show that mitochondria have the highest free NADH fraction while cytoplasm displayed the lowest free NADH among the three subcellular compartments (ANOVA for compartment effect, in male, both NTg and 3xTg-AD $p < 0.001$; For female, NTg and 3xTg-AD $p < 0.001$). In NTg male young neurons (**Fig. 2.3a**), free NADH fraction in mitochondria was 37% higher than the levels in cytoplasm. This difference reached a maximum of 41% higher in the middle age followed by a 36% higher in mitochondrial free NADH in old aged neurons. 3xTg-AD male young neurons presented the same 37% higher in mitochondrial free NADH fraction compared to that of cytoplasm, with further increases in the mitochondria-cytoplasm differences to 46% in middle and old ages. Similar magnitude changes in free NADH with age and genotype were seen in female neurons (**Fig. 2.3b**). The relative order of compartmental free to bound NADH redox states was independent of age and genotype. Overall, the largest changes in free NADH were associated with age, then compartment, genotype and gender. The highest free NADH fraction in mitochondria suggests that mitochondria have the highest capacity for free NADH production compared to nuclei and cytoplasm.

Genotype Effect

As illustrated in **Fig. 2.3a** and **2.3b**, the age-matched 3xTg-AD neurons present consistently lower free NADH levels compared to the free NADH levels of NTg neurons in each compartment of each gender. The cytoplasm responded most to the genetic loads of 3xTg-AD, ranging from 6% at young age to 12% at old age lower in free NADH levels of both male and female (young, $p < 0.05$; old $p < 0.01$). Under the genetic loads of 3xTg-

AD, free NADH levels in mitochondria and nuclei were 5%-10% lower than the age-matched NTg neurons from young to old ages of each gender ($p < 0.001$). The comparatively lower free NADH levels in 3xTg-AD neurons than that of the age- and gender- matched NTg neurons suggests an AD genotype-driven decline in capacity of free NADH regeneration of 3xTg-AD mouse brains. We infer that the genetic load of 3xTg-AD promoted age-related oxidative shifts to more bound NADH redox states by either consuming more free NADH or impairing the capacity for free NADH production.

2.4.4 Male Free/Bound NADH Fraction Slightly Less than that of Female Neurons

To gain insights into gender differences in free NADH depletion during aging in the NTg and 3xTg-AD mouse model, we compared the free NADH fractions in male and female neurons of mitochondria, nucleus and cytoplasm as a function of age and genotype. To more easily compare gender effects, the same data was expressed as male percent of female free NADH (**Fig. 2.3c, d**). Male neurons displayed less reducing free NADH states compared to the age-matched female neurons in these compartments (**Fig. 2.3c, d**), but these gender differences in free NADH diminished in old age. The average free NADH levels of male neurons was significantly 7% lower than that in female, across all ages and compartments of both genotypes ($p < 0.01$). Multiple comparison analysis demonstrated gender differences in the young and middle age of all compartments, but no significant gender differences at old ages. This suggests that higher reductive capacity in females than males is gradually lost in old age.

2.4.5 Mitochondrial Free NADH Concentrations Decline with Age and AD-genotype in Hippocampal Neurons

A variety of approaches have been reported for measurement of NAD(P)H concentrations (Sporty et al., 2008; Zhu et al., 2015; Coremans et al., 1997; Yu and Heikal, 2009; Ghosh et al., 2012). Neither HPLC or steady state fluorescence measures distinguish the bound form with a higher quantum yield from the free form (Ma et al., 2016; Ghosh et al., 2012). However, absolute measurement of concentration of both the free and bound NADH *in situ* is possible by a FLIM phasor method (Ma et al., 2016). We determined the absolute free NADH concentrations in live neurons from young and old age mouse hippocampal neurons specifically in mitochondria (**Fig. 2.4**). In NTg female neurons from young to old ages, mitochondrial free NADH concentrations declined 43% from 442 to 250 μM (**Fig. 2.4**). In 3xTg-AD neurons, age drove a roughly 50% loss in mitochondrial free NADH levels from 410 down to 207 μM. In addition, comparison of genotype effects indicated 8% less free NADH in the young ($p < 0.05$) and 21% in the old ($p < 0.001$). With a lower NAD total pool size in aging and AD, the declines in free/bound NADH fraction with age result from larger declines in free NADH concentration. In our results, we observed 43-50% age-related declines in concentrations of mitochondrial free NADH, which were much larger than the 23%-26% declines in free NADH fractions. Thus, the concentration of mitochondrial free NADH was depleted 2-fold more with aging in the 3xTg-AD than the NTg neurons. These results suggest both an age- and AD-related decrease in capacity for NADH regeneration or increase in consumption of NADH.

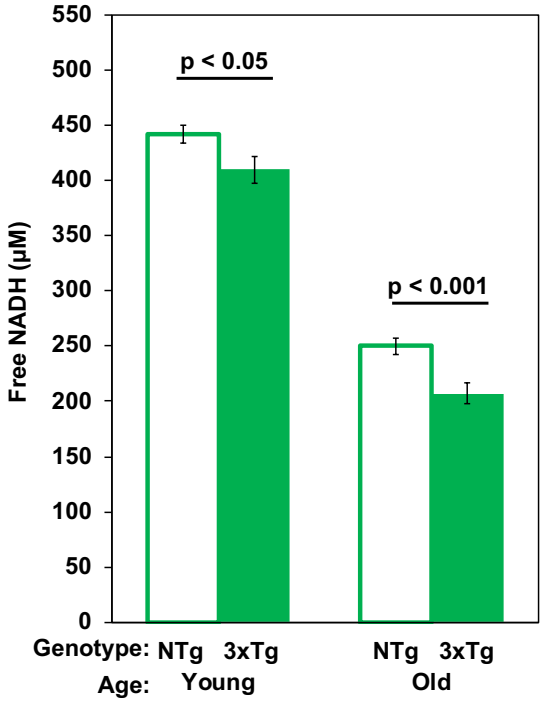

Figure 2.4. Free NADH concentrations decline from young to old mitochondria *in situ* exacerbated by the 3xTg-AD genotype. Two way ANOVA shows age effects $F(1, 63)= 466$, $p<0.001$ and for genotype effects $F(1, 63)= 16$, $p<0.001$ (n=16 neurons/age/genotype).

2.5 Discussion

2.5.1 Age- and AD- Dependent Decline in Free NADH

Free NADH serves as a vital redox-energy intermediate, produced from NAD^+ in glycolysis, the TCA cycle and transhydrogenase. Energy generation at complex I of oxidative phosphorylation in neurons requires at least three elements: sufficient levels of complex I protein, favorable regulation of this complex and sufficient free NADH substrate. The three-minute lability of NADH (Chance and Thorell, 1959) likely precludes its measurement in human surgical samples or postmortem. Our previous work in cultured rat neurons reported here suggested that NADH substrate was at least part of the age-related limitation (Jones and Brewer, 2010). Here, we examined the free NADH levels as a function of age and AD-like genotype. With aging, we found a 43% loss of free NADH concentration at rest, which was diminished further to 50% under the load of the transgenes in the 3xTg-AD neurons. These numbers are larger than the steady state fluorescence declines with aging (Ghosh et al., 2012) in the same neuron preparations because free NADH gets oxidized when exposed in air during tissue extraction. The lower NADH concentrations with age are consistent with an age-dependent lower capacity of NADH regeneration in the same live neuron preparations (Ghosh et al., 2012) or increased NADH consumption. In 3xTg-AD mouse brain mitochondria with age, the activity of cytochrome *c* oxidase (COX) decreased by 51% and PDH by 55%, which exceeded the 31% age-driven declines in NTg mitochondria (Yao et al., 2009). These assays are performed with excess substrate. Therefore, a lower NAD pool could further slow these activities. Judged by steady-state fluorescence, neuronal NAD(P)H concentration peaks in middle age compared to young and old age neurons (Ghosh et

al., 2012). Similar to mouse brains, human postmortem AD brains exhibited 27%-57% declines in PDHC, ICDH and KGDHC activities relative to age-matched controls (Bubber et al., 2005). As these enzymes produce NADH in the TCA cycle, AD-related declines in these dehydrogenases would lead to lower free NADH production in mitochondria, in line with our findings of lower free NADH with age and further decreased with AD genetic load.

There can be concerns for how well primary cultures from aged brains represent the aging brain with age-related changes in hormones, inflammatory mediators and the vasculature. Many fundamental properties of brain neurons are maintained in culture such as dendrite and axon regeneration (Brewer, 1997), synapse formation (Brewer et al., 2009), action potential firing (Evans et al., 1998), NMDA receptor modulation (Cady et al., 2001) and response to redox shifts (Ghosh and Brewer, 2014a). Although a lower NAD pool can be measured in old brain homogenates (Gomes et al. 2013), the lability of NADH makes *in vivo* measurements difficult. *In vivo* circadian oscillation of NADH have been detected in stem cells within the epidermal basal layer of mice by two-photon excitation (Stringari et al., 2015). A controlling influence of NAD^+ levels on behavior was demonstrated in mice without the NAD-hydrolase CD38 (Sahar et al., 2011). As NADH needs to be measured noninvasively, studies on neuron cultures will be useful in attempts to remedy age and AD-related deficits in free NADH.

The age-related declines in NADH could be caused by age-associated sedentary behavior (Figueiredo et al., 2009; Lee Y et al., 2015; Stolle et al., 2018) that sets

epigenetic controls for metabolic changes (Walker et al., 2013; Intlekofer et al., 2013). Metabolic expression of enzymes of the TCA cycle and ETC that could impede NADH regeneration and ATP production need to be measured in activity-controlled studies of aging and AD. This type of study in aging mouse skeletal muscle showed a decline in respiratory activity with aged sedentary behavior (Figueiredo et al., 2009). A review of rat cardiac energy function highlighted decreased mitochondrial energetics with age (Yaniv et al., 2013). As compensatory effects, pathways may re-direct fluxes to replenish the decreasing NADH levels. The NNT reverses the direction of reaction to generate more NADH at the cost of NADPH. This begins a vicious cycle because NADPH is needed to regenerate GSH as the major redox buffer, when GSH levels are decreased by age-associated oxidative stress (Ghosh et al., 2014b). Age- and AD-related oxidative shifts stimulate up-regulation of glycolytic pathway to feed the NADH and energetic demand. Alternatively, to maintain redox balance within a viable range, NADH needs to be recycled via either lactate dehydrogenase (with associated acidosis) or the electron transport chain (with minimal oxyradicals) or plasma membrane NAD(P)H oxidoreductase (NOX, with one oxyradical per NADH) (Brewer, 2010; Aon et al., 2010). Moreover, rat neurons are more susceptible to stressors with aging (Brewer et al., 1998) and old mouse neurons are more vulnerable than young neurons to limits on NADH resynthesis and GSH depletion (Ghosh et al., 2014b). An upstream possible cause is the age-related 50% decline in the total NAD(P)H pool of whole 3xTg-AD neurons compared to 27% decrease in age-matched NTg neurons (Ghosh et al., 2012). The mitochondrial free NADH concentrations of NTg old neurons surpassed those of 3xTg-AD old neurons by 21%, further indicating

an even lower capacity to maintain free NADH levels with genetic load in 3xTg-AD old mouse brains.

2.5.2 NAD Pool Size Diminished with Aging and AD

Under normal physiology, the concentrations of NADH and NAD^+ are balanced by the NAD-synthesizing and NAD-consuming enzymes. In aging and AD, evidence suggests that consumption exceeds recycling and synthetic capabilities. NAD^+ levels are maintained via three biosynthetic pathways: the Preiss-Handler, de novo biosynthesis and salvage pathways (Verdin et al., 2015). Age- and AD-related changes in consumption and resynthesis of NAD^+ diminish the levels of free NADH (Prolla et al., 2014), which could further lead to a decrease in capacity for ATP synthesis. Either the age- and AD-related oxidative shift or the energy crisis with demand is insufficient to cause many downstream dysfunctions including amyloid and tau processing, LTP, calcium handling (Green and LaFerla, 2008), mitochondrial function and motility (Gibson and Blass, 1976; Calkins et al., 2011), DNA repair (Imam et al., 2006) and autophagy (Nixon, 2013).

With aging, the activity of NAD-biosynthesis decreases while the activities of NAD^+-consuming enzymes increase such as CD38 (Camacho-Pereira et al., 2016) and PARP (Bai and Canto, 2012) which together contribute to the age-associated decline in NAD pool size. PARP inhibitors together with NAD+ precursors boost ATP levels and increased gene expression of enzymes in TCA cycle and glycolysis, such as citrate synthase and hexokinase (Mouchiroud et al., 2013). Supplementation of the NAD^+ precursor, nicotinamide riboside improves learning and memory in AD/Polβ mouse model of

mitochondrial DNA damage (Hou et al., 2018). Mounting evidence supports the beneficial effects of nicotinamide (NAM) to ameliorate cognitive decline in AD mouse models associated with declines in Sirt3 activity (Green et al., 2008; Liu et al., 2013). Gomes et al. (2013) reported the reversibility of mitochondrial dysfunction in skeletal muscle of old mice by raising NAD^+ levels via the SIRT-1-HIF-1α-c-Myc pathway. Ghosh 2012 showed that neurons pretreated with nicotinamide reverse NAD(P)H levels and NADH regenerating capacity of both NTg and 3xTg-AD neurons (Ghosh et al., 2012). Nicotinamide pre-treatment improved recovery of hippocampal neuronal function, enhanced NADH reduction and ATP content in an acute model of hypoxia in rat (Shetty et al., 2014).

Tau protein is critical to stabilize microtubules of axons. Overexpression of tau in P301L tau mice alters the distribution of organelles including mitochondria that are dependent on microtubule motor proteins for transport and decrease the distribution of mitochondria in synapses of neurons (Rhein and Eckert, 2007). Furthermore, in P301L tau mice together with reduced NADH-ubiquinone oxidoreductase activity with age were found to impair mitochondrial respiration and ATP synthesis (Rhein and Eckert, 2007; David et al., 2005). Our results of decreased free NADH levels with age could impair energetic capacity to remove amyloid and tau through autophagy (Brewer 2010; Barnett 2011; Brewer submitted 2019).

2.5.3 Age-Related Oxidized Shifts in NADH/NAD^+ in Subcellular Compartments

The subcellular distribution of NADH and their signaling pathways are highly compartmentalized and function somewhat independently (Koch-Nolte et al., 2011). In our study with aging, free NADH shifted toward more bound and less free NADH in both NTg and 3xTg-AD mouse neurons. Of note, all ages of 3xTg-AD neurons display comparatively more oxidized redox state with less free NADH than the age-matched NTg neurons, indicating a further impaired in capacity of free NADH regeneration. The genetic load of 3xTg-AD neurons promoted age-related depletion in free NADH levels and oxidative shifts in NADH redox states starting as early as in young age. The NADH/NAD^+ redox states also mediates crosstalk of signaling between neurons and astrocytes in brain (Winkler and Hirrlinger, 2015). Both NADH and NAD^+ levels drop remarkably with aging and AD. However, growing evidence demonstrates the age- and AD- induced oxidative shifts in NADH/NAD^+ redox states (Zhu et al., 2015; Parihar et al., 2008; Ghosh et al., 2012). An important issue is whether redox state controls ROS production or ROS levels influence redox state. Based on more neurodegeneration from titrated inhibition of NADH production than GSH synthesis, we concluded that NADH redox state is upstream of ROS generation (Ghosh et al., 2014).

We found nuclear free NADH to be less affected by age than cytoplasmic or mitochondrial NADH. Cytoplasmic and nuclear NAD^+ pools can communicate by diffusion via the nuclear pore (Verdin, 2015). Given the important role of NADH shuttles in the communication between compartments, Easlon et al. (2008) reported beneficial effects on extending lifespan in yeast by overexpression of the functional component of the

NADH malate-aspartate shuttle and glycerldehyde-3-phosphate shuttle in the calorie restriction (CR) pathway. In addition to comparatively lower consumption of NADH in the nucleus, the nuclear-localization of NMNAT1, with its lower Km and higher Vmax than mitochondrial NMNAT3 (Berger et al., 2005) could be sufficient to regenerate NAD^+ consumed by Sirt1 and PARPs. Control of many redox-sensitive transcription factors (Lavrovsky et al., 2000) could buffer or exacerbate age-related changes in free NADH and the NAD pool. We found mitochondrial free NADH to be the most affected by age. The mitochondrial membrane is impermeable to both NAD^+ and NADH. Normal ratios of NADH/NAD^+ are maintained by the malate-aspartate and glutamate-aspartate shuttles and transhydrogenase. NAD^+ precursors such as nicotinamide and nicotinamide riboside can traverse the mitochondrial membrane (Pittelli et al., 2011) to be used for NADH/NAD^+ regeneration by nicotinamide phosphoribosyltransferase (NAMPT) and nicotinamide mononucleotide adenyl transferase (NMNAT) (Revollo et al., 2004) via the salvage pathway and transhydrogenase.

2.5.4 Redox States of NADH/NAD^+ Reflect Metabolic States of Neurons

The alterations of free/bound NADH provide insight on kinetic switches for modulation of metabolism based on NADH/NAD^+ redox states. We find in mouse hippocampal neurons across the age-span, both genotypes and both genders, that the NADH redox state is more reduced in mitochondria, than nuclei and that cytoplasm was the most oxidized. This order replicates the relative thiol redox states from most reducing to most oxidizing in Hela cells: mitochondria > nuclei > cytoplasm (Hansen et al., 2006). As the cytoplasmic and mitochondrial NADH/NAD^+ ratios are metabolic readouts (Christensen et al., 2014),

a shift from free to more bound NADH suggests a metabolic shift from glycolysis to more oxidative phosphorylation with more consumption of free NADH (Stringari et al., 2015). As we observed an age- and AD-related depletion of free NADH in mouse neurons, an oxidative shift in NADH/NAD^+ redox states predicts a downstream switch and re-direction in metabolic fluxes from higher TCA-dependent to higher reliance on glycolysis for energy supply and lactate generation for redox balance.

2.5.5 Relationship to Caloric Restriction (CR)

Caloric restriction (CR) and fasting can extend lifespan and increase NAD levels in the Alzheimer's mouse brain (Qin, 2006), rat or mouse liver (Yang et al., 2007; Nakagawa et al., 2009; Hayashida et al., 2010) and skeletal muscles (Canto et al., 2010) of animal models by inducing the expression of NAMPT in the salvage pathway. Protein restriction (PR), especially, methionine restriction was also found to extend lifespan (Schiff et al., 2011; López-Torres and Barja, 2008) and decrease mitochondrial reactive oxygen species (ROS) production in both brain and kidney mitochondria of rats (Caro et al., 2009) as well as free radical leak in rat mitochondria (Lopez-Torres and Barja, 2008). Paradoxically, the enzymatic activities needed by the brain for energy production, complex I and III are decreased in rat brain with MetR (Naudi et al., 2007). Martin et al. (2016) also found that CR decreased cytochrome c oxidase activity together with 40% increases in the levels of NAD(P)H in the molecular and polymorphic layers of the mouse dentate gyrus of the hippocampus. This CR paradox of lower activities of the electron transport chain so critical to brain energetics may be explained if CR forces higher turnover of leaky mitochondria so that higher efficiency is maintained (Yang et al., 2016).

CR mitochondria of higher efficiency could produce more energy with less consumption of NADH. Thus, CR could cause free NADH levels to rise above the age-related depletion that we observed. The overall effects can be described by antagonistic pleiotropy in which restriction results in higher autophagic quality control to maintain efficient function (Barnett and Brewer, 2011; Yang et al., 2016).

2.5.6 Gender-Differences in Age-Related Declines of Free NADH Levels

We found that levels of free NADH in male neurons were significantly lower than those of age- and genotype-matched female mouse brains, particularly in the cytoplasmic compartment. This protective effect of higher free NADH levels in female neurons appears to lessen with age, ending in similar free NADH levels in old neurons of female and male. This direction of lower male NADH levels follows the results of (Guevara et al., 2009) who found lower mitochondrial capacity of male brain mitochondria with lower respiratory capacity and lower antioxidant enzyme activities compared to that in aged female brains. Consistent with these studies, Grimm (2017) summarized a number of sex-specific changes with age in mitochondria, including mitochondrial dynamics and mitophagy (Guebel and Torres 2016), peroxide production (Borras et al., 2003), respiratory control rate, pyruvate dehydrogenase and cytochrome c oxidase (COX) activity (Yao et al., 2012). Many of these changes could be downstream of changes in the bioenergetics of NADH. However, in our studies with lower free NADH in males, sex-differences were smaller than the age- and genotype- effects. This protection seems to be lost after menopause in females or just older age in males (Borras et al. 2003; Brewer et al., 2006).

2.6 Conclusions

To our knowledge, this is the first time mitochondrial free NADH concentrations were measured in sub-compartments of live primary neurons using FLIM. The ability to distinguish free NADH from total NADH in live neurons across the age span from NTg and 3xTg-AD mice identified critical age-related deficits in energetic states of the neurons. Furthermore, imaging the intrinsic fluorescence of NADH in live neurons by two photon excitation avoids modifying or introducing any extra fluorophore probe or perturbation. Combined with subcellular analysis, we found an oxidative shift in free NADH levels in mitochondria, cytoplasm and nuclei of neurons as a function of age and AD-like genotype. The observed depletion of free NADH levels with age and AD-genotype suggests that less free NADH will be available for demand-critical energy supply to oxidative phosphorylation. The drop in free NADH could be caused by any combination of increased consumption by resting demand for ATP, decreased regeneration of NAD^+ by de novo and nicotinamide salvage pathways or relative metabolic changes, in glycolysis, lactate generation. Together with this work, our earlier work in rat neurons that found ATP levels unchanged with age but significantly lower NAD(P)H levels with age (Parihar et al., 2008), suggests that an age-associated oxidative shift in NADH redox state is upstream of the age-related metabolic shifts in rat and mouse brains. However, the consumption of NAD^+ by glycolysis or the TCA cycle for NADH demand at lower NAD pool sizes, together with increased lactate production may contribute to a lower redox ratio of NADH/NAD^+ (Brewer, 2010). Discrimination between excess consumption and regeneration in free NADH with age and genotype will require interventional studies (Dong & Brewer, in revision). Since free NADH is the substrate for numerous redox reactions as well as

energy generation, NADH target engagement and reversal of low free NADH levels could counter AD and extend lifespan via a series of NADH-sensor mechanisms involving oxidative stress, DNA repair and mitochondrial function.

2.7 Acknowledgements

This work was supported by the UC Irvine Foundation, NIH P41-GM103540 and a grant from the NIH RF1 AG058218. We appreciate Prof. Enrico Gratton for inspirational discussions and the help of Rachel Cinco-Hedde, Ning Ma and Sara Sameni at Laboratory for Fluorescence Dynamics, UC Irvine.

CHAPTER 3

REVERSIBILITY OF AGE-RELATED OXIDIZED FREE NADH REDOX STATES IN ALZHEIMER'S DISEASE NEURONS BY IMPOSED EXTERNAL CYS/CYSS REDOX SHIFTS (IN REVISION)

Yue Dong[1], Sara Sameni[1,2], Michelle A. Digman[1,2], Gregory J. Brewer[1,3]

[1]Department of Biomedical Engineering, University of California Irvine, Irvine, California, United States of America,

[2]Laboratory of Fluorescence Dynamics, Department of Biomedical Engineering, University of California Irvine, Irvine, California, United States of America,

[3]MIND Institute, Center for Neurobiology of Learning and Memory, University of California Irvine, Irvine, CA, United States of America

Keywords NADH • Aging brain • Alzheimer's disease • FLIM • Mitochondria • Redox States • Cys/CySS • Redox Manipulation

3.1 Abstract

Redox systems including extracellular cysteine/cystine (Cys/CySS), intracellular glutathione/oxidized glutathione (GSH/GSSG) and nicotinamide adenine dinucleotide reduced/oxidized forms (NADH/NAD^+) are critical for maintaining redox homeostasis. Aging as a major risk factor for Alzheimer's disease (AD) is associated with oxidative

shifts, decreases in anti-oxidant protection and dysfunction of mitochondria. Here, we examined the flexibility of mitochondrial-specific free NADH in live neurons from non-transgenic (NTg) or triple transgenic AD-like mice (3xTg-AD) of different ages under an imposed extracellular Cys/CySS oxidative or reductive condition. We used phasor fluorescence lifetime imaging microscopy (FLIM) to distinguish free and bound NADH in mitochondria, nuclei and cytoplasm. Under an external oxidative stress, a lower capacity for maintaining mitochondrial free NADH levels was found in old compared to young neurons and a further decline with genetic load. Remarkably, an imposed Cys/CySS reductive state rejuvenated the mitochondrial free NADH levels of old NTg neurons by 71% and old 3xTg-AD neurons by 89% to levels corresponding to the young neurons. Using FLIM as a non-invasive approach, we were able to measure the reversibility of subcellular free NADH levels in live neurons. Our results suggest a potential reductive treatment to reverse the loss of free NADH in old and Alzheimer's neurons.

3.2 Introduction

Neurons rely on redox couples to buffer oxidative and reductive stress using millimolar concentrations of extracellular Cysteine (Cys)/Cystine (CySS) and intracellular glutathione (GSH)/ glutathione disulfide (GSSG). Kinetically, intracellular glutathione is maintained by reduced nicotinamide adenine dinucleotide (NADH)/oxidized (NAD^+) and reduced nicotinamide adenine dinucleotide phosphate (NADPH)/oxidized ($NADP^+$). Each redox couple is compartmentalized and somewhat independent with distinct redox pools in the mitochondria, cytoplasm and nuclei (Circu and Aw, 2010; Koch-Nolte et al., 2011). Maintaining an independent mitochondrial GSH pool size is critical to preserve a reducing

environment for mitochondrial proteins against oxidative DNA damage (Chen et al., 2003). The crosstalk of reduced components between nuclear and other compartments has been demonstrated importantly in cell cycle progression (Markovic et al., 2007) and redox signaling (Sen, 1998; Ushio-Fukai, 2009). Additionally, the NADH/NAD+ redox states impact the regulation of gene expression (Winkler and Hirrlinger, 2015) by affecting the activity of transcription factors (Hirrlinger and Dringen, 2010) and cellular signaling (Ying, 2008). Thus, systematic studies of changes in the redox environment with aging could inform age-related bioenergetic aspects of neurodegeneration.

Age is the most important risk factor for Alzheimer's disease (AD). Aging promotes the oxidation of redox couples. In human plasma, aging is associated with the oxidation of the GSH/GSSG as well as the Cys/CySS redox state after middle-age (Jones, 2006). In rat brain, NAD(P)H levels decrease after middle age (Parihar et al., 2008). In brain neurons, NADH is kinetically upstream of GSH (Ghosh and Brewer, 2014b) and therefore, manipulating NADH levels influences GSH levels. Free NADH is generated from a cytoplasmic dehydrogenase in glycolysis (glyceraldehyde 3-phosphate dehydrogenase, GAPDH) and mitochondrial dehydrogenases (pyruvate dehydrogenase, PDHC, and other the TCA cycle dehydrogenases). The produced free NADH is used to power oxidative phosphorylation for ATP generation. NADH exists in two states, either in a protein-bound form or a free form. Our previous study used steady-state fluorescence imaging without being able to distinguish between bound and free NADH (Ghosh et al., 2014b). Studies of imposed Cys/CySS redox states demonstrated the feasibility to manipulate internal NAD(P)H levels (Ghosh and Brewer, 2014a) in mouse neurons and internal glutathione

(GSH) levels of human retinal pigment epithelial cells (Jiang et al., 2005). We recently reported an age-related decrease in intracellular free NADH of brain neurons (Dong et al., 2019). Since aging manifests as greater vulnerability to external stress and energetic shortage, here we non-invasively measured free NADH in mitochondria, cytoplasm and nuclei of aged neurons at various redox states. In order to examine the capacity to maintain free NADH levels, we imposed an external Cys/CySS oxidative stress. More importantly, we tested whether free NADH can be restored to young levels by imposing an extracellular reductive state. We applied a non-invasive and sensitive imaging technique to measure the intrinsic NADH fluorescence. Using fluorescence lifetime imaging microscopy (FLIM), we distinguish the bound and free NADH based on the long and short intrinsic fluorescent lifetimes of NADH (Yu and Heikal, 2009; Stringari et al., 2012) and also resolve subcellular compartments for free NADH re-distribution in response to an imposed external oxidative and reductive states in live neurons.

3.3 Materials and Methods

Mouse Model

As described before (Dong, 2019), we used LaFerla's triple transgenic mouse model of AD (3xTg-AD) with human transgenes *βAPP* (SWE), *PS1* (M146V), and *Tau* (P301L) to mimic the neuropathological features of AD (Odd et al., 2003). Nontransgenic (NTg) C57BL/6 (Charles River) with normal NNT (Ghosh et al., 2014b) were used as controls. All mice underwent genotyping before using in experiments. All experiments involving mice were approved by the Institutional Animal Care and Use Committee (AUP-17-65) and performed according to guidelines and regulations.

Primary Neuron Culture

As describe previously (Brewer and Torricelli, 2007), adult hippocampal neurons were isolated from NTg and 3xTg-AD age-matched mouse brains at young (3-4 months old), middle ages (9-10 months old) and old ages (18- 23 months old). Hippocampi were sliced at 0.5 mm, digested with papain (Worthington) and triturated in Hibernate A (BrainBits LLC, Springfield, IL) with 2% B27 supplement (Fisher Scientific) with 0.5 mM Glutamax (Fisher Scientific). Neurons were separated from debris and microglia on an Optiprep (Sigma-Aldrich) density gradient. The neuron-enriched fraction was collected. Neurons were plated at 50,000 cells/cm^2 on 15 mm glass coverslips and cultured in NbActiv1 (BrainBits) with 5 ng/mL mouse FGF2 and 5 ng/mL PDGFbb (Fisher Scientific) for trophic support. Prior to plating, glass coverslips (Assistant; Carolina Biological) were coated overnight with 100 µg/mL poly-D-lysine. Neurons were cultured for 9-12 days at 37°C in 5% CO_2, 9% O_2 at saturated humidity. Viability in our neuronal cultures was similar to previous studies of neurons from all ages and both genotypes (Dong et al., 2019; Ghosh et al., 2012). The neuronal densities of all ages and genotypes in culture were similar, without fragmented axons or dendrites, indicating the capacity to withstand the imposed redox shifts. The mitochondria of neurons were prelabeled with 10 nM TMRE (tetramethylrhodamine ethyl ester) for 20 minutes under 5% CO_2 at 37°C (Dong et al., 2019). In the same fields as used for FLIM, mitochondria were imaged by 561 nm laser excitation and 597-737 nm filtered emission. Nuclear subcellular regions were selected by their central circular appearance. Cytoplasmic sub-regions were chosen in regions lacking mitochondria in TMRE images.

Variation of Cys/CySS Redox State

Fresh stock solutions of 10 mM cysteine and 5 mM cystine were made in culture medium NbActiv1 (BrainBits). The Cys/CySS redox state for NbActiv1 is -50 mV. As described before (Ghosh and Brewer, 2014a), oxidized and reduced Cys/CySS redox states were modulated by varying cysteine and cystine concentrations based on the Nernst equation: Eh (mV)= -250 + 30 log ($CySS/[Cys]^2$). The modulated reductive and oxidative potentials of Cys/CySS were made by the adjusting the proportions of Cys and CySS stock solution in the NbActiv1 medium, 100 µM CySS for 0 mV and 180 µM Cys for -150 mV. Neurons were incubated under different Cys/CySS redox states for 6 hours at 37°C in 5% CO_2, 9% O_2.

Free NADH Calibration

According to Ma et al. (2016), the β-Nicotinamide adenine dinucleotide (NADH, Sigma-Aldrich) was prepared fresh each time as a stock solution of 428 µM in a 0.2 mM Tris-HCl, pH 7.5 and stored at 4°C. The absolute concentration of the free NADH stock solution for calibration was determined prior to use in a NanoDrop 2000 UV-Vis Spectrophotometer (Thermo Fisher Scientific Inc) at 340 nm. The actual free NADH concentration was calculated based on the Beer-Lambert law

$$\boldsymbol{A = \varepsilon bc}$$

where ***A*** is the readout absorbance; **ε** is the extinction coefficient of NADH (6.22 at 340 nm); **b** is the length of light path (1 mm) and **c** refers to concentration of NADH in the solution.

FLIM Imaging

As described previously (Dong et al., 2019), fluorescence lifetime images were acquired at 37° C in 5% CO_2 on a Zeiss LSM 710 microscope (Carl Zeiss, Jena, Germany) using a 63x oil immersion objective, 1.2 N.A. (Carl Zeiss, Oberkochen, Germany). The 2-Photon excitation laser source was a Titanium:Sapphire MaiTai laser (Spectra-Physics, Mountain View, CA) with 120 fs pulses and 80 MHz repetition rate. Pixel dwell time was 25.21 µs and image size was 256 x 256 pixels. The cultured neurons were excited at 740 nm employing an emission band pass filter at 460/80 nm. The signal (autofluorescence) was collected with a photomultiplier tube (H7422P-40, Hamamatsu, Japan).

FLIM Phasor and Sub-regional Data Analysis

Analyses were performed using a phasor method (Digman et al., 2008) and SimFCS software (LFD,UCI). From Stringari (Stringar, 2012; 2015), every pixel of the FLIM image was transformed to one pixel in the phasor plot by a Fast Fourier Transform (FFT) of the intensity decay I(t). The coordinates g and s in the phasor plot are the real and imaginary part of the FFT by using the following transformations:

$$g_{i,j}(\omega) = \frac{\int_0^t I_{i,j}(t)cos(\omega t)dt}{\int_0^t I_{i,j}(t)dt}$$

$$s_{i,j}(\omega) = \frac{\int_0^t I_{i,j}(t)sin(\omega t)dt}{\int_0^t I_{i,j}(t)dt}$$

Where the indices *i* and *j* identify a pixel of the image and ω represents the frequency ($\omega=2\pi f$), with f is the laser repetition rate (80 MHz) and t is the period of the laser, 12.5 ns. Based on the linearity of the phasor coordinates, the g and s position of each pixel represents the fraction of free to bound NADH in the image (Stringari, 2015).

To study the free NADH levels of mitochondria, regions of interest (ROI) were selected based on TMRE staining of mitochondria (Dong et al., 2019). Cytoplasmic regions replete of mitochondria were selected. Circular nuclear regions were readily evident from their low NADH signal. Five ROIs were measured in each compartment of each neuron. Measurements of compartments from 20 female neurons and 10 male neurons from each age and genotype mouse group were averaged.

Measurements of Total NADH Pool and Free NADH Concentrations in Mitochondria.

Before calibration with free NADH for absolute NADH quantification, we calibrated the instrument response function with a known standard, 100 µM Coumarin 6 with lifetime at 2.5 ns. In the phasor plot, the pure free NADH lifetime is 0.4 ns. Whereas, the NADH bound to LDH (lactate dehydrogenase) has a longer lifetime of 3.4 ns. The lifetime distribution of the NADH signal from the cells represents the fractional combination of free and bound NADH along the line between the pure free NADH and bound NADH. To measure the total NADH pool in the neurons, we first acquired a FLIM image of a known concentration of free NADH calibrated using the absorbance spectrophotometer. We then corrected for the difference between a lower quantum yield of the free and higher quantum

yield of the bound form of NADH as described by Ma et al. (2016) To determine the mitochondrial free NADH concentration, we multiplied the measured total NADH pool by the corresponding free NADH fraction in mitochondria.

Statistical Analysis

One-way or Two-way ANOVA analysis was used to assess the difference of means and variances in Excel. Multifactorial ANOVA analysis was conducted in IBM SPSS Statistics software. The level of significance was set at $p < 0.05$ to reject the null hypothesis. Means and SEs are presented.

3.4 Results

3.4.1 Imposed Extracellular Cys/CySS Redox States Modulate Intracellular NADH Levels

Age-associated oxidative stress lowers total (bound + free) NADH levels (Parihar et al., 2008; Ghosh et al., 2012) as well as free NADH in neurons (Dong et al., 2019). To study free NADH in live neurons as a function of age and transgenic AD genotype, we isolated and cultured neurons in a uniform medium from mice at young, middle and old ages, removed from a complicated aging context *in vivo* including age-related inflammation, hormones and vasculature. To study how the external redox shifts impact intracellular free NADH levels and distributions, we applied a 120 fs pulsed laser excitation for fluorescence lifetime imaging microscopy (FLIM) to distinguish free NADH from bound forms (**Fig. 3.1**) at a normal balance of extracellular Cys/CySS (-50 mV), an imposed oxidative state (0 mV, excess CySS) and an imposed reductive treatment (-150 mV,

excess Cys). The FLIM intensity images of neurons attest to the ability of withstand measurements with a Cys/CySS oxidative and reductive state in young NTg neurons **(Fig. 3.1A-C)** and 3xTg-AD neurons **(Fig. 3.1a-c)**, compared to old NTg **(Fig. 3.1H-J)** and 3xTg-AD neurons **(Fig. 3.1 h-j)**.

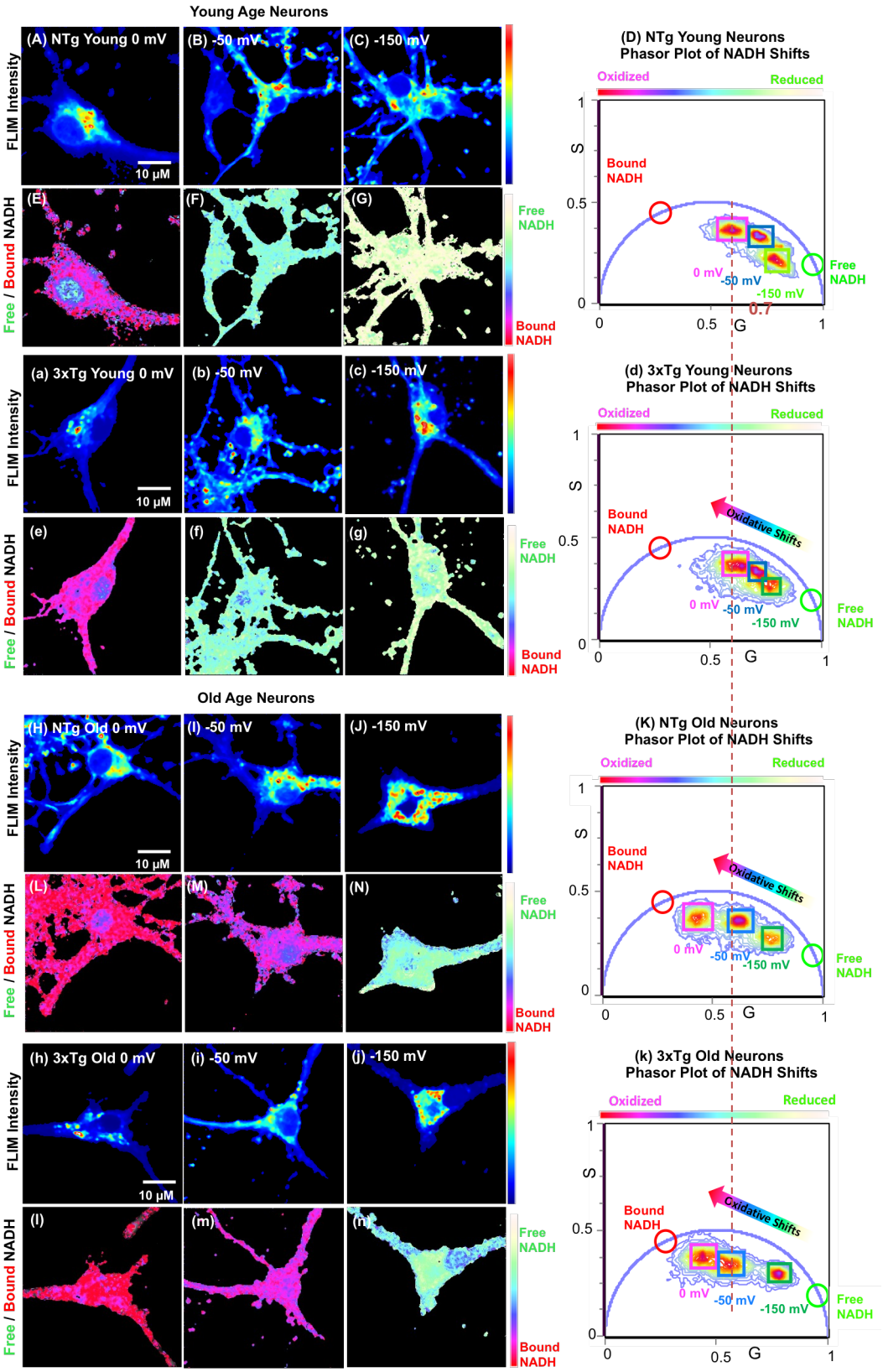
Young Age Neurons
(A) NTg Young 0 mV
(B) -50 mV
(C) -150 mV
FLIM Intensity
10 µM
(E)
(F)
(G)
Free / Bound NADH
Free NADH
Bound NADH
(D) NTg Young Neurons
Phasor Plot of NADH Shifts
Oxidized
Reduced
Bound NADH
Free NADH
0 mV
-50 mV
-150 mV
0.7
S
G
(a) 3xTg Young 0 mV
(b) -50 mV
(c) -150 mV
(e)
(f)
(g)
(d) 3xTg Young Neurons
Phasor Plot of NADH Shifts
Oxidative Shifts
Old Age Neurons
(H) NTg Old 0 mV
(I) -50 mV
(J) -150 mV
(L)
(M)
(N)
(K) NTg Old Neurons
Phasor Plot of NADH Shifts
(h) 3xTg Old 0 mV
(i) -50 mV
(j) -150 mV
(l)
(m)
(n)
(k) 3xTg Old Neurons
Phasor Plot of NADH Shifts

Figure 3.1. Imposed external Cys/CySS oxidative and reductive states shift the internal NADH redox state in neurons from NTg and 3xTg-AD mice. FLIM NADH Intensities were collected from NTg **(A, B, C)** and 3xTg-AD **(a, b, c)** in young age neurons under 0 mV (oxidative), -50 mV (normal medium as control, no treatment) and -150 mV Cys/CySS (reductive) redox states. **(D)** Phasor plot of the same NTg and **(d)** 3xTg-AD young age neurons illustrate the shifts of the intracellular free/bound NADH ratios toward more free NADH at reductive -150mV and to more bound NADH with imposed external oxidative state of 0 mV. The colored arrow indicates the direction of shifts from free to bound NADH with imposed reductive to oxidative states. Corresponding free /bound NADH FLIM color maps of the NTg **(E, F, G)** and 3xTg-AD **(e, f, g)** of young age neurons demonstrate intracellular NADH shifts to higher free/bound NADH proportions with an external reductive shift showing more cyan-green. In the FLIM fraction colormap, pink-purple regions indicate more bound NADH and green-cyan refers to more free NADH fraction. An imposed oxidative stress to 0 mV shifted the cellular distribution of NADH free/bound ratio toward more red-purple, indicating a shift to a lower free/bound NADH fraction. Similarly, FLIM NADH intensities were collected in old age neurons from NTg **(H, I, J)** and 3xTg-AD mouse neurons **(h, i, j)** following the indicated redox treatments. Phasor plot of the same NTg **(N)** and **(n)** 3xTg-AD old neurons shows the manipulation of intracellular free/ bound NADH ratios of neurons in response to the imposed external Cys/CySS oxidative and reductive states. The dashed vertical orange line indicates the G value at the center of NTg young cluster at the -50 mV (normal) Cys/CySS condition for reference. Corresponding free and bound NADH distributions from old neurons of NTg **(L, M, N)** and 3xTg-AD **(l, m, n)** mice with imposed redox states.

Mitochondria were localized and selected by imaging TMRE fluorescence (Dong et al., 2019). Since each pixel contains information of the lifetimes of free and bound NADH molecules, we transformed the signal from each pixel onto a phasor plot to visualize the proportions of free and bound in young age neurons of NTg (**Fig. 3.1D**) and 3xTg-AD (**Fig. 3.1d**) as well as old age neurons of NTg (**Fig. 3.1K**) and 3xTg-AD (**Fig. 3.1k**). In the phasor plot, the coordinates G and S represent the real and the imaginary part of the fast Fourier transformation (FFT) respectively (Stringari et al., 2015). As a combination of free and bound lifetimes, the cellular signal clusters along the line between the bound NADH lifetime of 3.4 ns (red circle) and pure free NADH lifetime of 0.4 ns (green circle). In response to the imposed oxidative Cys/CySS redox states, the NADH cluster from a whole neuron shifted toward more bound NADH, relative to the cluster of the untreated condition in both young (**Fig. 3.1D, d**) and old neurons of both genotypes (**Fig. 3.1K, k**). Under the imposed reductive states, the neuronal NADH lifetime cluster shifted to more free NADH compared to the untreated condition. In the free and bound NADH distribution map **(Fig. 3.1E-G)**, the cyan-green color refers to more free NADH while red-purple indicates more bound NADH. Neurons treated with an oxidative condition showed a shift in NADH fraction from free to more bound NADH (**Fig. 3.1E, e, L, l**). In contrast, an imposed external reductive state caused a shift in cellular distribution toward more free NADH (**Fig. 3.1 G, g, N, n).**

3.4.2 Mitochondrial Free/Bound NADH Proportions Respond to Imposed Oxidative and Reductive States

Free NADH levels in mitochondria are critical for complex I to maintain the proton gradient across the mitochondrial membrane to power ATP production in the process of oxidative phosphorylation (OXPHOS). We used 2-photon excitation microscopy to resolve mitochondrial free and bound proportions in the NADH pool. We determined whether the mitochondrial free NADH levels can be manipulated with imposed extracellular Cys/CySS oxidative and reductive states. **Fig. 3.2** shows (G, S) data plotted from 10 cells of each age and genotype as a function of external oxidative and reductive shifts. In general, for both genotypes and 3 ages, the extracellular oxidative stress (pink circle) caused a shift toward more bound NADH relative to untreated mitochondria. The imposed external reductive state (green circle) caused dramatic shifts toward higher free NADH in the (G, S) plot of all ages and both genotypes. These results indicate the ability to shift mitochondrial free and bound NADH fractions of all ages and both genotypes by imposed external redox shifts.

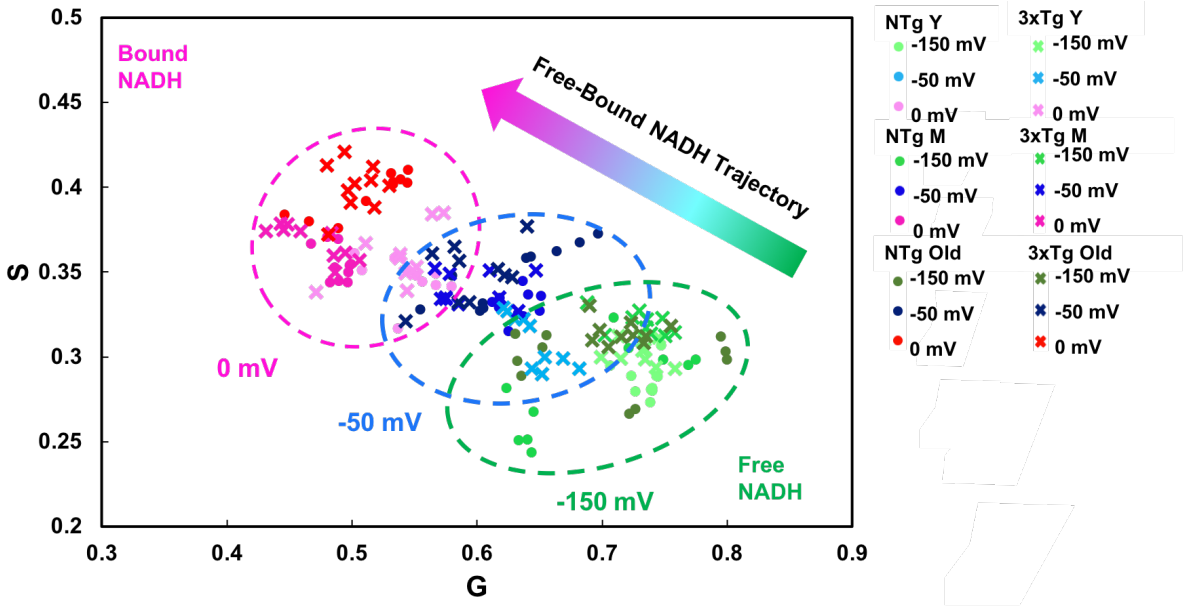

Figure 3.2 Mitochondrial NADH shifts toward more bound NADH with oxidative states and toward more free form in response to the imposed external reductive treatment. Each dot or cross point represents the average measurements in mitochondrial regions (ROIs) from a single NTg or 3xTg-AD neuron (n= 10 neurons/age/genotype/redox state = 180 points). Mitochondrial free/bound NADH re-distributes in response to the manipulated external Cys/CySS redox states from reductive (-150 mV) to oxidative (0 mV) in both genotypes and three ages are shown by the colored arrow (ANOVA for G, $F(2, 179)= 547$, $p< 0.001$; for S, $F(2, 179)= 356$, $p< 0.001$).

3.4.3 Imposed External Cys/CySS Redox States Modulate NADH at Mitochondria, Cytoplasm and Nuclei by Age, AD-genotype and Gender

Given that the age- and AD-associated declines in free NADH levels (Dong et al., 2019), we investigated 1) age- and AD-related differences of compartment-specific free NADH proportions in response to the external oxidative stress and further determine if old age diminishes the capacity to maintain free NADH against external imposed oxidative stress; 2) More importantly, whether the lower free NADH levels in old neurons could be restored by imposed external Cys/CySS reductive state in either genotype. Note that measures of the free NADH fraction are relative to the total NADH pool size (free + bound). Therefore, as the total NADH pool size diminishes with age and AD, computed changes in absolute free NADH concentrations could be larger than the changes in free NADH fraction of the total. From these measures of free NADH fraction, we further measured the free NADH concentrations in mitochondria across the age span to adjust for different total NADH pool sizes. We describe each of these effects first for mitochondria at each redox state, then cytoplasm and nucleus in terms of age, genotype and sex effects.

Mitochondrial Free NADH Fractions

(1) At 0 mV Oxidative State

The imposed external Cys/CySS oxidative stress (0 mV) caused declines in mitochondrial free NADH fractions in all ages (Two Way ANOVA for ages, female $F(2,119)= 165$, $p< 0.001$ and male $F(2,59)= 112$, $p< 0.001$) and genotypes (Two Way ANOVA for genotypes, female $F(1,119)= 35$, $p< 0.001$ and male $F(1,59)= 26$, $p< 0.001$) (**Fig. 3.3A, D**). Interestingly, under the external oxidative stress, the declines of mitochondrial free NADH

fractions from -50 to 0 mV of all ages and genotypes ranged narrowly from 30-35% in female (**Fig. 3.3A**) and 37-40% in male neurons (**Fig. 3.3D**). Specifically, at the 0 mV oxidative condition the old-age free NADH fraction were 21-30% lower than young neurons in mitochondria of both genders and genotypes. However, since the old neurons started at a 23-26% lower free NADH fraction, at 0 mV the old neurons were shifted closer toward a viable limit of free NADH.

(2) At -150 mV Reductive State

To determine if the lower free NADH fractions in old age neurons can be rescued by a reductive treatment, we imposed an extracellular Cys/CySS reductive state of -150 mV in the culture media. **Fig. 3.3A, D** show that this reductive stress elevated mitochondrial free NADH fraction in all ages, genotypes and genders compared to the untreated conditions (Two Way ANOVA for age, female $F(2,119)= 37$, $p< 0.001$ and male $F(2,59)= 60$, $p< 0.001$) and genotypes (Two Way ANOVA for genotypes, female $F(1,119)= 13$, $p< 0.001$ and male $F(1,59)= 164$, $p< 0.001$). Under the imposed reductive state, mitochondrial free NADH of young neurons increased 6%-15% and old neurons rose by 23%-26% for both genotypes and genders. The external reductive state enhanced the mitochondrial free NADH fraction in old neurons to values approaching the those of young age under the untreated condition (orange circles) of both genotypes and genders. This indicates the lower mitochondrial free NADH in old age can be restored with an external reductive shift. Additionally, successful rejuvenation of the mitochondrial free NADH fractions in old age neurons suggests a reversible latent capacity to regenerate free NADH in old age neurons. With external reductive state, the lesser 6%-15% rise of free NADH fractions in

young than the 23%-36% in old age neurons suggests an approach toward a maximal capacity for free NADH regeneration.

(3) Manipulability

Over the range of imposed oxidative to reductive conditions, the mitochondrial free NADH fractions of young neurons could be manipulated by 64-74% and old age neurons were affected 105-111% (treatment*age interaction for female $F(4, 359)= 9$, $p< 0.001$; for male $F(4, 179)= 36$, $p< 0.001$) for both genotypes and genders. The higher manipulability in old age neurons suggests a higher vulnerability to resist external redox stress and a lower capacity to maintain mitochondrial free NADH levels.

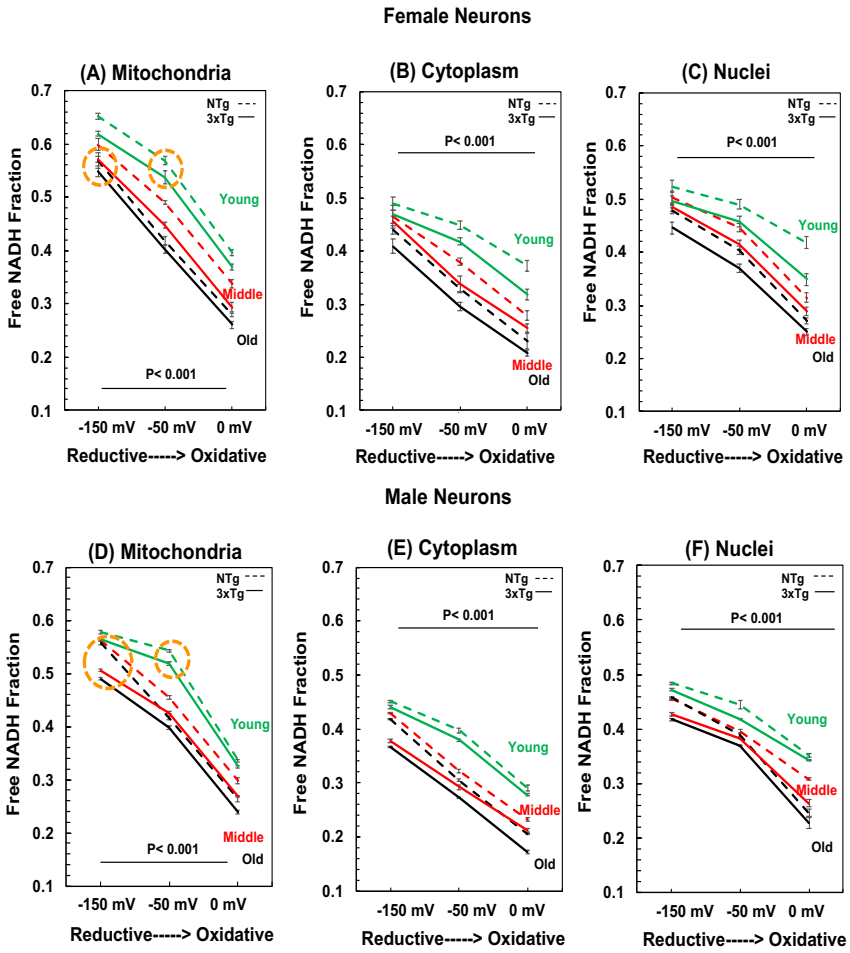

Figure 3.3. Compartment-specific changes in free NADH fractions with imposed extracellular oxidative (0 mV) and reductive (-150 mV) states across ages of NTg and 3xTg-AD mice for both female (A-C) and male (D-F) neurons. (A, D) Mitochondrial free NADH fractions in response to the imposed external Cys/CySS reductive states at -150 mV and imposed oxidized state at 0 mV in all ages ($p < 0.001$) of both NTg and 3xTg-AD mice. With external reductive treatment, mitochondrial free NADH fractions can be rescued to the levels of young age at untreated condition (orange circles). Untreated condition of -50 mV was a control for comparison. At the untreated condition, age effect drove declines in mitochondrial free NADH from young to old age of each genotype ($p < 0.001$). Moreover, free NADH fractions with genetic load appear to be lower than that of age- and redox- matched NTg neurons ($p < 0.001$). The imposed oxidative stress depleted free NADH fractions in all ages ($p < 0.001$). Notably, mitochondrial free NADH fractions in young age always presented highest than the levels of middle and old age in response to the external redox shifts. **(B, E)** Cytoplasmic free NADH fractions and **(C, F)** Nuclear free NADH fractions of female neurons illustrated depletion with oxidative stress ($p < 0.001$) and elevation in reductive states ($p < 0.001$) across ages in NTg and 3xTg-AD mice. Similarly, in male neurons. For gender difference, male neurons exhibited lower free NADH fractions than the age-, genotype- and redox-matched female neurons in each compartment, (Mito. $F(1,59)=13$, $p<0.001$; Cytoplasm $F(1,59)=25$, $p<0.001$; Nuclei $F(1,59)=13$, $p<0.001$); This sex-driven redox orders remain unchanged with external oxidized stress, (Mito. $F(1,59)=33$, $p<0.001$; Cytoplasm $F(1,59)=24$, $p<0.001$; Nuclei $F(1,59)=5$, $p=0.03$) and with the imposed reductive state (Mito. $F(1,59)=22$, $p<0.001$; Cytoplasm $F(1,59)=3.7$, $p=0.06$; Nuclei $F(1,59)=22$, $p<0.001$); Genotype effect drove a lower free NADH fraction in 3xTg-AD neurons than the NTg neurons in each age, redox state and compartment (n=20 female neurons or n=10 male neurons/compartment/redox state/age/genotype).

3.4.4 Cytoplasmic and Nuclear Compartment-Specific Changes in Free NADH Fractions

To explore compartment-specific responses in free NADH fractions with extracellular reductive and oxidative stress, we further measured free NADH fractions in cytoplasm **(Fig. 3.3B, E)** and nuclei **(Fig. 3.3C, F)** for all ages, both genotypes and genders. In the untreated condition, cytoplasmic free NADH fractions of old neurons were 23-29% lower than young neurons for both genotypes and genders (treatment*age for female $F(4, 359)= 8$, $p< 0.001$; male $F(4, 179)= 19$, $p< 0.001$). Nuclear differences in free NADH fractions at the untreated redox state were 11-19% lower in old than young neurons (treatment*age in nuclei for female $F(4, 359)= 11$, $p< 0.001$; male $F(4, 179)= 20$, $p< 0.001$). Under the imposed external oxidative stress to 0 mV, cytoplasmic free NADH fractions decreased 17-27% in young and 30-37% in old age neurons of both genotypes and genders. Similar to that of mitochondria, an external imposed reductive shift to -150 mV nearly restored both cytoplasmic and nuclear free NADH fractions in old age neurons to the levels of young neurons under the untreated condition. Of note, over the entire redox range, the manipulability of nuclear free NADH fractions by external redox shifts was 25-43% in young and 77-87% in old neurons of both genotypes and genders. These percentages are lower than the changes in the cytoplasm of old-age (91-103%) or the mitochondria (105-111%), suggesting a stronger capacity in nuclei to maintain free NADH levels relative to the total NADH pool size and minimize impacts on changes in free NADH with external redox stress. Remarkably, mitochondria were the most reduced with highest free NADH fractions, followed by more oxidized nuclei and most oxidized cytoplasm. This

order was affected little by the imposed reductive and oxidized conditions, genotype age or gender.

3.4.5 More Oxidized State in Male Neurons than Female Neurons

Females have a higher incidence of AD than males as well as other neurodegenerative diseases (Payami et al., 1996; Vina and Lloret, 2010). In response to redox shifts, we found the free NADH fractions to be consistently higher in female than male neurons across the age-span in both genotypes and three compartments (gender effects $F(1,1619)= 375$, $p< 0.001$; treatment*gender*compartment interaction $F(4, 1619)= 3$, $p=0.02$). Under the same external oxidative and reductive stress, the free NADH fraction in female neurons was 5%-15%, 6-22% and 3-16% higher than that of male in mitochondria, cytoplasm and nuclei respectively. The largest gender-difference of free NADH fractions was found in cytoplasm, suggesting a more glycolytic metabolism in female neurons under various external redox states.

3.4.6 Free NADH Concentrations and Total NADH Pool Size in Mitochondria with Imposed Redox States

As the NADH pool size changes with age, genotype, redox environments and energetic states, free NADH fraction reflects a change of free NADH level relative to the current NADH pool size (free + bound). To assess absolute free NADH concentrations in mitochondria of live neurons, we adjusted the FLIM phasor measures for the lower quantum yield of the free and higher quantum yield of the bound form of NADH (Ma et al., 2016). Under oxidative stress of 0 mV, in NTg neurons (**Fig 3.4A**), mitochondrial free

NADH concentrations of young age neurons declined by 37% to 280 μM ($F(1,31)= 112$, $p<0.001$) and old age neurons decreased 55% to 110 μM ($F(1,31)= 338$, $p<0.001$) compared to the untreated condition (-50 mV). In 3xTg-AD neurons, the free NADH concentration in young neurons declined 46% ($F(1,31)= 128$, $p<0.001$) and that in old neurons dropped 63% ($F(1,31)= 198$, $p<0.001$) compared to the untreated condition (-50 mV). AD genetic load drove a further 10% depletion in mitochondrial free NADH concentrations compared to the age-matched NTg neurons. This indicates that with external oxidative stress, old neurons had lower capacity to maintain mitochondrial free NADH concentrations than the young neurons of both genotypes. Furthermore, neurons with the genetic load were even lower than NTg neurons in their capacity to conserve mitochondrial free NADH in response to the oxidative stress.

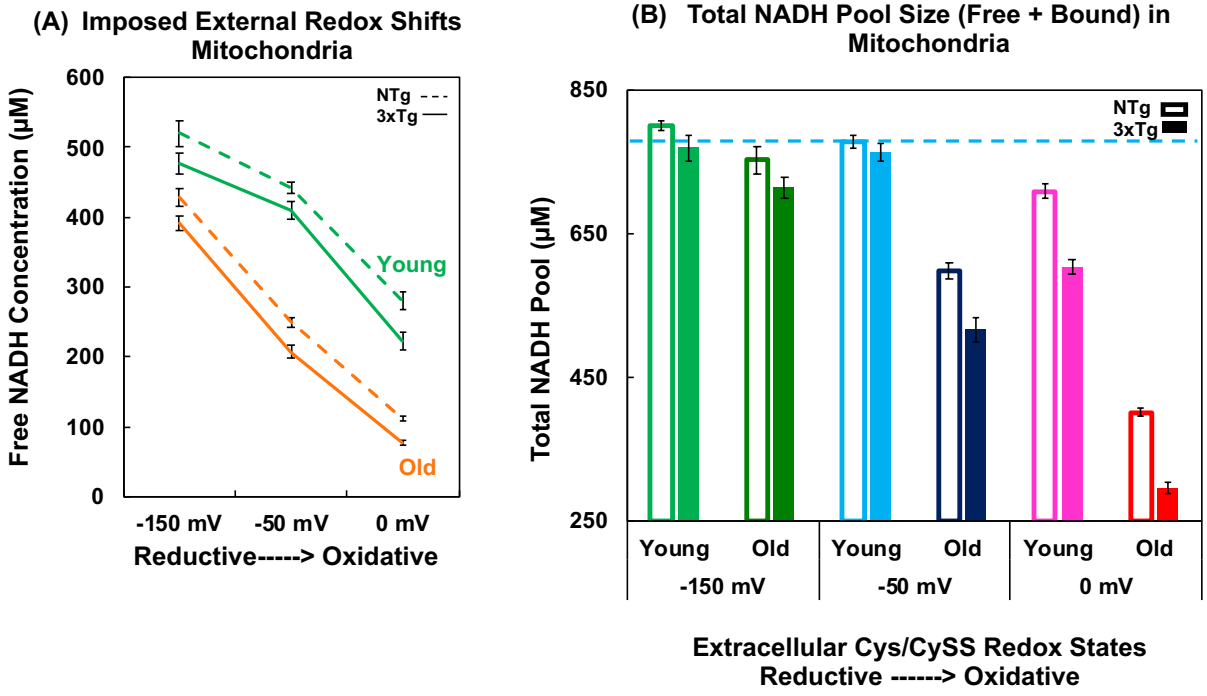

Figure 3.4. Absolute free NADH concentrations and total NADH pool size shift in mitochondria in response to an imposed external Cys/CySS reductive (-150 mV) or oxidative (0 mV) state for young and old age neurons from NTg and 3xTg-AD female mouse brains. (A) Under the imposed external oxidative stress, free NADH in mitochondria of both young and old neurons, both genotypes was depleted compared to that of untreated condition at -50 mV (at 0 mV, NTg young $F(1, 31)= 112$, $p< 0.001$; NTg old $F(1, 31)= 338$, $p< 0.001$; 3xTg young $F(1, 31)= 128$, $p< 0.001$; 3xTg-AD old $F(1, 31)= 198$, $p<0.001$) and was elevated with external reductive state to -150 mV (at -150 mV NTg young $F(1, 31)= 16$, $p< 0.001$; NTg old $F(1, 31)= 154$, $p< 0.001$; 3xTg young $F(1, 31)= 13$, $p=0.0013$; 3xTg-AD old $F(1, 31)= 183$, $p< 0.001$) (n=16 neurons/treatment/age/genotype). **(B)** Mitochondrial total NADH pool size in each redox state of female of both genotypes. As a reference, the blue dashed line indicates the total NADH pool in young NTg neurons at -50 mV redox state.

With imposed external reductive state to -150 mV, the mitochondrial free NADH concentration of old neurons was elevated by 71% to 430 μM in NTg ($F(1,31)=598$, $p< 0.001$) and by 89% to 390 μM in 3xTg-AD neurons ($F(1,31)=183$, $p< 0.001$). Under the reductive environment, the free NADH levels in old neurons approach the levels in young neurons of 442 μM in NTg and 410 μM in 3xTg-AD at the untreated condition (-50 mV). The successful rejuvenation of mitochondrial free NADH concentrations in old neurons under the external reductive treatment indicates a latent capacity to restore free NADH back to the young levels of both genotypes. However, reductive treatment on young neurons only drove a 18% increase of mitochondria free NADH concentrations in NTg ($F(1,31)=16$, $p= 0.0004$) and 16% elevation in 3xTg-AD neurons ($F(1,31)=13$, $p= 0.0013$) respectively. This suggests an approach to the maximal capacity for free NADH regeneration (or minimal consumption) in the young age with this reductive condition at -150 mV. Though the increment was smaller in young neurons with the reductive shift, the mitochondrial free NADH concentrations were still 22% higher than the old neurons with reductive treatment in both genotypes.

From the range of external oxidative to reductive stress, the overall flexibility for alteration of mitochondrial free NADH concentration in old neurons was 30% higher that of young neurons in both genotypes (n=16 neurons/treatment/age/genotype) (redox treatment*age interaction $F (2, 191) = 25$, $p< 0.001$). This suggests that old neurons were more susceptible to external redox stress than young neurons. By comparison of the pattern of young and old differences in **Fig. 3.4A to 3.3A** for the same neurons, the percent changes driven by age in mitochondrial free NADH concentrations in Fig. 3.4A were 2-fold larger

than that in free NADH fractions in Fig. 3.3A. **Fig. 3.4B** indicates the reason as a smaller NADH pool (free+ bound) size in old neurons compared to young neurons at each redox state (ANOVA for treatment*age $F(2,191)= 53$, $p< 0.001$; treatment*genotype $F(2, 191)= 8$, $p= 0.001$). The commonly reported free (or bound) NADH fraction can be compared to that of free (or bound) NADH concentrations only if the NADH pool is constant (free + bound NADH). **Fig. 3.4B** shows large changes in the NADH pool with age and genotype under each redox state. Thus, the changes in free NADH concentration can be larger than the fractional changes because of these changes of NADH pool. The smaller size of the NADH pool in old-age was exacerbated by an external oxidative stress but can be nearly restored to the untreated young levels by a reductive shift to -150 mV.

3.5 Discussion

Free mitochondrial NADH provides the major source of energy in neurons. The redox environment is critical for regulating NADH and NAD levels (Stein and Imai, 2012). How aging influences the free NADH regenerating capacity of mitochondria is less clear. Here for the first time we have reported the reversibility of free NADH levels even in old age and AD with an external oxidative or reductive stress. By using a non-invasive method of FLIM, we were able to quantify free and bound NADH fractions, concentrations and pool sizes in live neurons in response to the modified external redox states and distinguish separate responses in neuronal mitochondria, cytoplasm and nuclei. With 6 hours of an external oxidative shift in Cys/CySS redox state, the intracellular free NADH levels were lowered in mitochondria, cytoplasm and nuclei of all ages, approaching levels needed for survival (Ghosh and Brewer, 2014a). Subcellular free NADH in old neurons moved lower

than the that in young age neurons of both genotypes, suggesting a lower capacity to preserve free NADH in old age. Additionally, the 3xTg-AD genotype resulted in further lowering of levels of free NADH compared to that of age-matched NTg neurons. Remarkably, a reductive shift could rejuvenate free NADH in old neurons to the levels of untreated young neurons. We propose that the extracellular reductive Cys/CySS states not only enhance the internal free NADH concentrations, but provide substrate energy for enzymatic functions to reverse the energetic deficit in aging and AD. Though the redox systems and signaling of each compartment remain somewhat independent, the imposed Cys/CySS reductive states dramatically rescued the loss of capacity in regenerating free NADH of old age neurons in mitochondria, cytoplasm and nuclei of both genders and genotypes. Under all redox states, we observed that mitochondria had higher NADH levels than nuclei or cytoplasm, indicating a compartment-specific distribution of free NADH levels. This reductive privilege of mitochondria enables maximum generation of ATP from feeding free NADH to the electron transport chain. Our findings suggest the potential for reductive treatments in aging and AD to reverse the course of oxidative shifts.

Protein cysteine residues serve as redox molecular switches to signal regulatory and adaptive responses (Fra et al., 2017). A prototypic instance is given by the Kelch-like ECH-associated protein 1 (Keap1)- nuclear factor erythroid 2-related factor 2 (Nrf2)-antioxidant response elements (ARE) (Keap1-Nrf2-ARE) pathway. An oxidized redox state causes an oxidation of cysteines in Keap1 to promote dissociation from Nrf2 (Magesh et al., 2012). This allows Nrf2 to translocate to the nucleus to promote transcription of antioxidant response genes (Dinkova-Kostova et al., 2002). As the critical

feature of reversible thiol redox switches, we investigated whether an imposed external Cys/CySS reductive state could reverse the age- and AD-related loss of intracellular free NADH levels in neurons. In support, dietary supplementation of glutathione precursors cysteine and glycine in elderly subjects can dramatically drive a 95% increase in glutathione concentration and 79% elevation in fractional synthesis rate in plasma (Sekhar et al., 2011). Protective effects on cysteine-rich proteins were seen in dietary supplementation with SelenoCysteine, which is also available from milk proteins and egg to improve antioxidant status (McPherson and Hardy, 2011).

Though intracellular free NADH levels decline with age and AD-genotype, our data suggests that the free NADH levels in old age NTg and AD-model neurons can be restored back to the young age levels by the external manipulation of Cys/CySS redox circumstances. This restoration to youthful levels of free NADH could provide the reductive energy for higher rates of oxidative phosphorylation. Higher ATP flux could explain the improved survival of these old neurons with reductive shifts through a mechanism of higher pAKT (Ghosh and Brewer, 2014a). More generally, redox biology interfaces the individual exposome (e.g. diet and exercise; here redox shift) and functional metabolome and genome (Go and Jones, 2014). Our imposed redox shifts are important because extracellular redox states play critical roles in numerous biological processes including proliferation (Hutter et al., 1997), differentiation (Smith et al., 2000) and apoptosis (Voehringer, 1999). Systemically, the thiol/disulfide couples of cysteine/cystine (Cys/CySS) and glutathione/glutathione disulfide (GSH/GSSG) are in thermodynamic disequilibrium in plasma (Go and Jones, 2017). Inside cells, the GSH/GSSG couple

buffers the redox state, but NADH is kinetically upstream of GSH (Ghosh et al., 2014b). Cys residues and most thiols in proteins can be kinetically manipulated for redox control (Go and Jones, 2017; Kirlin et al., 1999).

Our results demonstrate that the free NADH concentration and NADH pool are under direct and rapid redox control by external Cys/CySS oxidative and reductive shifts. The reductive shift in the circadian rhythm of plasma Cys/CySS with eating (Blanco et al., 2007) indicates the opportunity for in vivo manipulation. These results suggest a potential use of redox-based therapy as an effective tool to delay or even reverse the course of aging and AD by reversing the depletion of free NADH levels to improve ATP generating capacity. Here we only evaluated one level of reductive shift and less reductive shift may be necessary to avoid reductive stress (Aon et al., 2010). *In vivo*, this will require titration to biomarker targets. In previous work, neuronal (free + bound) NAD(P)H levels were compared after titrated inhibition of NAD(P)H regeneration or inhibition of glutathione re-synthesis, which consumes NADPH (Ghosh et al., 2014b). The results in old neurons indicated that regeneration of NADH was more important than consumption of NAD(P)H for regeneration of glutathione.

Our studies were motivated by reported changes in the Cys/CySS redox state in human plasma which was progressively oxidized with age 0.2 mV per year from 18 to 93 years (Jones, 2006). In neurons, the excitatory amino acid transporter EAAT3 facilitates entry of the zwitterionic amino acid L-cysteine (Watts et al., 2014). The cystine/glutamate antiporter SLC7A11/xCT is also responsible for uptake of extracellular cystine and

release of intracellular glutamate (Soria et al., 2016; Koppula et al., 2017). The activity of EAAT3 maintains the intracellular pool of free cysteine for glutathione synthesis (Aoyama and Nakaki, 2013). Addition of extracellular L-cysteine elevates intracellular GSH levels (Dinkova-Kostova et al., 2002). CySS is immediately reduced to Cys in the more reducing cytoplasm (Aoyama and Nakaki, 2013). However, the mechanism for increasing intracellular free NADH levels by the imposed reductive Cys/CySS states remains unclear. If NADH also serves as an anti-oxidant, then higher levels of GSH could relieve some ROS-dependent consumption of NADH. Additionally, NADH is in equilibrium with NADPH via transhydrogenase (Ying, 2008) and malate enzyme (Singh et al., 2008). NADPH is used for reductive energy by glutathione reductase to regenerate GSH from GSSG. Therefore, a reductive shift that elevates GSH (Ghosh and Brewer, 2014a), would lessen consumption of NADPH and thus NADH. A reductive shift may indirectly improve the free NADH levels by reducing the oxidized protein thiols and reversing the activities of thiol-containing redox couples and enzymes. Cysteine residues at active sites of proteins, such as thioredoxin (Trx), glutaredoxin (Grx) and peroxiredoxin (Prx), dominate oxidative detoxification (Winterbourn, 2008). These characteristics facilitate a reversible redox switch in response to the extracellular reductive and oxidative circumstances. These responses have been especially well documented for NMDA receptors as protein cysteines dimerize in an oxidized redox state to limit Ca^{++} flux in aging hippocampal neurons (Kumar and Foster, 2018). As a fast response to the environmental stimuli, reversible changes of protein thiols provide rapid post-translational switches in control of the functions of mitochondrial proteins (Mailloux et al., 2014).

Clinical attempts to modulate cysteine were reported recently. Placebo-controlled clinical trials with *N*-acetylcysteine (NAC) as the supplement in psychosis patients showed significant improvements on neurocognition and increase of GSH levels in brain and blood cells (Conus et al., 2018; Sepehrmanesh et al., 2018) as well as working memory performance (Rapado-Castro et al., 2017). NAC functions as a powerful antioxidant for detoxification because of its role as a precursor of L-cysteine for glutathione biosynthesis (Mokhtari et al., 2017). In fibroblasts of AD patients, the combinatorial intervention of lipoic acid (1 mM) and NAC (100 μM) pronouncedly decreased mitochondrial-related oxidative stress (Moreira et al., 2007). Due to its safety as a nutritional supplement, NAC was also examined for AD treatment in clinical trials. In some clinical trials, L-cysteine is used as an auxiliary treatment for AD patients. A phase II randomized clinical trial of a nutraceutical formulation (including NAC, α-tocopherol, acetyl-L-carnitine, folate, B12, S-adenosyl methioinine) on 106 AD patients showed a stable or improved cognitive performance and mood/behavior (Remington et al., 2015). Administration of a supplement cocktail of antioxidants including L-cysteine, vitamin E, vitamin C, β-carotene, selenium, vitamins B1, 2, 3, 6, 9 and 12 may augment pharmacological approaches in AD treatment (Shea and Remington, 2015). In this study, we presented the successful reversibility of oxidized free NADH in mitochondria of old age neurons to the young levels from NTg and 3xTg-AD mouse brains by imposing an externally reductive Cys/CySS shift to -150 mV. This provides additional motivation for therapy for AD by administration of reductive cysteine redox states *in vivo*.

Free NADH functions critically to power energetic supply and maintain intracellular redox homeostasis. In an advance over previous *in vitro* NADH studies of brain aging and Alzheimer's, this work used FLIM, to discriminate free and bound NADH in segregated mitochondrial, cytoplasmic and nuclear compartments of live primary neurons in response to the external imposed Cys/CySS oxidative and reductive manipulation. Our method is label-free and non-invasive probing the intrinsic fluorescence of NADH in live neurons by two-photon excitation. Since the total NADH pool size varied by age, genotype and external redox shifts and free NADH fraction is relative to the total NADH pool size, a further quantification of free NADH concentrations and total NADH pool sizes in mitochondria facilitated comparison of their capacity to maintain or regenerate free NADH. With external reductive treatment, the free NADH fractions in old neurons can be reversed and rejuvenated to the levels of young age, indicating a potential reductive intervention to reverse or slow down the progression of aging and AD. The measured free NADH concentrations suggests a lower capacity in maintaining or regeneration of free NADH in old neurons than the young neurons and a further diminish with genetic load in the age-matched 3xTg-AD neurons. Additionally, in line with the compartmental redox order in HeLa cells (Hansen et al., 2006), we found in neurons, regardless of external redox states, mitochondria displayed the most reduced with highest free NADH fractions, followed by nuclei and most oxidized in cytoplasm with lowest free NADH fractions. The successful reversibility of free NADH concentrations in old age neurons back to the levels of healthy young age by an external reductive state suggests a potential reductive intervention to counter AD and extend lifespan.

3.6 Acknowledgements

This work was supported by grants from NIH R01AG058218 to G.J.B. and NIH P41-GM103540 to M.A.D. We appreciate the help from Rachel Cinco-Hedde and Ning Ma in the Digman lab.

CHAPTER 4

GLOBAL METABOLIC SHIFTS IN AGE AND ALZHEIMER'S MOUSE BRAINS PIVOT AT NAD^+/NADH REDOX SITES (SUBMITTED)

Yue Dong[1] and Gregory J. Brewer[1,2]

1Department of Biomedical Engineering, University of California Irvine, Irvine, California, United States of America

2MIND Institute, Center for Neurobiology of Learning and Memory, University of California, Irvine, CA, United States of America

Keywords Alzheimer's disease, aging, hippocampus, energy metabolism, NAD, dehydrogenase, oxidation-reduction, glycolysis, citric acid cycle, fatty acids

4.1 Abstract

Age and Alzheimer's disease (AD) share some common features such as cognitive impairments, memory loss, metabolic disturbances, bioenergetic deficits and inflammation. Yet little is known on how systematic shifts in metabolic networks depend on age and AD. In this work, we investigated the global metabolomic alterations in non-transgenic (NTg) and triple-transgenic (3xTg-AD) mouse brain hippocampus as a function of age by using untargeted Ultrahigh Performance Liquid Chromatography-tandem Mass Spectroscopy (UPLC-MS/MS). We observed common metabolic patterns with aging in

both NTg and 3xTg-AD brains involved in energy-generating pathways, fatty acids oxidation, glutamate and sphingolipid metabolism. We found age-related down-regulation of metabolites from reactions in glycolysis that consumed ATP and in the TCA cycle, especially at NAD^+/NADH-dependent redox sites, where age- and AD-associated limitations in the free NADH may alter reactions. Conversely, metabolites increased in glycolytic reactions in which ATP is produced. With age, inputs to the TCA cycle were increased including fatty acid β-oxidation and glutamine. Overall age- and AD-related changes were >2-fold when comparing the declines of upstream metabolites of NAD^+/NADH-dependent reactions to the increases of downstream metabolites ($p=10^{-5}$, n=8 redox reactions). Inflammatory metabolites such as ceramides and sphingosine-1-phosphate also increased with age. Age-related decreases in glutamate, GABA and sphingolipid were seen which worsened with AD genetic load in 3xTg-AD brains, possibly contributing to synaptic, learning- and memory-related deficits. The data support the novel hypothesis that age- and AD-associated metabolic shifts respond to $NAD(P)^+$/NAD(P)H redox-dependent reactions, which may contribute to decreased energetic capacity.

4.2 Introduction

Alzheimer's disease (AD) is a neurodegenerative disease characterized by extracellular β-amyloid plaque accumulation, intracellular neurofibrillary tangles, metabolic disturbances (Bubber et al., 2005), oxidative stress (Zhu et al., 2007), inflammation (Wang et al., 2015), autophagic (Reddy et al., 2018) and bioenergetic deficits (Perez and Swerdlow, 2019; Wu et al., 2018). Despite abundant associations, based on clinical trials, it is unclear which of these are primal. AD affects an estimated 5.7 million in America in

2016 and is projected to grow to 13.8 million by 2050 (Alzheimer's Association, 2016). Age is the greatest risk factor for neurodegenerative AD. Aging and AD share some common features including neurodegeneration (Wirth et al., 2013), metabolic perturbances (Culter et al., 2004; Müller et al., 2010; Mattson and Arumugam, 2018), bioenergetic deficits (Du et al., 2013) and inflammation (Yin et al., 2016). According to the epigenetic oxidative redox shift (EORS) theory of aging, age- and AD- associated sedentary life style promote oxidative shifts upstream of ROS to initiate a vicious cycle of oxidized membrane receptors, signaling molecules, transcription factors and epigenetic transcriptional regulators, which further impose a metabolic shift away from the mitochondrial energy supply (Brewer, 2010).

"Omics" technologies including genome (Seshadri et al., 2010), epigenome (Gjoneska et al., 2015), transcriptome (Miller et al., 2010), proteome (Manavalan et al., 2013; Kiddle et al., 2014) and metabolome (Trushina et al., 2013) studies of mice and human have examined age- and AD-associated changes in gene and protein expression (Zierer et al., 2015; De Magalhães et al., 2009). Metabolome studies integrate the effects of expression of the genome, epigenome, transcriptome, proteome and post-translational modulation of activity by the exposome to provide a downstream snap shot of regulatory signaling networks (Gomase et al., 2008). An age-associated sedentary low-energy state is implicated in AD morbidity and is coincident with observations of metabolic shifts and decline in glucose uptake with age (Ding et al., 2013; Gage et al., 1984; Gumbiner et al., 1992; Mattson and Arumugam, 2018). AD-associated metabolic perturbation was reported in tryptophan, tyrosine, methionine, purine in cerebrospinal fluid (CSF) of AD

patients (n=40) (Kaddurah-Daouk et al., 2013), ceramides and sphingomyelins in plasma of 26 AD patients (Han et al., 2011) relative to age-matched controls. Significant metabolic disturbances in transgenic APP/PS1 AD mouse model include essential amino acids, branched-chain amino acids, neurotransmitter serotonin, phospholipid and acylcarnitine (Pan et al., 2016). Additionally, changes in energy metabolism result in metabolic shifts in different regions of aging mouse brains (Ivanisevic et al., 2014; 2016). We specifically studied metabolic shifts in hippocampal regions of different ages which are implicated in impaired episodic memory, short- and long-term memory, spatial memory and navigation. Gene expression in 129/C57BL/6 mouse brains revealed that from 6- to 9- months, almost two-thirds of the genes relative to energy and amyloid metabolism were downregulated, whereas in the age-matched male brains, only 5% genes were altered (Zhao et al., 2016). In our work, we extended the studies to global metabolism gender-differences across the age-span in the hippocampus. Further, since aging increases the risk for AD incidence, whether the normal age and AD share some common shifts or signatures in metabolic profiles and patterns in brains and if so, which pathways are most affected are poorly understood. Moreover, correlations of metabolic shifts in old age of hippocampal brains relative to the Alzheimer's model brains at the sites of redox bioenergetics were examined to strengthen the redox hypothesis of aging.

Interest in metabolic alterations in AD is anchored by reduced glucose uptake in AD patients. A study of 20 patients with early-onset dementia of Alzheimer type (DAT) revealed a 50% reduced metabolic rate of glucose uptake in the brain and significant elevation of lactate compared to non-demented subjects (Hoyer, 1988). At the end of glycolysis, pyruvate is either oxidized to acetyl-CoA for entry into the TCA cycle or

reduced to lactate, dependent on the redox status of nicotinamide adenine dinucleotide oxidized/reduced forms (NAD^+/NADH). Since this redox state becomes more oxidized and the NADH pool declines with age and in AD-transgenic mice (Ghosh et al., 2012; Dong et al., 2019), we further explored how these age- and AD-related oxidative shifts in NADH affected metabolic networks, especially NAD^+/NADH-dependent substrates in glycolysis and NADH production in the TCA cycle. Lactate serves as an alternative energy supply for neurons during hypoglycemia (Aubert et al., 2005) and it also functions as a neuroprotective metabolite (Newington et al., 2013) via transcriptional activation of brain-derived neurotrophic factor (BDNF) expression (Coco et al., 2013). In addition to lactate, Ding et al. (2013) demonstrated the utilization of ketone bodies as an alternative energy supply during early glucose insufficiency in mouse brain. Yao et al. (2011), proposed that during an energetic crisis, a compensatory metabolic shift from glycolysis to ketogenic/ fatty acid oxidation caused white matter degradation. Here, we compared the age-related shifts of metabolomic profiles in both NTg and triple-transgenic (3xTg-AD) mouse brain hippocampus of both sexes by using ultrahigh performance liquid chromatography-tandem mass spectroscopy (UPLC-MS/MS). We observed major age and AD-associated shifts of metabolic patterns linked to energy production and NADPH antioxidant intermediates in the PPP, fatty acid metabolism, glutamine and sphingolipid metabolism. The prospect of correlating age- and AD- related shifts in metabolic profiles with impaired brain energy and antioxidant defense offers a novel way to study the mechanism of AD, diagnose early stages of AD among aged population with possible prognostic implications.

4.3 Materials and Methods

Mouse Model

We used LaFerla's triple transgenic mouse model of AD (3xTg-AD) with human transgenes AβPP (SWE) and Tau (P301L) driven by the Thy1.2 promoter and knock-in PS1 (M146V) to mimic the neuropathological features of AD (Oddo et al., 2003). Non-transgenic (NTg) C57BL/6 mice (Charles River, San Diego) were used as controls with normal NNT (Ghosh et al., 2014b). In each genotype and each gender, five young (1-3 month), five middle (8-14 month) and five old (18-23 month) ages of mice were used. All mice underwent genotyping before use in experiments. All experiments involving animals were approved by the Institutional Animal Care and Use Committee (AUP-17-65) and performed according to NIH guidelines and regulations.

Hippocampal Tissue Collection

Mice were anesthetized by isoflurane vapor with subsequent collection of whole brains. Hippocampi and overlaying entorhinal cortex were isolated, followed by immediate flash freezing in liquid nitrogen for 1 min (n=5 mice /age/genotype/gender). All samples were stored at -80°C until shipping to Metabolon (Durham, NC, USA) on dry ice for metabolomics analysis. Samples were randomized and coded for blinding in the repeated ages and genotypes.

Sample Preparation

Samples were prepared using the automated MicroLab STAR system from Hamilton Company. Several recovery standards were added before tissue extraction for quality

control (QC). Proteins in the samples were precipitated with methanol under vigorous shaking for 2 min (Glen Mills GenoGrinder 2000) followed by centrifugation. The resulting extract was divided into five aliquots: two for analysis by two separate reverse-phase (RP)/UPLC-MS/MS methods with positive ion mode electrospray (ESI), one with negative ion mode ESI, one for analysis by HILIC/UPLC-MS/MS with negative ion mode ESI, and one sample was stored for backup. Samples were placed briefly on a TurboVap (Zymark) to remove the organic solvent. Sample extracts were stored overnight under nitrogen before preparation for analysis.

Quality Control (QC)

Several types of controls were analyzed in concert with the experimental samples: 1) pooled matrix sample generated by taking a small volume of each experimental sample, serving as a technical replicate; 2) extracted water sample as process blanks; 3) a cocktail of QC standards that were carefully chosen not to interfere with the measurement of endogenous compounds were spiked into each analyzed sample to monitor instrumental performance and aided chromatographic alignment. Instrument variability was determined by calculating the median relative standard deviation (RSD) for the standards that were added to each sample before injection into the mass spec machine. Overall process variability was determined by calculating the median RSD for all endogenous metabolites present in 100% of the pooled matrix samples. The median RSD of instrument variability and total process variability was 4% and 11% respectively. Experimental samples were randomized across the platform run with QC samples spaced evenly among the injections.

Ultrahigh Performance Liquid Chromatography-Tandem Mass Spectroscopy (UPLC-MS/MS)

All methods utilized a Waters ACQUITY ultra-performance liquid chromatography (UPLC) and a Thermo Scientific Q-Exactive high resolution/accurate mass spectrometer interfaced with a heated electrospray ionization (HESI-II) source and Orbitrap mass analyzer operated at 35,000 mass resolution. The sample extract was dried followed by reconstitution in solvents compatible to each of the four methods. Each reconstitution solvent contained a series of standards at fixed concentrations to ensure injection and chromatographic consistency. For hydrophilic compounds analyzed using acidic positive ion condition, the extract was gradient eluted from a C18 column (Water UPLC BEH C18-2.1x100 mm, 1.7 µm) using water and methanol, containing 0.05% perfluoropentanoic acid (PFPA) and 0.1% formic acid (FA). For hydrophobic compounds analyzed using acidic positive ion conditions, the extract was gradient eluted from the same C18 column using methanol, acetonitrile, water, 0.05% PFPA and 0.01% FA. Another aliquot was analyzed using a basic negative ion optimized condition and a separate dedicated C18 column. The basic extracts were gradient eluted form the column using methanol and water, with 6.5 mM ammonium bicarbonate at pH 8. The fourth aliquot was analyzed via negative ionization following elution from a HILIC column (Waters UPLC BEH Amide 2.1x150 mm, 1.7 µm) with a gradient of water and acetonitrile with 10 mM ammonium formate, pH 10.8. The scan range covered 70-1000 m/z.

Compound Identification, Quantification

Compounds were identified by comparison to library entries of purified standards or recurrent unknown entities. Biochemical identifications are based on three criteria: retention index within a narrow RI window of the proposed identification, accurate mass match to the library +/- 10 ppm, and the MS/MS forward and reverse score between the experimental data and authentic standards.

Metabolite Quantification and Data Normalization

Peaks were quantified using area-under-the-curve. Each compound was corrected in run-day blocks by registering the median to equal one (1.00) and normalizing each data point proportionately. Each biochemical in the original scale is rescaled to set the median equal to 1 and presented as scaled intensities.

Statistical analysis

Following log transformation and imputation of missing values, if any, with the minimum observed value for each compound, ANOVA contrasts were used to identify biochemicals that differed significantly between experimental groups. Two-way and three-way ANOVAs were used to identify biochemicals of significant interaction and main effects for experimental parameters of genotype, age and gender. A hierarchical clustering method was applied to the fatty acids with calculation of Euclidian distances and clustering by complete-linkage method in R statistical software.

4.4 Results

4.4.1 Overview of Global Metabolic Shifts in Aging and AD Mouse Brains

We determined the age and AD-associated shifts in brain metabolomics by unbiased untargeted UPLC/MS/MS. By methanol extraction of freshly isolated mouse hippocampus with overlying cortex (hereafter hippocampus) from NTg and 3xTg-AD mice of young, middle and old ages, we were able to detect and identify 567 metabolites including amino acids, peptides, carbohydrates, energic intermediates and lipids from a wide range of pathways. Significance of changes in metabolites were calculated by ANOVA for age, genotype and gender effects based on fold change of those metabolites. Notably, a large 44% of the detected metabolites were affected by age and 57% by gender **(Fig. 4.1)**. Additionally, 36% differed by genotype. 21% of the metabolites showed an interaction of genotype and age. To explore how much age contributes to the metabolic shifts in AD, we grouped metabolites into three categories: both genotypes decreased with age, increased or were discordant as presented in Venn diagrams (female and male combined) **(Fig. 4.1)**. Each circle area is proportional to the total number of metabolites. The overlapped area in **Fig. 4.1A** indicates proportions of down-regulated metabolites in both old age and AD, accounting for 43% of the NTg and 63% of the 3xTg-AD metabolites. Similarly, **Fig. 4.1B** shows the common up-regulated metabolites in both normal old age and 3xTg-AD mouse brains, constituting 62% and 54% respectively. This high level of coordinate responses in either down-regulation or up-regulation (50-60%) suggests age and AD share common patterns of metabolic shifts. Additionally, this may indicate old age metabolism increases the risk for AD incidence. Discordant metabolites shifted in opposite directions with age in NTg and 3xTg-AD samples were just 20% of the total ($p<$

0.05, genders combined, **Fig. 4.1C**). Among these disparate metabolites, 60% of the metabolites decreased in NTg but increased in 3xTg-AD samples with age (purple circle, **Fig. 4.1C**). 40% of the metabolites were enhanced in NTg old age but lowered in 3xTg-AD samples (orange circle, **Fig. 4.1C**). These disparate metabolites distinguished normal aging from AD, and therefore indicates specific metabolic features involved in the AD genotype.

Two-Way or Three-Way ANOVA (p≤ 0.05)	Genotype Main Effect	Age Main Effect	Gender Main Effect	Genotype, Gender Interaction	Genotype, Age Interaction	Age, Gender Interaction	Genotype, Age, Gender Interaction
567 Metabolites identified	204 (36%)	248 (44%)	322 (57%)	125 (22%)	121 (21%)	82 (14%)	95 (17%)

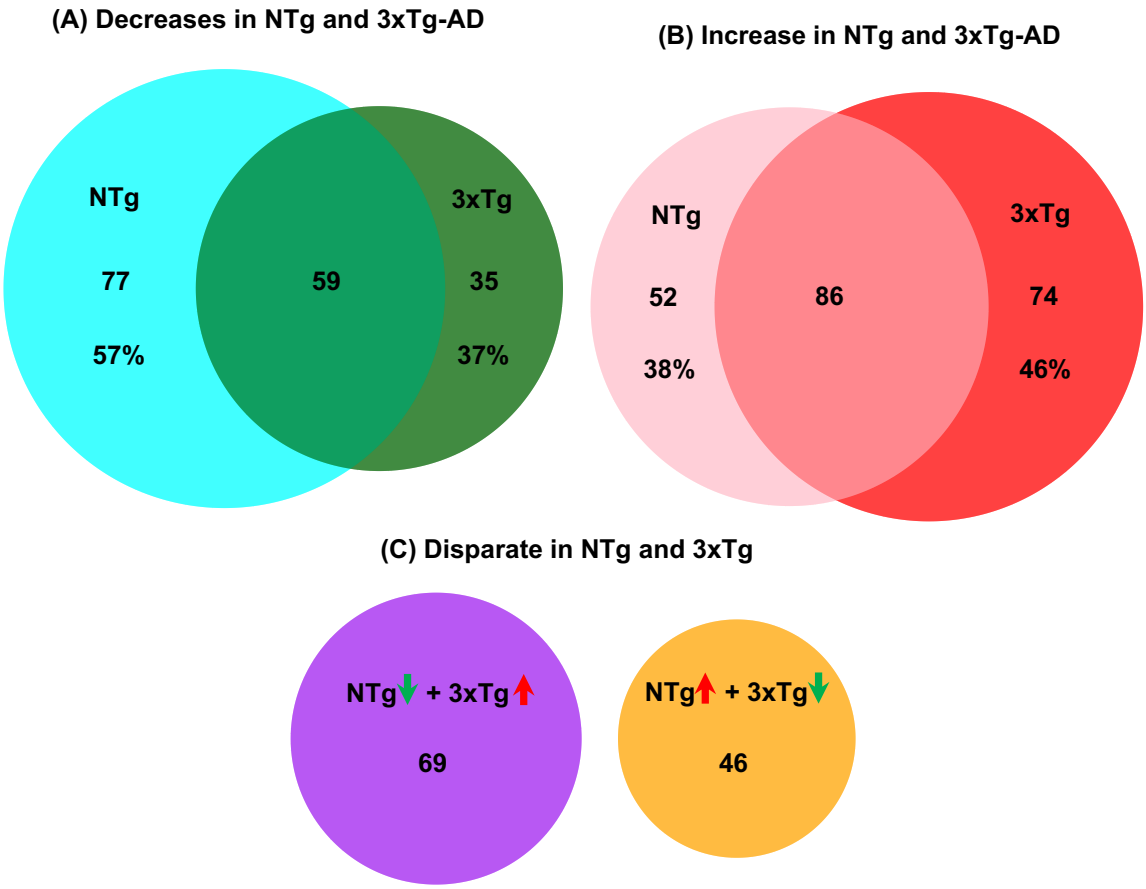

Figure 4.1. Majority of metabolites that change with age (old relative to young) coordinately respond in both NTg and 3xTg-AD mouse brains (female and male combined). Three-way ANOVA for genotype, age and gender identify 121 metabolites affected commonly by both genotype and age, accounting for 59% of genotype effects and 49% of age main effects**.** Numbers of biochemicals exhibiting main effects ($p \leq 0.05$) and significant interactions. **(A)** metabolites that decreased significantly in both NTg and 3xTg-AD ($p<0.05$). The cyan circle area represents the number of decreases in old NTg mouse brains (136 metabolites in total), similar to the dark green circle for 3xTg-AD mouse brains (94 total). The overlap area represents the common metabolites that decreased with aging in both NTg and 3xTg-AD. **(B)** significantly increased metabolites similarly age-related in NTg ($p<0.05$; pink circle, 138 in total) and 3xTg-AD (red circle, 160 metabolites total). with a large overlap area. **(C)** Number of NTg metabolites with significant opposite change with age of in 3xTg-AD mouse brains ($p<0.05$; purple circle NTg decreased; yellow circle NTg increased). Circle areas and overlaps are proportional to the number of metabolites.

4.4.2 Age-Related Metabolic Shift in Glycolytic and Pentose Phosphate Pathway (PPP) Metabolites

We examined the glycolytic pathway for low human utilization of glucose with age and AD in female mouse hippocampus and extended the specificity into steps of the glycolytic and PPP (**Fig. 4.2**). As glycolysis and the pentose phosphate pathways initially consume all the glucose from glucose-6-phosphate, we determined whether age and AD were associated with greater consumption of metabolites in these pathways. We observed that metabolites involved in consumption of ATP, including glucose, glucose 6-phosphate, fructose 6-phosphate and dihydroxyacetone phosphate (DHAP), decreased significantly with age of both genotypes. The largest decreases were found in glucose 6-phosphate and fructose-6 phosphate, which declined 51-52% in NTg and 27-38% in 3xTg-AD female with similar decreases in male. Given that glucose only declined 8-12% in female brains and less than 9% in male of both genotypes, this may indicate an age-related increase in consumption by energy producing steps of glycolysis and/or diversion into the PPP. Following glycolytic consumption of ATP and oxidation by NAD^+, the energy-generating steps of glycolysis were elevated with age (**Fig. 4.2**). 3-phosphoglycerate and phosphoenolpyruvate (PEP) were elevated 63-75% in NTg and 170-180% 3xTg-AD hippocampus in females with age, while these metabolites in males rose 114-119% in NTg and 90-91% in 3xTg-AD. This indicates that the input exceeds the consumption with age near the end of glycolysis. By genotype, these metabolites were 34-50% higher from 3xTg-AD hippocampi than NTg.

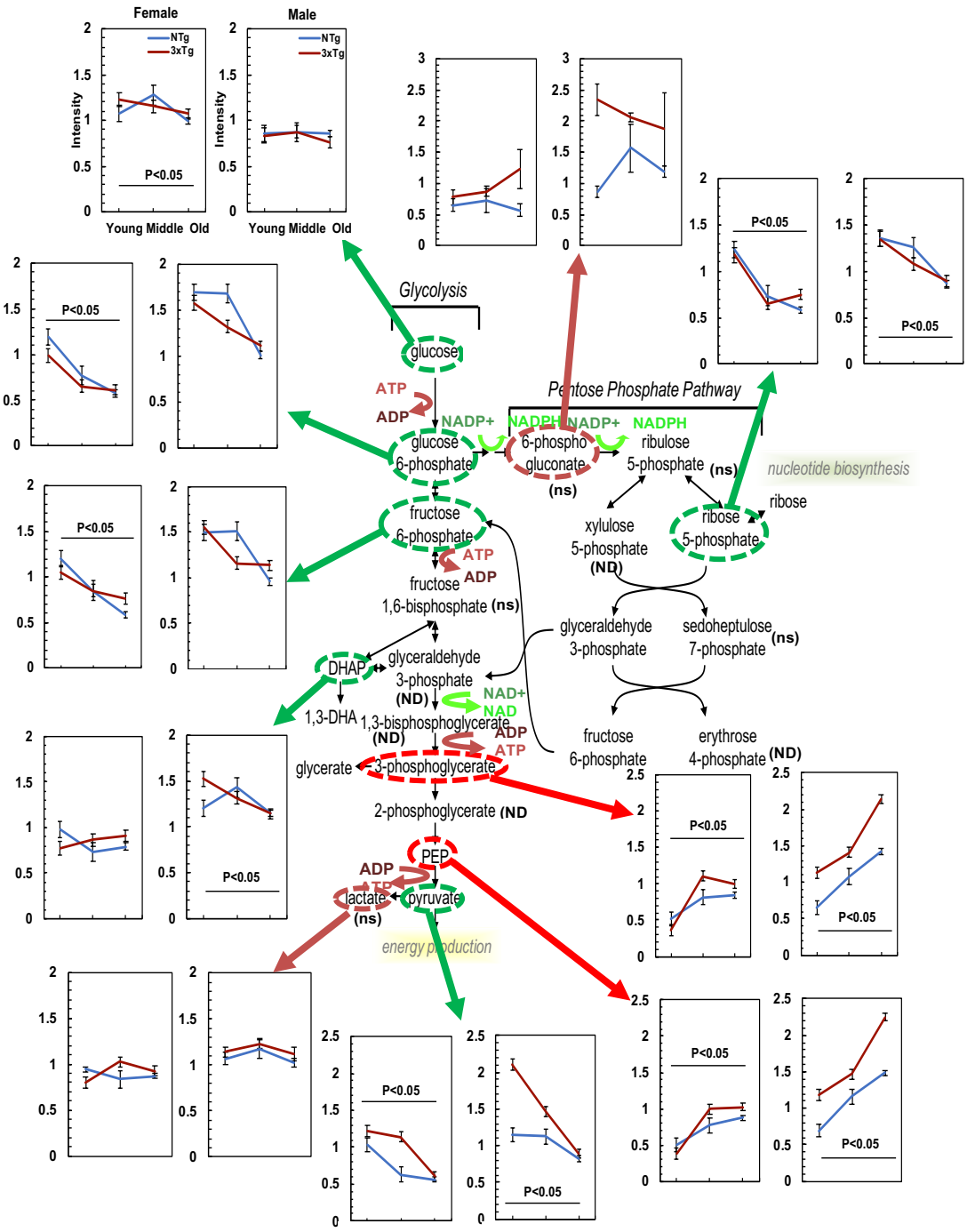

Figure 4.2. In glycolysis and the pentose phosphate pathway (PPP), hippocampal metabolites declined with age in reactions in which ATP was consumed (green circles with green arrows) and metabolites increased in reactions involved in ATP generation (red circle with red arrows). Intensities of identified metabolites from mass spectrometry in each hippocampal sample were normalized (n=5 mouse brain samples/age/genotype/gender). Mean intensity with standard errors in female (left) and male (right) for 3 ages of young, middle and old age. Two-way ANOVA was used to calculate statistical significance for each metabolite ($p<0.05$ indicates significant age effect). Ns indicates detection but not significantly affected by age; ND, no detectable.

The other possible pathway that could account for the age-related decrease in metabolites at the beginning of glycolysis would be diversion into the PPP (**Fig. 4.2**). As the first committed step in the PPP, we detected higher levels of 6-phosphogluconate, in 3xTg-AD than the age-matched NTg mouse brains (combined genders, $p < 0.05$), although it was not significantly changed with age. However, the downstream metabolite of ribose 5-phosphate in the PPP was 36-52% lower from young to old age of both genotypes and genders (**Fig. 4.2**). Age-related increased metabolic inputs in PPP from glycolysis with reduced levels in the downstream metabolite of ribose 5-phosphate suggests a higher consumption of intermediates in PPP to support NADPH generation for antioxidant defense. Ribulose 5-phosphate and sedoheptulose 7-phosphate in the PPP were not significantly changed with age. The PPP partially fluxes back into glycolysis at the points of glyceraldehyde 3-phosphate and fructose 6-phosphate (also decreased with age). Among the intermediates of ATP-consumed steps in glycolysis, only fructose 1,6-bisphosphate was found to be not significantly changed with age in either NTg and 3xTg-AD samples. In PPP, 6-phosphogluconate levels were 1.6 to 2-fold higher in 3xTg-AD old samples compared to age-matched NTg for both genders. The downstream intermediate ribose 5-phosphate showed remarkably age-dependent declines in both genotypes. These metabolites in the PPP pathway suggest either an age-dependent loss of antioxidant capacity in the PPP or a comparatively higher utilization of the PPP for more NADPH production and antioxidant defense with AD genetic load.

At the end of glycolysis, PEP is metabolized to pyruvate. Pyruvate is at a critical intersection to either branch to produce lactate or enter into the TCA cycle after

conversion into acetyl-CoA. Our results showed age-related 30-45% decreases in pyruvate of both genders for NTg and 50-58% decreases in 3xTg-AD samples (**Fig. 4.2**). This remarkable switch from an age-related increase in the PEP precursor to an age-related drop in pyruvate suggests an increased consumption of pyruvate with age, a re-direction in metabolic fluxes either into lactate or acetyl-CoA. A ratio of lactate to pyruvate (lactate/pyruvate) increased with age in female (Two-way ANOVA for age and genotype $F(2,29)= 14$, $p<0.001$) and male (Two-way ANOVA $F(2,29)= 12$, $p<0.001$). Compared to the young age, the lactate/pyruvate ratio in old-age brains increased 34-52% in NTg and 131-134% in 3xTg-AD samples of both genders. With age, the 30-50% drop in pyruvate of both genotypes and genders was not propagated to lactate levels (< 10% shifts with age), suggesting a balance between production and utilization of lactate or removal from the brain into the blood. The decreased levels of pyruvate suggest more output to branches of lactate or the TCA cycle. The lactate/pyruvate ratio can be regulated by the NAD/NADH ratio (Tilton et al., 1991). Metabolic flux experiments are needed for a definitive conclusion of an age-related decline in ATP production from glycolysis.

4.4.3 Age-Related Increased Inputs to the TCA Cycle with Decreased Cycle Metabolites

Increased fatty acid β-oxidation

To further explore if the age-related metabolic transition to lower pyruvate results in a lower metabolic state of the TCA cycle with age, we studied the age-related shifts in metabolite levels of the TCA cycle (**Fig. 4.3**). We first consider the inputs to the TCA cycle from fatty acids, glutamine and branched chain amino acids, followed by metabolites in

the cycle. Pyruvate enters the TCA cycle after conversion into acetyl-CoA. Fatty acid β-oxidation, also produces acetyl-CoA (pink highlight in **Fig. 4.3**). With age, acetyl-CoA levels increased 2 to 2.5-fold in both genotypes and genders. With AD genetic load, acetyl-CoA was 23% and 121% higher in 3xTg-AD old samples with comparatively larger in male brains with age. This suggests an increased production or a decreased consumption of acetyl-CoA in the TCA cycle with age that was further exacerbated with AD genetic load, indicating higher demand for energy.

Elevated glutamine

Other increased input to the TCA cycle occurs from glutamine and branched chain amino acids (BCAA). Glutamine feeds into the TCA cycle at the level of α-ketoglutarate (**Fig. 4.3**) and serves as an important source of intermediary metabolites (Waagepetersen et al., 1999). With aging, glutamine levels rose 7 to 27 % for both genotypes and genders. Yet another metabolite branch to α-ketoglutarate, 2-hydroxyglutarate levels increased 1.5 to 6.5-fold in 3xTg-AD compared to NTg samples in both genders ($p < 0.001$). However, α-ketoglutarate levels changed little with aging. The age- and AD-associated accumulation in glutamine and 2-hydroxyglutarate levels without significant change in α-ketoglutarate levels indicates a possible age- and AD-related blockage at the site of α-ketoglutarate for metabolic input to the TCA cycle.

Branched Chain Amino Acids (BCAAs) Increased in Females

BCAAs include leucine, isoleucine and valine. Since BCAA are converted into acetyl or succinyl-CoA in the TCA cycle for NADH and for eventual ATP generation, we examined

their changes with age, genotype and gender. Leucine, isoleucine and valine were1.2-1.3-fold higher in female samples than male ($p < 0.05$). Changes with age or genotype were not detected.

Decreased Metabolites in TCA Cycle

In the TCA cycle itself, metabolites decreased considerably with age, including citrate, cis-aconitate in both genders and succinate in males (green circles and green arrows in **Fig. 3**). In females, citrate and cis-aconitate dropped 46-47% in NTg and 30-35% in 3xTg-AD with age. In males, age drove decreases of citrate and cis-aconitate by 26-28% in NTg and 8-13% in 3xTg-AD. Succinate declined from middle to old age by 25%-28% in males of both genotypes, but not in females. TCA cycle metabolites of the 3xTg-AD brains were generally lower than the age-matched NTg mouse brains. Other metabolites in the TCA cycle including α-ketoglutarate, fumarate and malate were detected with little age-related changes. Isocitrate, succinyl-CoA and oxaloacetate were not detected. In summary, the combination of age-related increased inputs to the TCA cycle together with decreased TCA cycle metabolites suggests age-related limitations in utilization of the inputs by the TCA cycle and consequent decreased output of NADH with age and AD.

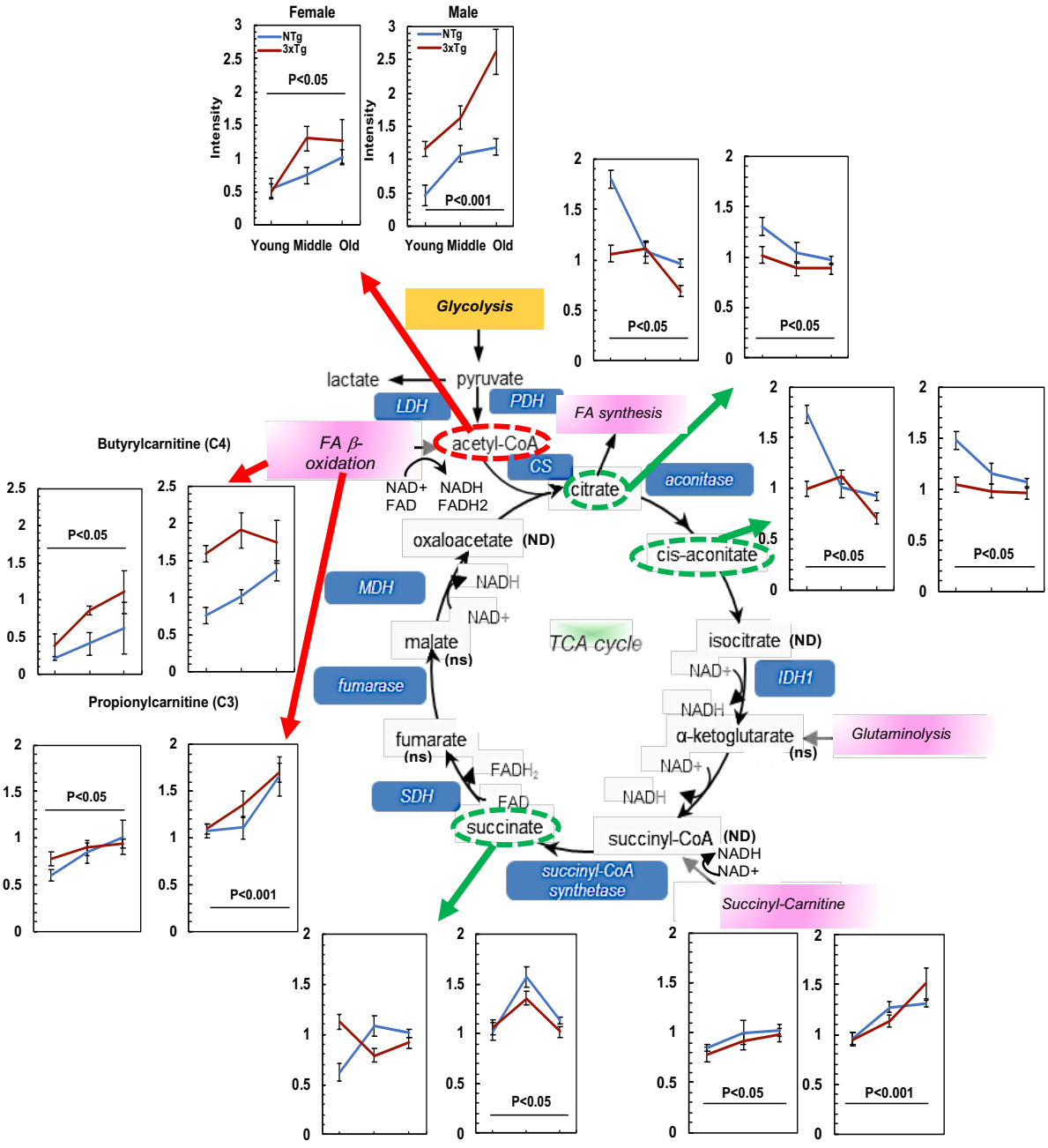

Figure 4.3. Age-related declines in the substrates of the TCA cycle from increased inputs at acetyl-CoA, succinyl carnitine and fatty acid metabolism. Ns indicates detection but not significantly affected by age; ND, not detectable.

4.4.4 Age- and AD-Associated Redox Pivot at Glutamate-α-Ketoglutarate in Glutamine Metabolism

In the glutamate-glutamine cycle, astrocytic release of glutamine is transported into neurons to synthesize neurotransmitters glutamate or GABA and maintain glutamine/ glutamate pools (Kam and Nicoli, 2007) and redox balance. Glutamate dehydrogenase (GDH) catalyzes the interconversion of glutamate to α-ketoglutarate modulated by a redox sensitive site depending on NAD+/NADH levels (Ödman et al., 2004). Depletion of glutamate-glutamine and gamma-aminobutyric acid (GABA) were reported recently in normal aged human brains and cognitively impaired patients by magnetic resonance spectroscopy (MRS) (Huang et al., 2017). These metabolites feed into α-ketoglutarate which functions as a critical NAD^+/NADH-dependent substrate in the TCA cycle. We determined metabolic shifts in glutamate with aging as an important upstream substrate via glutamate dehydrogenase (GDH). Glutamine increased 7-27% with age in both genotypes and genders (**Fig 4.4**). Glutamate levels declined 7% with age in males of both genotypes, but female levels were unchanged (**Fig 4.4**). Gamma-aminobutyric acid (GABA) as a major inhibitory transmitter in the brain declined 14-16% with age in females of both NTg and 3xTg-AD samples. N-acetylaspartyl glutamate (NAAG) decreased 9-36% in both genders and N-acetylaspartate (NAA) declined 10-23% with age in males of both genotypes (**Fig 4.4**). Given that the brain levels of NAA correlate with cognitive function (Meyerhoff et al., 1993), the lower levels of NAAG and NAA may contribute to cognitive impairments in age and AD. Aspartate was detected with less significant shifts with age of both genotypes in female ($p=0.12$) and male ($p=0.25$) (figure not shown). Our results are in accordance with decreased glutamate neurotransmission in AD patients

(Lin et al., 2003). Taken together, these shifts in glutamate metabolism with age may impair neuronal transmission.

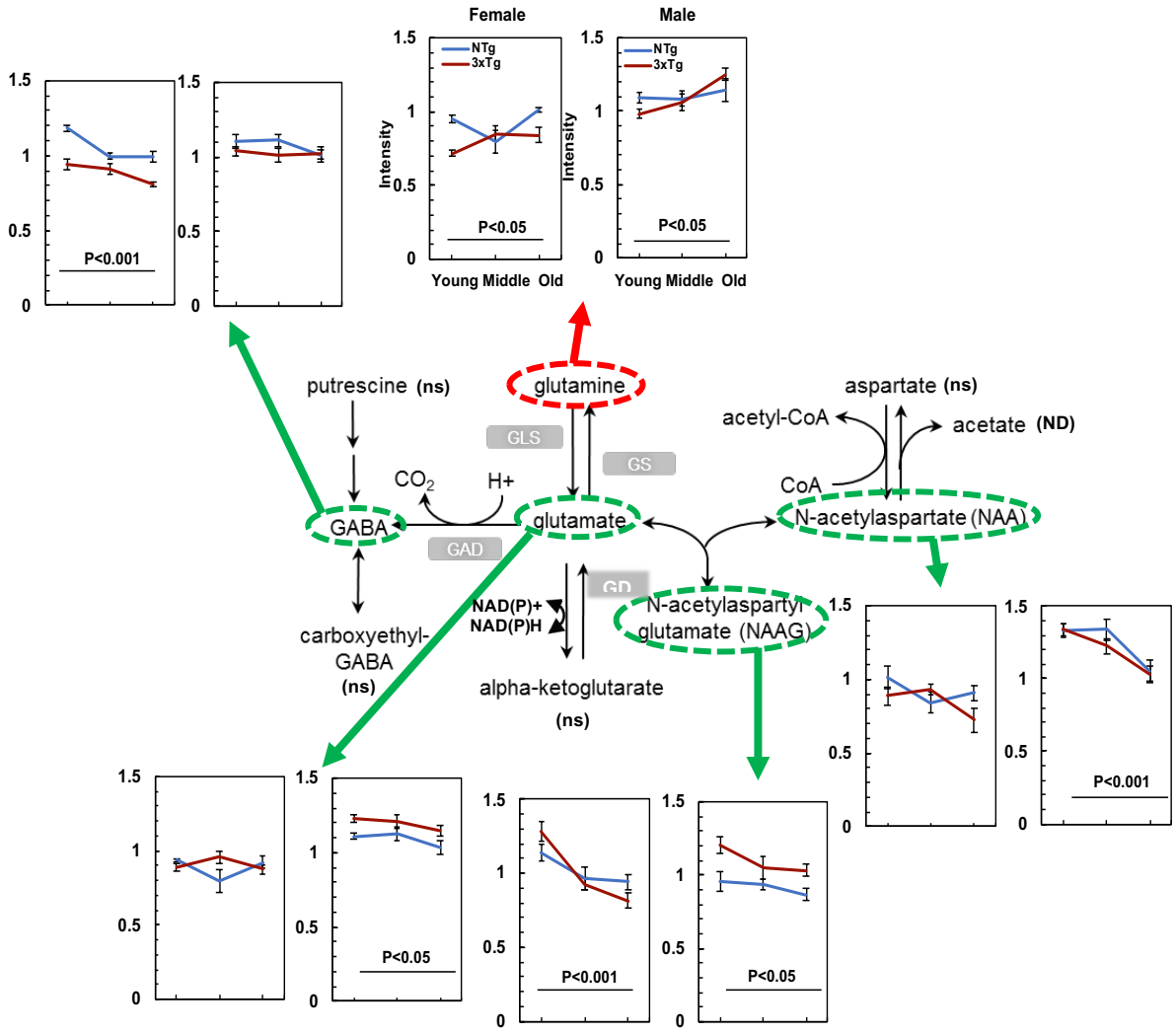

Figure 4.4. Age-related decreased glutamate metabolism from increased glutamine in both NTg and 3xTg-AD mice. Age drove decreases in the levels of glutamate, NAA and NAAG, which suggests a lower input to α-ketoglutarate in the TCA cycle or greater consumption. Ns indicates detection but not significantly affected by age; ND, no detectable. GLS: Glutaminase, GS: Glutamine synthetase, GAD: Glutamate decarboxylase, GDH: Glutamate dehydrogenase

4.4.5 Increased Fatty Acid Metabolites with Age

During energetic shortage with lower glucose intake or lower ATP generation via glycolysis and the TCA cycle, fatty acids undergo β-oxidation with production of acetyl-CoA and NADH to power energy production and maintain redox balance (Houten and Wander, 2010). Carnitine is conjugated to fatty acids for transport into mitochondria. **Fig. 4.3** shows that metabolites of butyrylcarnitine (C4) and propionylcarnitine (C3) in the short chain fatty acid pathway increased with age 1.2-2.9-fold in female and 1.1-1.8-fold in male as their dehydrogenase consumes NAD^+ to provide acetyl-CoA and NADH inputs. Compared to NTg, in old age, the AD genetic load increased levels of butyrylcarnitine (C4) 77% in female and 28% in male. Other metabolites of carnitine metabolism including carnitine and acetylcarnitine (C2) showed 1.5 to 2.5-fold elevations with aging in both NTg and 3xTg-AD samples (not shown, $p< 0.05$). To globally view fatty acid metabolites, their direction and magnitude were clustered to demonstrate a wide range of age-related increases with both genotypes and genders (**Fig. 4.5**). Each metabolite with a significant age-associated (gender and genotype) shift by two-way ANOVA is shown. After calculation of Euclidean distances and clustering distances, the heatmap pattern showed a strong age effect for up-regulation of fatty acid metabolism (x-axis). After clustering of the levels of fatty acids, we observed a strong age effect that drove 2-fold elevations of fatty acids (**Fig. 4.5**). Further, AD genetic load drove 21-22% more elevations of fatty acid metabolism in old 3xTg-AD samples compared to those of NTg for both female ($p<10^{-23}$) and male ($p< 10^{-17}$) samples. The age and AD up-regulation in fatty acid metabolism drove 1.8 to 2.6-fold elevations of acetyl-CoA in old versus young neurons as a final product of fatty acid β-oxidation for entry into the TCA cycle (**Fig. 4.3**). The global

upregulation in fatty acid metabolism with age suggests an age-related demand for more energetically dense substrates than carbohydrates to generate maximum NADH from 3-hydroxyacyl-CoA dehydrogenase or impairment the TCA cycle to use the resulting CoA with aging [49]. Furthermore, the greater upregulation in fatty acid metabolism in 3xTg-AD old brains compared to old NTg suggests a greater demand for energy in the aged 3xTg-AD brains. Elevation of numerous fatty acids with age and AD together with their carnitine conjugates could supply energy by their β-oxidation.

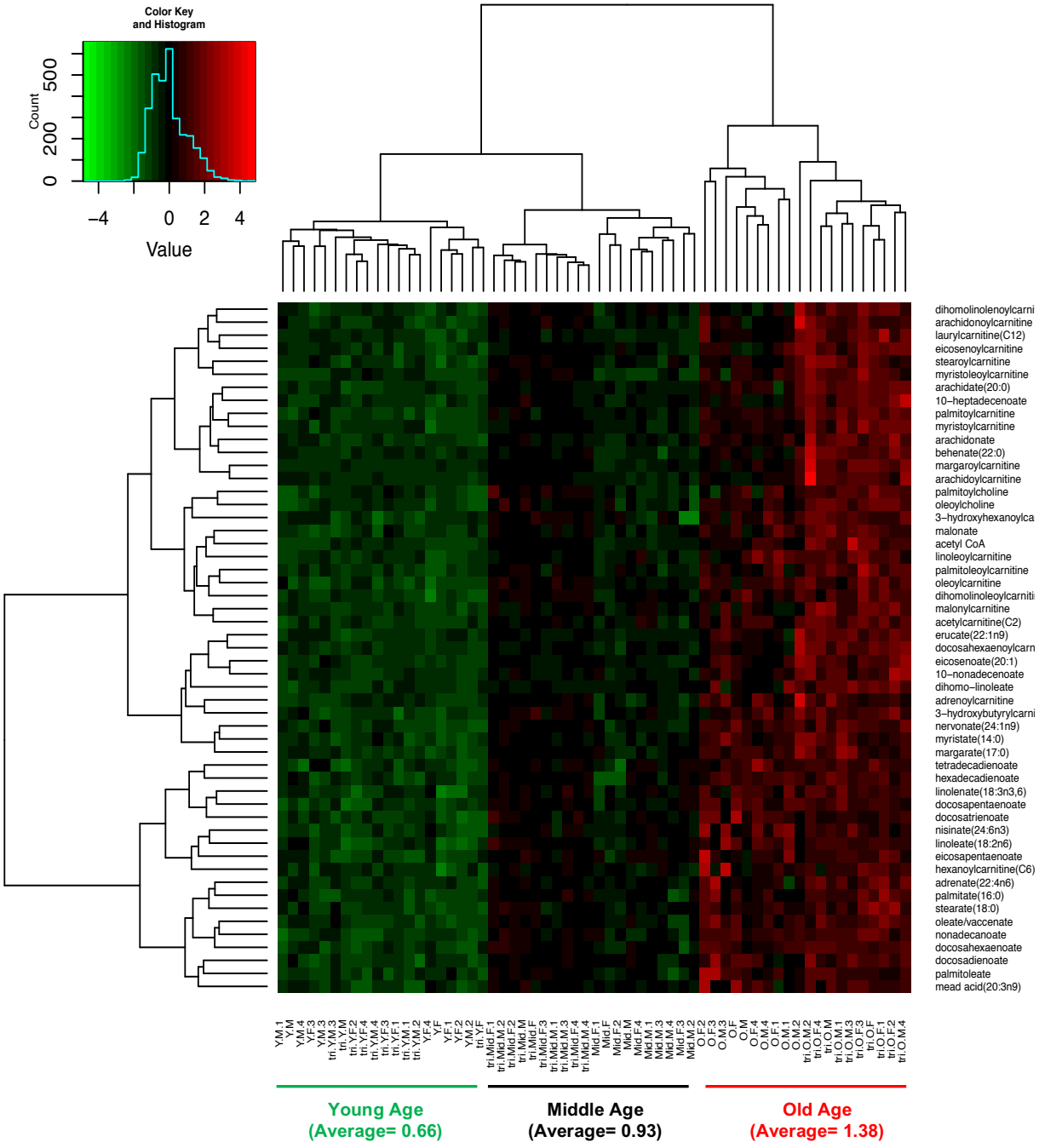

Figure 4.5. Elevated fatty acid metabolites cluster by age and genotype in both females and males. Scaled intensity of each metabolite in each sample was clustered in rows and columns. Differences in levels were clustered predominantly by age. Genotype effects were remarkably distinguished starting from middle age. Gender was less affected. Green indicates a lower scaled intensity and red indicates a higher scaled intensity. tri=3xTg-AD, non-tri=NTg, Y=young, M=middle-age, O=old, un-numbered, 1, 2, 3, 4 = sample number from different mice.

4.4.6 Age- and AD-Related Lower Expression in Sphingolipid Metabolism in Mouse Brains

Sphingolipids play numerous functions in cells, from structural components (sphingomyelins) to signaling (ceramides, sphingosine-1-phosphate). Sphingomyelins are important constituents of lipid rafts, which are particularly enriched in the central nervous system [50]. With age, sphinganine decreased 31-42% (**Fig. 4.6**) and sphingomyelin declined 14-29% with age of both genotypes and genders. Ceramides serve signaling functions, including apoptosis and inflammation, which have been associated with pathogenesis of AD [51]. In sphingolipid metabolism, the downstream intermediates including ceramide, sphingosine and sphingosine-1-phosphate were increased 27-143% with age in 3xTg-AD male brains (**Fig. 4.6**). The increased ceramides are consistent with higher inflammation with age, especially in the male AD genotype.

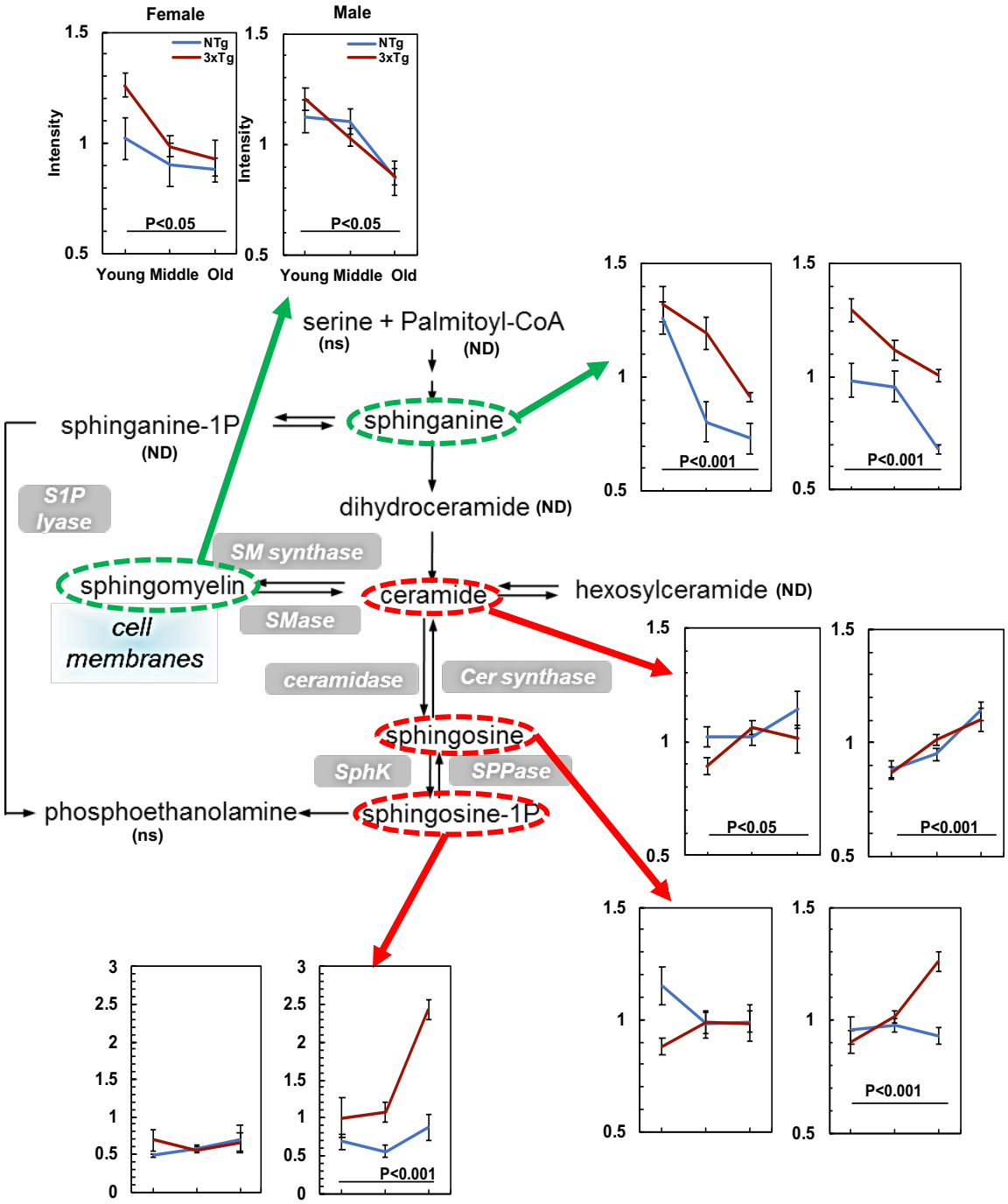

Figure 4.6. Age-related changes in sphingolipid metabolism of both NTg and 3xTg-AD suggest increased inflammation. Age drove significant declines in sphinganine and sphingomyelin (green ovals and arrows), but elevated the downstream metabolites of sphingolipid metabolism, including ceramide, sphingosine and sphingosine-1P in both NTg and 3xTg-AD female and male samples (red ovals and arrows). Ns indicates detection but not significantly affected by age; ND, no detectable.

4.4.7 Age-related Metabolic Shifts Sensed at NAD^+/NADH Redox Reactions

Since we found age- and AD-related depletion in the NAD pool size and free NADH levels in mitochondria of hippocampal neurons from NTg and 3xTg-AD mouse brains (Dong et al., 2019) and an increased ratio of NAD^+/NADH indicating an oxidative shift in these mice (Ghosh et al., 2012) we specifically examined metabolite levels upstream and downstream of dehydrogenases that sense the NAD^+/NADH redox sites. **Table 4.1** dichotomizes fold-changes with age in upstream substrates of 9 dehydrogenases compared to their downstream metabolites. Interestingly, in energy-producing metabolic pathways, including glycolysis and the TCA cycle, age drove decreased levels of the upstream substrates of dehydrogenases while downstream substrates increased in both of NTg (T-test upstream vs. downstream substrates, $p= 3x10^{-7}$, n=8 reactions, 18 upstream metabolites vs. 10 downstream metabolites) and 3xTg-AD (T-test, $p= 4x10^{-5}$). Glycolytic substrates were markedly depleted upstream of GAPDH, while GAPDH downstream products were enriched 2.7- 2.8-fold, especially in female 3xTg-AD. Small decrease in lactate in NTg product may indicate utilization by neurons as described; small increase in 3xTg-AD may indicate failure to do so because of susceptibility to acidosis (Brewer, 1997). In the TCA cycle, αKG was actually decreased, but only 1.1- 1.2-fold in 3xTg-AD. Overall, for NTg, age drove a 2.5-fold metabolic shift in the upstream versus downstream substrates of dehydrogenases and a slightly lower with 2.3-fold metabolic shift in 3xTg-AD samples (**Table 4.1**). These overall age-associated effects on decreased upstream substrate levels with increased downstream substrate levels suggests an age-related rise in NAD^+-dependent dehydrogenase rates to make NADH with a decreased ability to process the products leading to accumulated levels of downstream metabolites.

Other energy-redox components were detected but showed less significant changes with age, including coenzyme A (CoA), flavin adenine dinucleotide (FAD), flavin mononucleotide (FMN) and NAD ($p \geq 0.05$). Further redox-controlled enzymatic measurements in aging and 3xTg-AD mouse brains will need to be completed for validation. In BCAA metabolism catalyzed by branched-chain α-ketoacid dehydrogenase complex (BCKDH complex), the last step is to re-oxidize $FADH_2$ to FAD while reducing NAD^+ to NADH. BCKDH converts BCAAs into acyl-CoA derivatives, which are converted into acetyl-CoA or succinyl-CoA. Overall, we found age-related 2-fold increases in acetyl-CoA for input into the TCA cycle in hippocampal neurons from both NTg and 3xTg-AD genotypes.

Based on our observations, we considered whether age- and AD- associated oxidized in NAD^+/NADH redox potentials, triggered the metabolic shifts sensed at the NAD^+/NADH redox sites in the enzymatic reactions and drove the direction for more NADH and ATP generation as a compensatory effect in response to the energetic deficits for NADH and ATP replenishment. However, age- and AD- related oxidized shifts impaired mitochondrial functions and lower the activities in TCA cycle and ETC-OXPHOS resulting in declines NADH production from the TCA cycle and further leading to an energetic shortage state with insufficient ATP levels. Supported by our results, we observed dramatically up-regulated metabolic branches feeding into the TCA cycle including fatty acid oxidation, BCAA metabolism and glutaminolysis. Whereas the metabolite levels in TCA cycle decreased with aging and AD. This suggests the either lower activities of the

enzymatic rates or blockage in TCA cycle and ETC-OXPHOS due to oxidized impairment in mitochondria during aging and AD.

Table 4.1. Age-related metabolic shifts in upstream and downstream of redox dehydrogenases (fold change with age)

	Upstream Substrate	NTg			3xTg-AD			Downstream Product	NTg			3xTg-AD		
		F	M	**Avg.**	F	M	**Avg.**		F	M	**Avg.**	F	M	**Avg.**
Glycolysis														
GAPDH	**G6P**	-2	-1.7		-1.6	-1.4		**3PG**	1.6	2		2.8	1.9	
	F6P	-2	-1.6		-1.4	-1.4		**PEP**	1.7	2		2.7	1.9	
	DHAP	-1.2	-1.1		1.2	-1.3		***c**						
LDH	**Pyruvate**	-1.8	-1.4		-2	-2.4		**lactate**	-1.08	*b		1.15	*b	
	Avg.(F+M)			-1.60			-1.29	**Avg.(F+M)**			1.24			2.09
	S.E.			0.13			0.41	**S.E.**			0.66			0.34
	N =			8			8	**N =**			5			5
TCA cycle														
PDH	**Pyruvate**	-1.8	-1.4		-2	-2.4		**Acetyl-CoA**	1.8	2.6		2.5	2.3	
IDH	**Cis-aconitate**	-1.9	-1.4		-1.4	-1.1		**a-KG**	1.17	-1.1		-1.08	-1.2	
GDH	**Glutamate**	*b	-1.1		*b	-1.1		***c**						
KGDHC	**a-KG**	1.17	-1.1		-1.08	-1.2		**ND**						
SDH	**Succinate**	-1.1	-1.4	*a	-1.2	-1.3	*a	**Fumarate**	*b	1.4		-1.2	-1.3	
MDH	**Malate**	*b	-1.1		*b	-1.1		**ND**						
	Avg.(F+M)			-1.11			-1.39	**Avg.(F+M)**			1.17			0.0033
	S.E.			0.28			0.15	**S.E.**			0.69			0.83
	N =			10			10	**N =**			5			6
Total Effect	**Avg.(F+M)**			-1.33			-1.34	**Avg.(F+M)**			1.21			0.95
	S.E.			0.17			0.19	**S.E.**			0.42			0.56
	N =			18			18	**N =**			10			11

T-test (Up vs Down)

	NTg	**3xTg**
p value	**3E-07**	**4E-05**

Fold change with age = larger values / smaller values in young vs. old measurements
*a: middle-age vs. old
*b: missing value ratio was 1.0, which could not be assigned a negative or positive direction
*c: metabolites already listed
"+" indicates metabolite levels increased with age; "-" indicates metabolite level decreased with age

GAPDH: Glyceraldehyde 3-phosphate dehydrogenase
LDH: Lactate dehydrogenase

PDH: Pyruvate dehydrogenase
IDH: Isocitrate dehydrogenase
GDH: Glutamate dehydrogenase
KGDHC: Alpha-ketoglutarate-dehydrogenase complex
SDH: Succinate dehydrogenase

F: Female; M: Male

4.5 Discussion

In this work, we determined the age-, AD- and gender-associated global metabolomic shifts of mouse hippocampal tissue by using untargeted (unbiased) UPLC-MS/MS. We observed specific metabolic features and patterns in age and AD mouse brains including glycolysis, TCA cycle, glutamate metabolism, fatty acid metabolism and sphingolipid metabolism, suggesting shifts in metabolic pathways. Moreover, many of the metabolic shifts were common to both age and AD-genotype. Of note, our results showed age-related deficiencies in energy-generating pathways in glycolysis and the TCA cycle. In the glycolysis-PPP pathways, we observed declines in the first half of glycolysis involved in ATP consumption and downstream intermediates in PPP. Metabolites in the second half of glycolysis associated with ATP production were up-regulated in old age of both NTg and 3xTg-AD. As the detected metabolic profiles in different ages, genotypes and genders were steady-state snap shots, the metabolite levels reflect net effects of upstream enzymatic production and downstream enzymatic consumption. We propose that these metabolic shifts serve not only to maximize ATP production to meet increased age and AD-related demand, but also serve to maintain redox balance and maximize NADH production for maximum generation of ATP from oxidative phosphorylation (Brewer, 2010). Interestingly, this energetic shift occurs at the 9 NAD-dependent dehydrogenase steps in glycolysis, the TCA cycle and inputs to the TCA cycle that we feature in **Table 4.1.** We noticed remarkable declines in substrates with increases in products for both genotypes. This indicates that with age, dehydrogenases in old age neurons operate to consume substrates at faster rates than that of younger ages leading to age-related accumulations of downstream products. This scenario is consistent with

greater energy demands with age. However, since the NAD pool (NAD+NADH+NADP+NADPH) declines with age systemically (Imai and Guarente, 2014) and in our mouse brains (Ghosh et al., 2012), NADH available for oxidative phosphorylation would also decline. We found that the free NADH available in mitochondria declines with age by 43% in the same NTg mouse hippocampal regions and 50% with age in the 3xTg-AD (Dong et al., 2019). Together, these results suggest a critical NAD^+/NADH role in regulation of metabolism as a redox sensor in aging and AD. The age- and AD-related depletion on NAD and NADH pool sizes may limit the activities of dehydrogenases, metabolic shifts and ATP production. Besides, the age-and AD-related energy deficits, we observed enhanced input to the PPP pathway with lower downstream intermediates with age. This suggests a response to oxidative stress in age and AD brains that causes a rise in PPP with more NADPH production for antioxidant defense. Perturbations in glutamate and sphingolipid metabolisms suggested age- and AD-related impairments at synapses and in myelinated axons involved with memory.

4.5.1 Glycolysis and the TCA Cycle

Compared to non-demented controls, positron emission tomography with 2-deoxy-2-[fluorine-18]-D-glucose (^{18}F-FDG PET) in AD patients exhibit a metabolic pattern of bilateral temporo-parietal hypometabolism (Hoffman et al., 2000) and reduced blood flow (Maki and Resnick, 2000). We observed greater age- and AD-associated declines of glucose levels in hippocampal regions in females. Altered glucose levels were the net effects of a failure to increase glucose uptake under stress (Patel and Brewer, 2003) and consumption in the downstream metabolic pathways including the glycolysis-PPP

pathway. Further, we found aging dramatically up-regulated intermediates in glycolytic steps of ATP production including 3-phosphoglycerate and phosphoenol pyruvate. Moreover, AD genetic load drove increases two-fold higher than the age-matched NTg male samples. Downstream of the NAD^+-dependent GAPDH, pyruvate levels decreased as much as 2-fold, especially in the 3xTg-AD samples. Administration of pyruvate prevented the development of age-related cognitive impairments in 3xTg-AD mouse brains without reducing AD pathologies of amyloid and tau (Isopi et al., 2015). Pyruvate as the end metabolite in glycolysis is transported into mitochondria via the mitochondrial pyruvate carrier (MPC). Inhibition of MPC was reported to diminish the neurodegeneration in Parkinson's disease (PD) by augmentation of autophagy (Ghosh et al., 2016; Quansah et al., 2018). The TCA cycle plays a central role in glucose metabolism with multiple points of influx at different intermediate sites, such as fatty acid β-oxidation via acetyl-CoA, BCCA catabolism via succinyl-CoA and glutamine-glutamate metabolism via α-ketoglutarate, aspartate and phenylalanine. In AD patients, mitochondrial abnormalities are associated with decreases of enzymatic activity in the first half of the TCA cycle, including pyruvate dehydrogenase (PDHC), isocitrate dehydrogenase (ICDH) and α-ketoglutarate dehydrogenase (KGDHC) (Bubber et al., 2005), but an age-related basis for these changes has not been determined and their fluxes *in vivo* depend on substrate and product concentrations. When the thiamine-dependent KGDHC was deprived of thiamine in an AD mouse model, mitochondrial KGDHC activity decreased 43% and promoted early formation of plaques and tangles (Karuppagounder et al., 2007). Activity of cytochrome c oxidase (COX) decreased by 50% with age from 3 to 12-months in 3xTg-AD female mouse brain and PDH activity declined by 55% (Yao et al., 2009). PDH activity

in brain mitochondria was also found to be decreased by 25% and 45% in mitochondria from 14- month and 24- month old rat brains (Zhou et al., 2009). In our results, we observed up to 2-fold declines in pyruvate levels with age, worse in the AD-genotype, followed by 2-fold increases of acetyl-CoA with higher levels in the 3xTg-AD. Nearly 60% of nuclear genes encoding subunits of mitochondrial electron transport chain showed significantly lower expression in hippocampal CA1 of human AD cases brains (Liang et al., 2008). Together, these results suggest that during aging and AD, the lower activity of the TCA cycle may indicate a metabolic-energy blockage to power ATP generation in the ETC-OXPHOS pathways.

4.5.2 Inputs to the TCA Cycle

Among those metabolites that provide influx into the TCA cycle, fatty acids for β-oxidation and glutamine were upregulated with age and AD, possibly indicating a cellular need for maximizing generation of energy. The downregulated intermediates with age and AD in the TCA cycle together with accumulated inputs to TCA cycle suggest a lower capacity for load-driven demand for NADH to make ATP via the TCA cycle-OXPHOS pathways. A neuron energy crisis with reduced ATP synthesis can cascade into ionic pump dysfunction (Carageorgiou et al., 2008), signal transduction breakdown (Saitoh et al., 1993), neurotransmitter failure (Paula-Lima et al., 2013), increased cleavage of the amyloid precursor protein (APP) (Gabuzda et al., 1994), microtubule damage (Yanagisawa et al., 1999), tau hyperphosphorylation (Hoyer, 2007), which all promote neurodegeneration and region-specific neuroglial death (De La Torre, 2008). Together with the observation of “mitochondria-on-a-string” due to mitochondrial fission in 5

transgenic AD mouse models and brain tissue of AD patients (Zhang et al., 2016) and decreased free NADH levels with age and AD in 3xTg-AD brains (Dong et al., 2019), these results are consistent with the hypothesis that age-related mitochondrial metabolic deficits pivoting at NAD^+/NADH redox sensitive sites contribute to the systematic complexity of brain aging and AD.

4.5.3 Fatty Acid Oxidation

Redox steps in fatty acid β-oxidation first involve oxidation by FAD in acyl-CoA dehydrogenase followed by an oxidation by NAD^+ in 3-hydroxyacyl-CoA dehydrogenase inside mitochondria (Wakil, 1956). An age-related oxidized NAD^+/NADH redox state promote FA oxidation by converting NAD^+ to NADH and FAD into FADH2. We observed a 2-fold elevation in fatty acid oxidation with aging in NTg and 3xTg-AD mouse brains, suggesting that fatty acid β-oxidation may be driven by an oxidized redox state with aging. In each cycle of oxidation, two carbons are cleaved from a fatty acid to release acetyl-CoA. During the last step of each FA oxidation cycle, thiolase cleaves between the C2 and C3 of 3-ketoacyl-CoA to release two carbons as acetyl-CoA. The generated acetyl-CoA enters the TCA cycle for more NADH production to power OXPHOS and the generation of ATP. Interestingly, the thiolase that catalyzes two acetyl-CoA molecules to form acetoacetyl-CoA in Clostridium has a regulatory redox-switch (Kim et al., 2015). As the redox potential of NAD^+/NADH is oxidized with aging and AD, this could drive the direction of FA oxidation reactions for more acetyl-CoA production. The age- and AD-related increased fatty acid β-oxidation and elevated production of acetyl-CoA could be a metabolic response to lessen energetic shortages. Adiponectin secreted by adipocytes

plays an important role in stimulating glucose utilization and fatty acid oxidation via activation of 5'-AMP-activated protein kinase (AMPK), suggesting a novel intervention to regulate glucose and fatty acid metabolism (Yamauchi et al., 2002). Efforts to elevate acetyl-CoA by overexpression of AT-1 in mice results in a progeria phenotype (Peng et al., 2018), suggesting that raising acetyl-CoA is limited or outright pathologic. Moreover, disturbances of fatty acid metabolism and increased in PUFAs in age and AD brains is associated with up-regulation of inflammatory signaling in neurodegenerative diseases (DeLegge and Smoke, 2008). Increased PUFAs provide prostaglandins, leukotrienes and thromboxanes, which increase inflammatory signaling (Calder, 2006), further promoting neurodegenerative processes. An mRNA microarray study on 759 innate immune genes, from human brains with AD and normal cognitive controls, revealed widespread upregulation of genes associated with inflammation in human aging correlated to cognitive declines (Cribbs et al., 2012). Another study found elevated blood levels of fatty acids in MCI prognostic for conversion to AD (Mapstone et al., 2014).

4.5.4 Branched Chain Amino Acids (BCAAs)

Although we did not find age-related hippocampal changes in isoleucine, leucine or valine, their oxidation by NAD^+ in the BCKDH complex produces NADH, to maintain redox balance and feed OXPHOS. Increased BCAA metabolites in human plasma such as isoleucine are positively correlated with AD (Larsson and Markus, 2017). BCAAs are elevated with age in serum of human AD and 3xTg-AD mice (Li et al., 2018). The important question is whether this is protective or pathologic. In the 3xTg-AD mouse fed with a BCAA-supplemented high-fat diet for 2 months, tau and amyloid pathologies

worsened leading to an increase in the mortality of two-thirds of the mice from 6 to 16 months (Tournissac et al., 2018). This intervention suggests that BCAA and fatty acids are not limiting to energy production and that excess levels are pathologic, but systemic stress could also be important, independent of brain metabolism. Conversely, a low BCAA diet was found to improve recognition memory in 18-month-old 3xTg-AD mice (Tournissac et al., 2018). Taken together, the BCAA metabolites levels in plasma may serve as a biomarker for an AD metabolic switch and pathology.

4.5.5 Lactate

Our results showed remarkable increases in the ratio of lactate/pyruvate levels as a function of age in both NTg and 3xTg-AD mouse brains. Notably, declines in pyruvate with small changes in lactate levels with aging and AD, indicate a balance of rates between production of lactate by LDH and the rates of either utilization or removal into blood. Alternative energy supplies were found to be upregulated in age and AD brains, such as lactate (Magistretti and Allaman, 2018) and ketone bodies (KB) (Ding et al., 2013). Lactate increased 1.5-fold in AD patient serum compared to the healthy control subjects (González-Domínguez et al., 2015). CSF lactate levels in AD patients increased 20% compared to age-matched controls (Liguori et al., 2016). Lactate increased two-fold with age in mtDNA mutator mice with a metabolic shift from pyruvate to more lactate production (Ross et al., 2010). Lactate is a preferred energy substrate to maintain redox balance and neuronal activity especially during glucose deprivation (Magistretti and Allaman, 2018). Memory in rats was dependent on neuronal import of lactate from astrocytes via the monocarboxylate transporter (Newman et al., 2011). Astrocyte-neuron

lactate transport is critical for long-term memory formation (Suzuki et al., 2011). In aging wild-type mouse brains, improved memory performance correlated with elevated expression of glycolytic enzymes. Yet this age-related increase in glycolytic enzyme expression with elevated lactate levels in APP/PS1 mice were associated with poorer memory performance (Harris et al., 2016). Again, whether the age- and AD-correlated alterations in lactate levels play a rescue role to release the energetic deficits or in turn to exacerbate the AD pathologies needs to be further investigated. Our failure to detect significant changes in lactate in the hippocampus with age suggests though lactate may be an alternative energy source during age-related energetic shortage, it did not accumulate in old age NTg or 3xTg-AD hippocampus, likely by increased activity of LDH to maintain redox balance (Brewer, 2010).

4.5.6 Ketone Bodies as Another Alternative Energetic Source

In our results, we observed an age-related 40-55% decline in the levels of 3-hydroxybutyrate (BHBA) in the 3xTg-AD samples of both genders ($p < 0.05$), indicating a possible higher utilization of KB as an energetic source in aging and AD brains. Ketone bodies (KB) are another alternative energy substrate, which derive from the incomplete oxidation of fatty acids in the liver. Three KB including acetone, acetoacetate and β-hydroxybutyrate are interconvertible and metabolized to succinyl-CoA feeding into the TCA cycle with generation of NADH for energy production during energetic demand (Sokoloff, 1973; Wicks et al., 2015). As administration of KB can bypass the AD-related blockage in PDH and insulin resistance and provide needed NADH for redox balance, mild ketosis provides a potential therapy for AD (Veech, 2004). Diet supplementation with

pyruvate (5 mM) and β-hydroxybutyrate (4 mM) for 5 weeks showed diminished neuronal hyper-excitability in 3xTg-AD mice (Zilberter et al., 2013; Hertz et al., 2015). Compared to normal levels of KB less than 0.1 mM in blood and pathological ketoacidosis of 15-25 mM, nutritional ketosis from a low-carbohydrate- high-fat diet raised blood KB to 7-8 mM and reduced total Aβ loads in a mouse model of AD (Henderson, 2008; Paoli et al., 2015). Importantly, nutritional ketosis increases NAD^+/NADH redox states in young healthy human brains (Xin et al., 2018). Even though ketones cannot completely replace glucose for energy source, mild experimental ketonemia in rats improves brain glucose uptake (Pifferi et al., 2011; Cunnane et al., 2011), probably by improved redox balance. In another AD mouse model, a ketogenic diet reduced total Aβ40 and Aβ42 pathologic load (Van der Auwera et al., 2005). The expression of monocarboxylate transporters (MCTs) for transporting lactate and KB increased in female brains at 12-month in NTg but earlier at 3-month in 3xTg-AD, indicating the activation of the ketogenic pathway (Ding et al., 2013). Our data of an age-dependent decline in 3-hydroxybutyrate levels in 3xTg-AD hippocampus adds to the above findings to suggest that a therapeutic ketogenic diet may supply extra NADH reductive energy and maximize generation of energy. However, further studies are needed to uncover the mechanism of potential beneficial effect of dietary KB considering the contradictory roles of ketosis on anorexigenic and orexigenic signals (Paoli et al., 2015).

4.5.7 Glutamate

In our NTg and 3xTg-AD mouse model, glutamate, GABA, NAAG and NAA markedly declined with age, suggesting decreased availability of synaptic neurotransmitters. NMDA

receptors rely on glutamate to induce hippocampal long-term potentiation (LTP) of synapses for learning and memory (Collingridge, 1987; Butterfield and Pocernich, 2003). Decreased levels of glutamate (Peng et al., 2011), NAAG and NAA are associated with disorders of learning and memory (Kołodziejczyk et al., 2009) and pathogenesis of AD (McEntee and Crook, 1992). Glutamatergic neurotransmission in hippocampus is severely disrupted in AD (Greenamyre, 1986; Palmer and Gershon, 1990). The decline in neurotransmitters with age could be a response to decreased energy available to maintain ionic homeostasis associated with neurotransmission and feedback to reduce excitotoxicity.

4.5.8 Sphingolipids

Our results of age- and AD related patterns of up-regulation of ceramide and sphingosine-1-phosphate suggest increased inflammation with age and AD. Sphingolipid metabolism is deregulated in AD brains with a pattern of elevated acid sphingomyelinase (ASM) and acid ceramidase (AC) expression (He et al., 2008). Elevated ceramides and sphingosine-1-phosphate as signaling molecules correlate with inflammation (Maceyka and Spiegel, 2014). Since the oxidized redox potentials of Cys/CySS in human plasma were positively corelated with interleukin (IL)-1β levels (Iyer et al., 2009), our results of an oxidative shift with age in neurons could promote inflammation neurons (Dong, Digman, Brewer, unpublished data). Additionally, sphingolipids mediate synaptic plasticity (Sonnino and Prinetti, 2016), and disturbances in sphingolipid content correlated with impairment in memory and learning (Mielke et al., 2010). Studies of 30 human plasma samples from

each group of AD, MCI and normal control subjects revealed remarkable declines in sphingomyelin, especially in females (Armirotti et al., 2014).

4.5.9 Conclusions

According to the epigenetic oxidative redox shift (EORS) aging theory (Brewer, 2010), we hypothesized that an age-associated sedentary behavior triggers oxidative shifts and mitochondrial impairments, which cause downstream cascades. To offset the age-related energetic deficits, redox-sensitive epigenetic modification enforces metabolic shifts in aging brains. Here, we found evidence for a metabolic pivot at redox-dependent bioenergetic enzymes that generate NADH. Age- and AD-associated oxidized NAD^+/NADH redox states (increased ratio) (Jones, 2006; Parihar et al., 2008; Ghosh et al., 2012; Dong et al., 2019) could signal metabolic re-direction for more NADH generation by epigenetics, redox-sensitive transcription factors (Yang et al., 1999; Marina et al., 2016), redox sensing cysteines in the enzyme (Foster et al., 2017), nitration of KGDHC (Shi et al., 2011), acylation of KGDHC (Carrico et al., 2018) or NAD^+/NADH substrate limitations (Jones and Brewer, 2010). However, lower levels of metabolites in the TCA cycle suggests a limitation or blockage at the TCA cycle, depriving the ETC-OXPHOS of NADH for ATP generation (Bubber et al., 2005). The NAD^+/NADH redox couple is likely to function as a sensor for dehydrogenases at the pivot of upstream and downstream metabolites in pathways including glycolysis, the TCA cycle, fatty acid oxidation and BCAA metabolism. The age- and AD-related oxidative shifts with drops of NAD pool size are sensed by NADH redox sites in the metabolic pathways and serve as a switch to affect the rate or direction of metabolic flux. Taken together with the age- and AD-

associated energetic shortage, metabolic up-regulation in fatty acid metabolism likely generates NADH as an alternative to carbohydrate oxidation to maintain redox balance and maximize energetic capacity.

4.6 Acknowledgements

We appreciate the help of Justyna Maria Sosna for mouse genotyping in Prof. Charles Glabe‘s Lab and Robert Herrera for sample collection. This work was supported by the UC Irvine Foundation and a grant from the NIH RF1 AG058218.

CHAPTER 5

CONCLUSION AND FUTURE DIRECTIONS

5.1 Conclusion

Given that the no effective pharmacological therapies for cognitive impairment and AD result from little-known mechanisms on the upstream of AD pathologies and aging, my dissertation hypothesized and investigated an age- and AD-related oxidative shifts in NADH redox states as an upstream, reflecting by free/bound NADH ratios, free NADH levels and distributions in mitochondria, cytoplasm and nuclei as well as the mitochondria-specific total NADH pool sizes of neurons. By using fluorescence lifetime imaging microscopy (FLIM) technique as an invasive approach for intrinsic fluorescent NADH, after transformation of pixels of FLIM images by Fast Fourier Transform (FFT), we were able to distinguish and quantify free and enzyme-bound NADH based on different lifetimes at subcellular compartments in the phasor plot. We found age strongly drives declines in free NADH levels of mitochondria, cytoplasm and nuclei and remarkably depleted total mitochondrial NADH pool size. With AD genetic load, these depletion in free NADH and NADH pool size were exacerbated in 3xTg-AD mouse neurons. This indicates an age-related decreased capacity of free NADH regeneration, which further limits the power of oxidative phosphorylation for energetic supply.

To further study age- and AD-associated redox capacity of NADH, we imposed an oxidized Cysteine/Cystine (Cys/CySS) states to 0 mV in primary neuron cultures from

NTg and 3xTg-AD hippocampus across age-span. We observed that with the imposed external oxidative stress to 0 mV, the declines of mitochondrial free NADH concentrations and total NADH pool sizes in old neurons far more exceeded the levels in young neurons, which even worse with AD genetic load in 3xTg-AD mouse neurons. This suggests a lower capacity for maintaining free NADH levels in old neurons under oxidative stress and more so in AD-model mouse neurons. More importantly, as free NADH importantly pivots redox, energy and metabolic states, we examined whether these age-related oxidized free NADH redox states and depletion of NADH can be reversed and restored with external redox modification. We imposed reductive external Cys/CySS redox state to -150 mV in the culture medium on NTg and 3xTg-AD primary neurons from young, middle and old mouse hippocampal brains. We found that with an imposed Cys/CySS reductive state, the mitochondrial free NADH levels were rejuvenated to the levels of young age neurons in both NTg and 3xTg-AD mouse neurons. Being able to reverse the depleted free NADH in old neurons with an external reductive state suggest a potential therapy for Alzheimer's disease and a possible delay on the course of aging.

To support our hypothesis and build up causative correlations among redox system, metabolomics and energy, we used the untargeted Ultrahigh Performance Liquid Chromatography-Tandem Mass Spectroscopy (UPLC-MS/MS) Platform to globally measure metabolite levels from NTg and 3xTg-AD mouse hippocampal brain samples across age-span. Age and AD share some common metabolic patterns in pathways including energy-generating pathways, fatty acids oxidation, glutamate and sphingolipid metabolism. We observed strong age-related global elevations up to 2-3-fold in energy

metabolism including glycolytic ATP-produced steps, fatty acid β-oxidation, regulated and pivoted at NAD+/NADH redox sensitive sites in both NTg and 3xTg-AD mouse hippocampal samples. We find for the first-time age-related decreases in the upstream metabolites of dehydrogenases and increases in the downstream metabolites of glycolysis and the TCA cycle. Building up causative correlations among metabolomics, redox and energy and tracing the most upstream of AD pathologies and aging that initiate a series of downstream cascades, may provide potential treatments to delay or reverse the course of AD pathologies and aging as well as to prevent the initiation of Alzheimer's disease and prolong dementia-free health span.

5.2 Future Directions

5.2.1 How Could Deficits in Intracellular NADH be Assessed in the Elderly Non-Invasively and Cost-Effectively?

In Chapters 2 and 3, the declines of NADH levels with age and AD and their rejuvenation indicate NADH as a potential biomarker that could be used for AD diagnosis, prognosis and monitor the progression of AD. Additional rationale for the importance of NAD were reviewed for extension of longevity in model organisms (Yaku et al., 2018). Biomarkers from CSF, blood, gene and neuroimaging are possible for NADH evaluation. Often, a combination of biomarkers is needed to achieve a comparatively accurate assessment and diagnosis on AD. The mechanistic implications for energy generation resistance to oxidative stress make NADH advantageous as a biomarker. Issues that will need to be addressed include firstly, which non-invasive and cost-effectively sample source such as CSF, blood cells or plasma will provide more accurate information for AD prediction and

diagnosis. Further, the reductive components of redox couples are easily oxidized when exposed to air, which requires a chemical modification via a redox clamp to maintain in vivo levels (Klaidman et al., 1995; Jones et al., 2002). Which redox clamp of NADH is optimal for sample pre-treatment without interference of the NADH levels and properties? Moreover, measurements of NADH through the skin in vivo may be able to directly image red blood cells, platelets or lymphocytes (Stringari et al., 2015). Alternatively, plasma cysteine levels may be usefully measured to reflect intracellular NADH levels, as we have shown in Chapter 3.

5.2.2 How Could Intracellular NADH be Elevated Orally? Can Intracellular NADH Levels be Quantitatively Controlled?

Supplements to improve cognitive function in MCI and AD patients by reversing age- and AD-related oxidized states have been examined by oral supplementation of GSH. 500 mg/day was found remarkably enhanced the GSH levels in erythrocytes and greatly improved the cognitive score in MCI and AD patients (Mandal et al., 2019). Supplementations of a NAD^+ precursor vitamin, nicotinamide riboside (NR) for 500 mg twice/day, effectively stimulated NAD^+ metabolism (Martens et al., 2018), redox homeostasis and exercise performance in healthy elderly people (Dolopikou et al., 2019). Administrated a combination of NAD+ and NADPH supplements within 2 hours after reperfusion in mice effectively ameliorated ischemic brain damage (Huang et al., 2018). As NAD^+ and NADH can interconvert in the salvage pathways and supplements of NAD^+ precursors dramatically improve the cognitive functions in MCI and AD patients, a follow-up question may rose by if the orally administrate NADH can reverse cognitive

impairments and pathologically metabolic shifts in MCI and AD patients. Further, as NADH easily gets oxidized and how to quantitatively control intracellular NADH levels should also be addressed before NADH administration in clinical trials.

5.2.3 Can Elevated Intracellular NADH Slow Progression of AD, Stall Conversion from MCI to AD or Improve Cognitive Function in MCI Subjects?

Based on the EORS theory, we hypothesized that an age- and AD-related oxidative shift in NADH redox states triggers a downstream cascade of metabolic and energetic shifts, exacerbating cognitive impairments and AD pathologies. Since supplements of NAD precursors significantly improve mouse cognition (Hou et al., 2018), reversing declines in elderly NADH levels may improve and ameliorate cognitive function and stall the cognitive impairment at early stage of MCI before the development to AD (Dolopikou et al., 2019) Assessments of cognitive function with NADH administration in animals (Huang et al., 2018), and further on MCI and AD patients are proposed (Mandal et al., 2019).

5.2.4 Will Supplementary Intracellular NADH Rescue the Observed Age- and AD-Related Metabolic Shifts Implicated in AD?

In Chapter 4, we observed the age- and AD-associated shifts in redox-energy pivoted at NAD+/NADH redox sensitive sites. This leads to a follow-up study to determine if recovery of free NADH and total NAD pool re-directs metabolic shifts at NAD^+/NADH redox sensitive sites and if this can reverse the energetic deficits in aged and AD brains. Careful consideration of the question is critical to determine whether increased energy supplied by fatty acid oxidation is needed for example to handle a chronic need for age-related

repairs or whether the oxidation contributes to ensuing pathology. Several approaches are possible to non-invasively track and evaluate metabolic alterations of AD patients before and after NADH administration. Blood plasma can be rapidly monitored for lipid changes by capillary chromatography and mass spec (Mapstone et al., 2014) with prognostic utility already demonstrated for MCI. Alternatively, brain MRI spectroscopy after ingestion of ^{13}C-labeled glucose may provide dynamic tracing of certain metabolites.

BIBLIOGRAPHY

Aguilar-Arnal, L., Ranjit, S., Stringari, C., Orozco-Solis, R., Gratton, E., & Sassone-Corsi, P. (2016). Spatial dynamics of SIRT1 and the subnuclear distribution of NADH species. Proceedings of the National Academy of Sciences, 113(45), 12715-12720.

Aksenov, M. Y., Tucker, H. M., Nair, P., Aksenova, M. V., Butterfield, D. A., Estus, S., & Markesbery, W. R. (1999). The expression of several mitochondrial and nuclear genes encoding the subunits of electron transport chain enzyme complexes, cytochrome c oxidase, and NADH dehydrogenase, in different brain regions in Alzheimer's disease. Neurochemical research, 24(6), 767-774.

Alessenko, A. V., Bugrova, A. E., & Dudnik, L. B. (2004). Connection of lipid peroxide oxidation with the sphingomyelin pathway in the development of Alzheimer's disease.

Alzheimer's Association. (2016). 2016 Alzheimer's disease facts and figures. Alzheimer's & Dementia, 12(4), 459-509.

Alzheimer's Association. (2018). 2018 Alzheimer's disease facts and figures. Alzheimer's & Dementia, 14(3), 367-429.

Ansari, M. A., & Scheff, S. W. (2011). NADPH-oxidase activation and cognition in Alzheimer disease progression. Free Radical Biology and Medicine, 51(1), 171-178.

Aon, M. A., Cortassa, S., & O'Rourke, B. (2010). Redox-optimized ROS balance: a unifying hypothesis. Biochimica et Biophysica Acta (BBA)-Bioenergetics, 1797(6-7), 865-877.

Aoyama, K., & Nakaki, T. (2013). Neuroprotective properties of the excitatory amino acid carrier 1 (EAAC1). Amino acids, 45(1), 133-142.

Armirotti, A., Basit, A., Realini, N., Caltagirone, C., Bossù, P., Spalletta, G., & Piomelli, D. (2014). Sample preparation and orthogonal chromatography for broad polarity range plasma metabolomics: application to human subjects with neurodegenerative dementia. Analytical biochemistry, 455, 48-54.

Ashe, K. H. (2001). Learning and memory in transgenic mice modeling Alzheimer's disease. Learning & Memory, 8(6), 301-308.

Attwell, D., & Laughlin, S. B. (2001). An energy budget for signaling in the grey matter of the brain. Journal of Cerebral Blood Flow & Metabolism, 21(10), 1133-1145.

Aubert, A., Costalat, R., Magistretti, P. J., & Pellerin, L. (2005). Brain lactate kinetics: modeling evidence for neuronal lactate uptake upon activation. Proceedings of the National Academy of Sciences, 102(45), 16448-16453.

Baglietto-Vargas, D., Chen, Y., Suh, D., Ager, R. R., Rodriguez-Ortiz, C. J., Medeiros, R., ... & LaFerla, F. M. (2015). Short-term modern life-like stress exacerbates Aβ-pathology and synapse loss in 3xTg-AD mice. Journal of neurochemistry, 134(5), 915-926.

Baglietto-Vargas, D., Prieto, G. A., Limon, A., Forner, S., Rodriguez-Ortiz, C. J., Ikemura, K., ... & Kitazawa, M. (2018). Impaired AMPA signaling and cytoskeletal alterations induce early synaptic dysfunction in a mouse model of Alzheimer's disease. Aging cell, 17(4), e12791.

Bai, P., & Cantó, C. (2012). The role of PARP-1 and PARP-2 enzymes in metabolic regulation and disease. Cell metabolism, 16(3), 290-295.

Barnett, A., & Brewer, G. J. (2011). Autophagy in aging and Alzheimer's disease: pathologic or protective?. Journal of Alzheimer's Disease, 25(3), 385-394.

Barrientos, A., Casademont, J., Cardellach, F., Estivill, X., Urbano-Marquez, A., & Nunes, V. (1997). Reduced steady-state levels of mitochondrial RNA and increased mitochondrial DNA amount in human brain with aging. Molecular brain research, 52(2), 284-289.

Berger, F., Lau, C., Dahlmann, M., & Ziegler, M. (2005). Subcellular compartmentation and differential catalytic properties of the three human nicotinamide mononucleotide adenylyltransferase isoforms. Journal of Biological Chemistry, 280(43), 36334-36341.

Berndt, N., Bulik, S., & Holzhütter, H. G. (2012). Kinetic modeling of the mitochondrial energy metabolism of neuronal cells: The impact of reduced-ketoglutarate dehydrogenase activities on ATP production and generation of reactive oxygen species. International journal of cell biology, 2012.

Berndt, N., Kann, O., & Holzhütter, H. G. (2015). Physiology-based kinetic modeling of neuronal energy metabolism unravels the molecular basis of NAD (P) H fluorescence transients. Journal of Cerebral Blood Flow & Metabolism, 35(9), 1494-1506.

Bird, D. K., Yan, L., Vrotsos, K. M., Eliceiri, K. W., Vaughan, E. M., Keely, P. J., ... & Ramanujam, N. (2005). Metabolic mapping of MCF10A human breast cells via multiphoton fluorescence lifetime imaging of the coenzyme NADH. Cancer research, 65(19), 8766-8773.

Blanco, R. A., Ziegler, T. R., Carlson, B. A., Cheng, P. Y., Park, Y., Cotsonis, G. A., ... & Jones, D. P. (2007). Diurnal variation in glutathione and cysteine redox states in human plasma. The American journal of clinical nutrition, 86(4), 1016-1023.

Borrás, C., Sastre, J., García-Sala, D., Lloret, A., Pallardó, F. V., & Viña, J. (2003). Mitochondria from females exhibit higher antioxidant gene expression and lower oxidative damage than males. Free radical biology and medicine, 34(5), 546-552.

Boumezbeur, F., Mason, G. F., De Graaf, R. A., Behar, K. L., Cline, G. W., Shulman, G. I., ... & Petersen, K. F. (2010). Altered brain mitochondrial metabolism in healthy aging as assessed by in vivo magnetic resonance spectroscopy. Journal of Cerebral Blood Flow & Metabolism, 30(1), 211-221.

Bradshaw, P. C. (2019). Cytoplasmic and Mitochondrial NADPH-Coupled Redox Systems in the Regulation of Aging. Nutrients, 11(3), 504.

Braidy, N., Guillemin, G. J., Mansour, H., Chan-Ling, T., Poljak, A., & Grant, R. (2011). Age related changes in NAD+ metabolism oxidative stress and Sirt1 activity in wistar rats. PloS one, 6(4), e19194.

Brewer, G. J. (1997). Effects of acidosis on the distribution and processing of the β-amyloid precursor protein in cultured hippocampal neurons. Molecular and chemical neuropathology, 31(2), 171-186.

Brewer, G. J. (1998). Age-related toxicity to lactate, glutamate, and β-amyloid in cultured adult neurons. Neurobiology of aging, 19(6), 561-568.

Brewer, G. J. (2010). Epigenetic oxidative redox shift (EORS) theory of aging unifies the free radical and insulin signaling theories. Experimental gerontology, 45(3), 173-179.

Brewer, G. J., & Torricelli, J. R. (2007). Isolation and culture of adult neurons and neurospheres. Nature protocols, 2(6), 1490.

Brewer, G. J., Boehler, M. D., Pearson, R. A., DeMaris, A. A., Ide, A. N., & Wheeler, B. C. (2008). Neuron network activity scales exponentially with synapse density. Journal of neural engineering, 6(1), 014001.

Brewer, G. J., Reichensperger, J. D., & Brinton, R. D. (2006). Prevention of age-related dysregulation of calcium dynamics by estrogen in neurons. Neurobiology of aging, 27(2), 306-317.

Brouwers, N., Sleegers, K., & Van Broeckhoven, C. (2008). Molecular genetics of Alzheimer's disease: an update. Annals of medicine, 40(8), 562-583.

Bubber, P., Haroutunian, V., Fisch, G., Blass, J. P., & Gibson, G. E. (2005). Mitochondrial abnormalities in Alzheimer brain: mechanistic implications. Annals of Neurology: Official Journal of the American Neurological Association and the Child Neurology Society, 57(5), 695-703.

Butterfield, D. A., & Pocernich, C. B. (2003). The glutamatergic system and Alzheimer's disease. CNS drugs, 17(9), 641-652.

Cady, C., Evans, M. S., & Brewer, G. J. (2001). Age-related differences in NMDA responses in cultured rat hippocampal neurons. Brain research, 921(1-2), 1-11.

Calder, P. C. (2006). Polyunsaturated fatty acids and inflammation. Prostaglandins, leukotrienes and essential fatty acids, 75(3), 197-202.

Calkins, M. J., Manczak, M., Mao, P., Shirendeb, U., & Reddy, P. H. (2011). Impaired mitochondrial biogenesis, defective axonal transport of mitochondria, abnormal mitochondrial dynamics and synaptic degeneration in a mouse model of Alzheimer's disease. Human molecular genetics, 20(23), 4515-4529.

Camacho-Pereira, J., Tarragó, M. G., Chini, C. C., Nin, V., Escande, C., Warner, G. M., ... & Chini, E. N. (2016). CD38 dictates age-related NAD decline and mitochondrial dysfunction through an SIRT3-dependent mechanism. Cell metabolism, 23(6), 1127-1139.

Cantó, C., Jiang, L. Q., Deshmukh, A. S., Mataki, C., Coste, A., Lagouge, M., ... & Auwerx, J. (2010). Interdependence of AMPK and SIRT1 for metabolic adaptation to fasting and exercise in skeletal muscle. Cell metabolism, 11(3), 213-219.

Canto, C., Menzies, K. J., & Auwerx, J. (2015). NAD+ metabolism and the control of energy homeostasis: a balancing act between mitochondria and the nucleus. Cell metabolism, 22(1), 31-53.

Carageorgiou, H., Sideris, A. C., Messari, I., Liakou, C. I., & Tsakiris, S. (2008). The effects of rivastigmine plus selegiline on brain acetylcholinesterase,(Na+, K+)-, Mg2+-ATPase activities, antioxidant status, and learning performance of aged rats. Neuropsychiatric disease and treatment, 4(4), 687.

Carrico, C., Meyer, J. G., He, W., Gibson, B. W., & Verdin, E. (2018). The mitochondrial acylome emerges: proteomics, regulation by sirtuins, and metabolic and disease implications. Cell metabolism, 27(3), 497-512.
Chance, B., & Thorell, B. (1959). Localization and kinetics of reduced pyridine nucleotide in living cells by microfluorometry. Journal of Biological Chemistry, 234(11), 3044-3050.
Chen, J., Delannoy, M., Odwin, S., He, P., Trush, M. A., & Yager, J. D. (2003). Enhanced mitochondrial gene transcript, ATP, bcl-2 protein levels, and altered glutathione distribution in ethinyl estradiol-treated cultured female rat hepatocytes. Toxicological Sciences, 75(2), 271-278.
Chou, J. L., Shenoy, D. V., Thomas, N., Choudhary, P. K., LaFerla, F. M., Goodman, S. R., & Breen, G. A. (2011). Early dysregulation of the mitochondrial proteome in a mouse model of Alzheimer's disease. Journal of proteomics, 74(4), 466-479.
Christensen, C. E., Karlsson, M., Winther, J. R., Jensen, P. R., & Lerche, M. H. (2014). Non-invasive in-cell determination of free cytosolic [NAD+]/[NADH] ratios using hyperpolarized glucose show large variations in metabolic phenotypes. Journal of Biological Chemistry, 289(4), 2344-2352.
Circu, M. L., & Aw, T. Y. (2010). Reactive oxygen species, cellular redox systems, and apoptosis. Free Radical Biology and Medicine, 48(6), 749-762.
Collingridge, G. (1987). The role of NMDA receptors in learning and memory. Nature, 330(6149), 604.
Conus, P., Seidman, L. J., Fournier, M., Xin, L., Cleusix, M., Baumann, P. S., ... & Golay, P. (2017). N-acetylcysteine in a double-blind randomized placebo-controlled trial: toward biomarker-guided treatment in early psychosis. Schizophrenia bulletin, 44(2), 317-327.
Cooper, G. M. (2000). Metabolic energy. The cell: A molecular approach, 2.
Coremans, J., Ince, C., Bruining, H. A., & Puppels, G. J. (1997). (Semi-) quantitative analysis of reduced nicotinamide adenine dinucleotide fluorescence images of blood-perfused rat heart. Biophysical journal, 72(4), 1849-1860.
Cortassa, S., O'Rourke, B., & Aon, M. A. (2014). Redox-optimized ROS balance and the relationship between mitochondrial respiration and ROS. Biochimica et Biophysica Acta (BBA)-Bioenergetics, 1837(2), 287-295.
Cribbs, D. H., Berchtold, N. C., Perreau, V., Coleman, P. D., Rogers, J., Tenner, A. J., & Cotman, C. W. (2012). Extensive innate immune gene activation accompanies brain aging, increasing vulnerability to cognitive decline and neurodegeneration: a microarray study. Journal of neuroinflammation, 9(1), 179.
Cruts, M., & vanBroeckhoven, C. (1998). Molecular genetics of Alzheimer's disease. Annals of medicine, 30(6), 560-565.
Cui, H., Kong, Y., & Zhang, H. (2012). Oxidative stress, mitochondrial dysfunction, and aging. Journal of signal transduction, 2012.
Cunnane, S., Nugent, S., Roy, M., Courchesne-Loyer, A., Croteau, E., Tremblay, S., ... & Begdouri, H. (2011). Brain fuel metabolism, aging, and Alzheimer's disease. Nutrition, 27(1), 3-20.
Cutler, R. G., Kelly, J., Storie, K., Pedersen, W. A., Tammara, A., Hatanpaa, K., ... & Mattson, M. P. (2004). Involvement of oxidative stress-induced abnormalities in ceramide and cholesterol metabolism in brain aging and Alzheimer's disease. Proceedings of the National Academy of Sciences, 101(7), 2070-2075.
Dai, D. F., Chiao, Y. A., Marcinek, D. J., Szeto, H. H., & Rabinovitch, P. S. (2014). Mitochondrial oxidative stress in aging and healthspan. Longevity & healthspan, 3(1), 6.
Datta, R., Alfonso-García, A., Cinco, R., & Gratton, E. (2015). Fluorescence lifetime imaging of endogenous biomarker of oxidative stress. Scientific reports, 5, 9848.
David, D. C., Hauptmann, S., Scherping, I., Schuessel, K., Keil, U., Rizzu, P., ... & Eckert, A. (2005). Proteomic and functional analyses reveal a mitochondrial dysfunction in P301L tau transgenic mice. Journal of Biological Chemistry, 280(25), 23802-23814.
Davidson, Y. S., Robinson, A., Prasher, V. P., & Mann, D. M. (2018). The age of onset and evolution of Braak tangle stage and Thal amyloid pathology of Alzheimer's disease in individuals with Down syndrome. Acta neuropathologica communications, 6(1), 56.
De Magalhães, J. P., Curado, J., & Church, G. M. (2009). Meta-analysis of age-related gene expression profiles identifies common signatures of aging. Bioinformatics, 25(7), 875-881.
DeLegge, M. H., & Smoke, A. (2008). Neurodegeneration and inflammation. Nutrition in clinical practice, 23(1), 35-41.

Di Domenico, F., Pupo, G., Giraldo, E., Badìa, M. C., Monllor, P., Lloret, A., ... & Butterfield, D. A. (2016). Oxidative signature of cerebrospinal fluid from mild cognitive impairment and Alzheimer disease patients. Free Radical Biology and Medicine, 91, 1-9.
Digman, M. A., Caiolfa, V. R., Zamai, M., & Gratton, E. (2008). The phasor approach to fluorescence lifetime imaging analysis. Biophysical journal, 94(2), L14-L16.
Ding, F., Yao, J., Rettberg, J. R., Chen, S., & Brinton, R. D. (2013). Early decline in glucose transport and metabolism precedes shift to ketogenic system in female aging and Alzheimer's mouse brain: implication for bioenergetic intervention. PloS one, 8(11), e79977.
Dinkova-Kostova, A. T., Holtzclaw, W. D., Cole, R. N., Itoh, K., Wakabayashi, N., Katoh, Y., ... & Talalay, P. (2002). Direct evidence that sulfhydryl groups of Keap1 are the sensors regulating induction of phase 2 enzymes that protect against carcinogens and oxidants. Proceedings of the National Academy of Sciences, 99(18), 11908-11913.
Dolopikou, C. F., Kourtzidis, I. A., Margaritelis, N. V., Vrabas, I. S., Koidou, I., Kyparos, A., ... & Nikolaidis, M. G. (2019). Acute nicotinamide riboside supplementation improves redox homeostasis and exercise performance in old individuals: a double-blind cross-over study. European journal of nutrition, 1-11.
Dong, Y., Digman, M. A., & Brewer, G. J. (2019). Age-and AD-related redox state of NADH in subcellular compartments by fluorescence lifetime imaging microscopy. GeroScience, 1-17.
Du, J., Ma, M., Zhao, Q., Fang, L., Chang, J., Wang, Y., ... & Song, X. (2013). Mitochondrial bioenergetic deficits in the hippocampi of rats with chronic ischemia-induced vascular dementia. Neuroscience, 231, 345-352.
Easlon, E., Tsang, F., Skinner, C., Wang, C., & Lin, S. J. (2008). The malate–aspartate NADH shuttle components are novel metabolic longevity regulators required for calorie restriction-mediated life span extension in yeast. Genes & development, 22(7), 931-944.
Eckel-Mahan, K. L., Patel, V. R., De Mateo, S., Orozco-Solis, R., Ceglia, N. J., Sahar, S., ... & Sassone-Corsi, P. (2013). Reprogramming of the circadian clock by nutritional challenge. Cell, 155(7), 1464-1478.
Elder, G. A., Gama Sosa, M. A., & De Gasperi, R. (2010). Transgenic mouse models of Alzheimer's disease. Mount Sinai Journal of Medicine: A Journal of Translational and Personalized Medicine: A Journal of Translational and Personalized Medicine, 77(1), 69-81.
Eng, J., Lynch, R. M., & Balaban, R. S. (1989). Nicotinamide adenine dinucleotide fluorescence spectroscopy and imaging of isolated cardiac myocytes. Biophysical journal, 55(4), 621-630.
Evans, M. S., Collings, M. A., & Brewer, G. J. (1998). Electrophysiology of embryonic, adult and aged rat hippocampal neurons in serum-free culture. Journal of neuroscience methods, 79(1), 37-46.
Fattoretti, P., Balietti, M., Casoli, T., Giorgetti, B., Di Stefano, G., Bertoni-Freddari, C., ... & Sensi, S. L. (2010). Decreased numeric density of succinic dehydrogenase-positive mitochondria in CA1 pyramidal neurons of 3xTg-AD mice. Rejuvenation research, 13(2-3), 144-147.
Fernandez-Fernandez, S., Almeida, A., & Bolaños, J. P. (2012). Antioxidant and bioenergetic coupling between neurons and astrocytes. Biochemical Journal, 443(1), 3-11.
Ferreira, S. T., Clarke, J. R., Bomfim, T. R., & De Felice, F. G. (2014). Inflammation, defective insulin signaling, and neuronal dysfunction in Alzheimer's disease. Alzheimer's & dementia, 10(1), S76-S83.
Figueiredo, P. A., Powers, S. K., Ferreira, R. M., Amado, F., Appell, H. J., & Duarte, J. A. (2009). Impact of lifelong sedentary behavior on mitochondrial function of mice skeletal muscle. Journals of Gerontology Series A: Biomedical Sciences and Medical Sciences, 64(9), 927-939.
Foster, N. L., Wang, A. Y., Tasdizen, T., Fletcher, P. T., Hoffman, J. M., & Koeppe, R. A. (2008). Realizing the potential of positron emission tomography with 18F-fluorodeoxyglucose to improve the treatment of Alzheimer's disease.
Foster, T. C., Kyritsopoulos, C., & Kumar, A. (2017). Central role for NMDA receptors in redox mediated impairment of synaptic function during aging and Alzheimer's disease. Behavioural brain research, 322, 223-232.
Fra, A., Yoboue, E. D., & Sitia, R. (2017). Cysteines as redox molecular switches and targets of disease. Frontiers in molecular neuroscience, 10, 167.
Gabuzda, D., Busciglio, J., Chen, L. B., Matsudaira, P., & Yankner, B. A. (1994). Inhibition of energy metabolism alters the processing of amyloid precursor protein and induces a potentially amyloidogenic derivative. Journal of Biological Chemistry, 269(18), 13623-13628.
Gage, F. H., Kelly, P. A., & Bjorklund, A. (1984). Regional changes in brain glucose metabolism reflect cognitive impairments in aged rats. Journal of Neuroscience, 4(11), 2856-2865.

Games, D., Adams, D., Alessandrini, R., Barbour, R., Borthelette, P., Blackwell, C., ... & Guido, T. (1995). Alzheimer-type neuropathology in transgenic mice overexpressing V717F β-amyloid precursor protein. Nature, 373(6514), 523.
Gao, H. M., Zhou, H., & Hong, J. S. (2012). NADPH oxidases: novel therapeutic targets for neurodegenerative diseases. Trends in pharmacological sciences, 33(6), 295-303.
Gaugler, J., James, B., Johnson, T., Marin, A., & Weuve, J. (2019). 2019 Alzheimer's disease facts and figures. ALZHEIMERS & DEMENTIA, 15(3), 321-387.
Ghosh, A., Tyson, T., George, S., Hildebrandt, E. N., Steiner, J. A., Madaj, Z., ... & Kordower, J. H. (2016). Mitochondrial pyruvate carrier regulates autophagy, inflammation, and neurodegeneration in experimental models of Parkinson's disease. Science translational medicine, 8(368), 368ra174-368ra174.
Ghosh, D., & Brewer, G. J. (2014). External cys/cySS redox state modification controls the intracellular redox state and neurodegeneration via Akt in aging and Alzheimer's disease mouse model neurons. Journal of Alzheimer's Disease, 42(1), 313-324.
Ghosh, D., Levault, K. R., & Brewer, G. J. (2014). Relative importance of redox buffers GSH and NAD (P) H in age-related neurodegeneration and Alzheimer disease-like mouse neurons. Aging cell, 13(4), 631-640.
Ghosh, D., LeVault, K. R., Barnett, A. J., & Brewer, G. J. (2012). A reversible early oxidized redox state that precedes macromolecular ROS damage in aging nontransgenic and 3xTg-AD mouse neurons. Journal of Neuroscience, 32(17), 5821-5832.
Gibson, G. E., & Blass, J. P. (1976). Impaired synthesis of acetylcholine in brain accompanying mild hypoxia and hypoglycemia. Journal of neurochemistry, 27(1), 37-42.
Gjoneska, E., Pfenning, A. R., Mathys, H., Quon, G., Kundaje, A., Tsai, L. H., & Kellis, M. (2015). Conserved epigenomic signals in mice and humans reveal immune basis of Alzheimer's disease. Nature, 518(7539), 365.
Go, Y. M., & Jones, D. P. (2014). Redox biology: interface of the exposome with the proteome, epigenome and genome. Redox biology, 2, 358-360.
Go, Y. M., & Jones, D. P. (2017). Redox theory of aging: implications for health and disease. Clinical Science, 131(14), 1669-1688.
Godyń, J., Jończyk, J., Panek, D., & Malawska, B. (2016). Therapeutic strategies for Alzheimer's disease in clinical trials. Pharmacological Reports, 68(1), 127-138.
Gomase, V. S., Changbhale, S. S., Patil, S. A., & Kale, K. V. (2008). Metabolomics. Current drug metabolism, 9(1), 89-98.
Gomes, A. P., Price, N. L., Ling, A. J., Moslehi, J. J., Montgomery, M. K., Rajman, L., ... & Mercken, E. M. (2013). Declining NAD+ induces a pseudohypoxic state disrupting nuclear-mitochondrial communication during aging. Cell, 155(7), 1624-1638.
González-Domínguez, R., García-Barrera, T., & Gómez-Ariza, J. L. (2015). Metabolite profiling for the identification of altered metabolic pathways in Alzheimer's disease. Journal of pharmaceutical and biomedical analysis, 107, 75-81.
Graham, W. V., Bonito-Oliva, A., & Sakmar, T. P. (2017). Update on Alzheimer's disease therapy and prevention strategies. Annual review of medicine, 68, 413-430.
Green, K. N., & LaFerla, F. M. (2008). Linking calcium to Aβ and Alzheimer's disease. Neuron, 59(2), 190-194.
Green, K. N., Steffan, J. S., Martinez-Coria, H., Sun, X., Schreiber, S. S., Thompson, L. M., & LaFerla, F. M. (2008). Nicotinamide restores cognition in Alzheimer's disease transgenic mice via a mechanism involving sirtuin inhibition and selective reduction of Thr231-phosphotau. Journal of Neuroscience, 28(45), 11500-11510.
Greenamyre, J. T. (1986). The role of glutamate in neurotransmission and in neurologic disease. Archives of neurology, 43(10), 1058-1063.
Grimm, A., & Eckert, A. (2017). Brain aging and neurodegeneration: from a mitochondrial point of view. Journal of neurochemistry, 143(4), 418-431.
Guebel, D. V., & Torres, N. V. (2016). Sexual dimorphism and aging in the human hyppocampus: identification, validation, and impact of differentially expressed genes by factorial microarray and network analysis. Frontiers in aging neuroscience, 8, 229.

Guevara, R., Santandreu, F. M., Valle, A., Gianotti, M., Oliver, J., & Roca, P. (2009). Sex-dependent differences in aged rat brain mitochondrial function and oxidative stress. Free Radical Biology and Medicine, 46(2), 169-175.
Gumbiner, B., Thorburn, A. W., Ditzler, T. M., Bulacan, F., & Henry, R. R. (1992). Role of impaired intracellular glucose metabolism in the insulin resistance of aging. Metabolism, 41(10), 1115-1121.
Hajjar, I., Hayek, S. S., Goldstein, F. C., Martin, G., Jones, D. P., & Quyyumi, A. (2018). Oxidative stress predicts cognitive decline with aging in healthy adults: an observational study. Journal of neuroinflammation, 15(1), 17.
Hampel, H., Frank, R., Broich, K., Teipel, S. J., Katz, R. G., Hardy, J., ... & Sanhai, W. R. (2010). Biomarkers for Alzheimer's disease: academic, industry and regulatory perspectives. Nature reviews Drug discovery, 9(7), 560.
Han, X., Rozen, S., Boyle, S. H., Hellegers, C., Cheng, H., Burke, J. R., ... & Kaddurah-Daouk, R. (2011). Metabolomics in early Alzheimer's disease: identification of altered plasma sphingolipidome using shotgun lipidomics. PloS one, 6(7), e21643.
Hansen, J. M., Go, Y. M., & Jones, D. P. (2006). Nuclear and mitochondrial compartmentation of oxidative stress and redox signaling. Annu. Rev. Pharmacol. Toxicol., 46, 215-234.
Harari, O., Cruchaga, C., Kauwe, J. S., Ainscough, B. J., Bales, K., Pickering, E. H., ... & Goate, A. M. (2014). Phosphorylated tau-Aβ42 ratio as a continuous trait for biomarker discovery for early-stage Alzheimer's disease in multiplex immunoassay panels of cerebrospinal fluid. Biological psychiatry, 75(9), 723-731.
Hardy, J., & Selkoe, D. J. (2002). The amyloid hypothesis of Alzheimer's disease: progress and problems on the road to therapeutics. science, 297(5580), 353-356.
Harraan, D. (1955). Aging: a theory based on free radical and radiation chemistry.
Harris, R. A., Tindale, L., Lone, A., Singh, O., Macauley, S. L., Stanley, M., ... & Cumming, R. C. (2016). Aerobic glycolysis in the frontal cortex correlates with memory performance in wild-type mice but not the APP/PS1 mouse model of cerebral amyloidosis. Journal of Neuroscience, 36(6), 1871-1878.
Hauptmann, S., Scherping, I., Dröse, S., Brandt, U., Schulz, K. L., Jendrach, M., ... & Müller, W. E. (2009). Mitochondrial dysfunction: an early event in Alzheimer pathology accumulates with age in AD transgenic mice. Neurobiology of aging, 30(10), 1574-1586.
Hayashida, S., Arimoto, A., Kuramoto, Y., Kozako, T., Honda, S. I., Shimeno, H., & Soeda, S. (2010). Fasting promotes the expression of SIRT1, an NAD+-dependent protein deacetylase, via activation of PPARα in mice. Molecular and cellular biochemistry, 339(1-2), 285-292.
He, X., Huang, Y., Li, B., Gong, C. X., & Schuchman, E. H. (2010). Deregulation of sphingolipid metabolism in Alzheimer's disease. Neurobiology of aging, 31(3), 398-408.
Henderson, S. T. (2008). Ketone bodies as a therapeutic for Alzheimer's disease. Neurotherapeutics, 5(3), 470-480.
Hertz, L., Chen, Y., & Waagepetersen, H. S. (2015). Effects of ketone bodies in Alzheimer's disease in relation to neural hypometabolism, β-amyloid toxicity, and astrocyte function. Journal of neurochemistry, 134(1), 7-20.
Herukka, S. K., Rummukainen, J., Ihalainen, J., von und zu Fraunberg, M., Koivisto, A. M., Nerg, O., ... & Helisalmi, S. (2015). Amyloid-β and tau dynamics in human brain interstitial fluid in patients with suspected normal pressure hydrocephalus. Journal of Alzheimer's Disease, 46(1), 261-269.
Hirai, K., Aliev, G., Nunomura, A., Fujioka, H., Russell, R. L., Atwood, C. S., ... & Shimohama, S. (2001). Mitochondrial abnormalities in Alzheimer's disease. Journal of Neuroscience, 21(9), 3017-3023.
Hirrlinger, J., & Dringen, R. (2010). The cytosolic redox state of astrocytes: maintenance, regulation and functional implications for metabolite trafficking. Brain research reviews, 63(1-2), 177-188.
Hoffman, J. M., Welsh-Bohmer, K. A., Hanson, M., Crain, B., Hulette, C., Earl, N., & Coleman, R. E. (2000). FDG PET imaging in patients with pathologically verified dementia. Journal of Nuclear Medicine, 41(11), 1920-1928.
Hou, Y., Lautrup, S., Cordonnier, S., Wang, Y., Croteau, D. L., Zavala, E., ... & Stevnsner, T. V. (2018). NAD+ supplementation normalizes key Alzheimer's features and DNA damage responses in a new AD mouse model with introduced DNA repair deficiency. Proceedings of the National Academy of Sciences, 115(8), E1876-E1885.
Houten, S. M., & Wanders, R. J. (2010). A general introduction to the biochemistry of mitochondrial fatty acid β-oxidation. Journal of inherited metabolic disease, 33(5), 469-477.

Hoyer, S. (1998). Risk factors for Azheimer's disease during aging. Impacts of glucose/energy metabolism. In Alzheimer's Disease—From Basic Research to Clinical Applications (pp. 187-194). Springer, Vienna.
Hoyer, S., & Lannert, H. (2007). Long-term abnormalities in brain glucose/energy metabolism after inhibition of the neuronal insulin receptor: implication of tau-protein. In Neuropsychiatric Disorders An Integrative Approach (pp. 195-202). Springer, Vienna.
Hsiao, K., Chapman, P., Nilsen, S., Eckman, C., Harigaya, Y., Younkin, S., ... & Cole, G. (1996). Correlative memory deficits, Aβ elevation, and amyloid plaques in transgenic mice. Science, 274(5284), 99-103.
Huang, D., Liu, D., Yin, J., Qian, T., Shrestha, S., & Ni, H. (2017). Glutamate-glutamine and GABA in brain of normal aged and patients with cognitive impairment. European radiology, 27(7), 2698-2705.
Huang, Q., Sun, M., Li, M., Zhang, D., Han, F., Wu, J. C., ... & Qin, Z. H. (2018). Combination of NAD+ and NADPH offers greater neuroprotection in ischemic stroke models by relieving metabolic stress. Molecular neurobiology, 55(7), 6063-6075.
Humphries, K. M., Szweda, P. A., & Szweda, L. I. (2006). Aging: a shift from redox regulation to oxidative damage. Free radical research, 40(12), 1239-1243.
Hutter, D. E., Till, B. G., & Greene, J. J. (1997). Redox state changes in density-dependent regulation of proliferation. Experimental cell research, 232(2), 435-438.
Ibáñez, C., Simó, C., Martín-Álvarez, P. J., Kivipelto, M., Winblad, B., Cedazo-Mínguez, A., & Cifuentes, A. (2012). Toward a predictive model of Alzheimer's disease progression using capillary electrophoresis–mass spectrometry metabolomics. Analytical chemistry, 84(20), 8532-8540.
Imai, S. I., & Guarente, L. (2014). NAD+ and sirtuins in aging and disease. Trends in cell biology, 24(8), 464-471.
Imam, S. Z., Karahalil, B., Hogue, B. A., Souza-Pinto, N. C., & Bohr, V. A. (2006). Mitochondrial and nuclear DNA-repair capacity of various brain regions in mouse is altered in an age-dependent manner. Neurobiology of aging, 27(8), 1129-1136.
Intlekofer, K. A., Berchtold, N. C., Malvaez, M., Carlos, A. J., McQuown, S. C., Cunningham, M. J., ... & Cotman, C. W. (2013). Exercise and sodium butyrate transform a subthreshold learning event into long-term memory via a brain-derived neurotrophic factor-dependent mechanism. Neuropsychopharmacology, 38(10), 2027.
Inui, Y., Ito, K., & Kato, T. (2017). Longer-term investigation of the value of 18F-FDG-PET and magnetic resonance imaging for predicting the conversion of mild cognitive impairment to Alzheimer's disease: A multicenter study. Journal of Alzheimer's Disease, 60(3), 877-887.
Isopi, E., Granzotto, A., Corona, C., Bomba, M., Ciavardelli, D., Curcio, M., ... & Sensi, S. L. (2015). Pyruvate prevents the development of age-dependent cognitive deficits in a mouse model of Alzheimer's disease without reducing amyloid and tau pathology. Neurobiology of disease, 81, 214-224.
Ivanisevic, J., Epstein, A. A., Kurczy, M. E., Benton, P. H., Uritboonthai, W., Fox, H. S., ... & Siuzdak, G. (2014). Brain region mapping using global metabolomics. Chemistry & biology, 21(11), 1575-1584.
Ivanisevic, J., Stauch, K. L., Petrascheck, M., Benton, H. P., Epstein, A. A., Fang, M., ... & Boska, M. D. (2016). Metabolic drift in the aging brain. Aging (Albany NY), 8(5), 1000.
Iyer, S. S., Accardi, C. J., Ziegler, T. R., Blanco, R. A., Ritzenthaler, J. D., Rojas, M., ... & Jones, D. P. (2009). Cysteine redox potential determines pro-inflammatory IL-1β levels. PloS one, 4(3), e5017.
Jack, C. (2008). Pathophysiology of neuronal energy crisis in Alzheimer's disease. Neurodegenerative diseases, 5(3-4), 126-132.
Jiang, S., Moriarty-Craige, S. E., Orr, M., Cai, J., Sternberg, P., & Jones, D. P. (2005). Oxidant-induced apoptosis in human retinal pigment epithelial cells: dependence on extracellular redox state. Investigative ophthalmology & visual science, 46(3), 1054-1061.
Jones, D. P. (2006). Redefining oxidative stress. Antioxidants & redox signaling, 8(9-10), 1865-1879.
Jones, D. P., & Go, Y. M. (2010). Redox compartmentalization and cellular stress. Diabetes, Obesity and Metabolism, 12, 116-125.
Jones, D. P., Go, Y. M., Anderson, C. L., Ziegler, T. R., Kinkade Jr, J. M., & Kirlin, W. G. (2004). Cysteine/cystine couple is a newly recognized node in the circuitry for biologic redox signaling and control. The FASEB journal, 18(11), 1246-1248.
Jones, D. P., Mody Jr, V. C., Carlson, J. L., Lynn, M. J., & Sternberg Jr, P. (2002). Redox analysis of human plasma allows separation of pro-oxidant events of aging from decline in antioxidant defenses. Free Radical Biology and Medicine, 33(9), 1290-1300.

Jones, T. T., & Brewer, G. J. (2010). Age-related deficiencies in complex I endogenous substrate availability and reserve capacity of complex IV in cortical neuron electron transport. Biochimica et Biophysica Acta (BBA)-Bioenergetics, 1797(2), 167-176.
Jové, M., Portero-Otín, M., Naudí, A., Ferrer, I., & Pamplona, R. (2014). Metabolomics of human brain aging and age-related neurodegenerative diseases. Journal of Neuropathology & Experimental Neurology, 73(7), 640-657.
Kaddurah-Daouk, R., Zhu, H., Sharma, S., Bogdanov, M., Rozen, S. G., Matson, W., ... & Appleby, D. (2013). Alterations in metabolic pathways and networks in Alzheimer's disease. Translational psychiatry, 3(4), e244.
Kam, K., & Nicoll, R. (2007). Excitatory synaptic transmission persists independently of the glutamate–glutamine cycle. Journal of Neuroscience, 27(34), 9192-9200.
Karuppagounder, S. S., Xu, H., Shi, Q., Chen, L. H., Pedrini, S., Pechman, D., ... & Gibson, G. E. (2009). Thiamine deficiency induces oxidative stress and exacerbates the plaque pathology in Alzheimer's mouse model. Neurobiology of aging, 30(10), 1587-1600.
Khan, R. S., Fonseca-Kelly, Z., Callinan, C., Zuo, L., Sachdeva, M. M., & Shindler, K. S. (2012). SIRT1 activating compounds reduce oxidative stress and prevent cell death in neuronal cells. Frontiers in Cellular Neuroscience, 6, 63.
Kiddle, S. J., Sattlecker, M., Proitsi, P., Simmons, A., Westman, E., Bazenet, C., ... & Soininen, H. (2014). Candidate blood proteome markers of Alzheimer's disease onset and progression: a systematic review and replication study. Journal of Alzheimer's Disease, 38(3), 515-531.
Kim, D., Nguyen, M. D., Dobbin, M. M., Fischer, A., Sananbenesi, F., Rodgers, J. T., ... & Puigserver, P. (2007). SIRT1 deacetylase protects against neurodegeneration in models for Alzheimer's disease and amyotrophic lateral sclerosis. The EMBO journal, 26(13), 3169-3179.
Kim, S., Jang, Y. S., Ha, S. C., Ahn, J. W., Kim, E. J., Lim, J. H., ... & Kim, K. J. (2015). Redox-switch regulatory mechanism of thiolase from Clostridium acetobutylicum. Nature communications, 6, 8410.
Kim, S., Kim, T., Lee, H. R., Jang, E. H., Ryu, H. H., Kang, M., ... & Lim, C. S. (2016). Impaired learning and memory in CD38 null mutant mice. Molecular brain, 9(1), 16.
Kirlin, W. G., Cai, J., Thompson, S. A., Diaz, D., Kavanagh, T. J., & Jones, D. P. (1999). Glutathione redox potential in response to differentiation and enzyme inducers. Free Radical Biology and Medicine, 27(11-12), 1208-1218.
Klaidman, L. K., Leung, A. C., & Adams, J. D. (1995). High-performance liquid chromatography analysis of oxidized and reduced pyridine dinucleotides in specific brain regions. Analytical biochemistry, 228(2), 312-317.
Koch-Nolte, F., Fischer, S., Haag, F., & Ziegler, M. (2011). Compartmentation of NAD+-dependent signalling. FEBS letters, 585(11), 1651-1656.
Kołodziejczyk, K., Hamilton, N. B., Wade, A., Karadottir, R., & Attwell, D. (2009). The effect of N-acetyl-aspartyl-glutamate and N-acetyl-aspartate on white matter oligodendrocytes. Brain, 132(6), 1496-1508.
Koppula, P., Zhang, Y., Shi, J., Li, W., & Gan, B. (2017). The glutamate/cystine antiporter SLC7A11/xCT enhances cancer cell dependency on glucose by exporting glutamate. Journal of Biological Chemistry, 292(34), 14240-14249.
Krüger, A., Grüning, N. M., Wamelink, M. M., Kerick, M., Kirpy, A., Parkhomchuk, D., ... & Jakobs, C. (2011). The pentose phosphate pathway is a metabolic redox sensor and regulates transcription during the antioxidant response. Antioxidants & redox signaling, 15(2), 311-324.
Kuhla, A., Blei, T., Jaster, R., & Vollmar, B. (2011). Aging is associated with a shift of fatty metabolism toward lipogenesis. Journals of Gerontology Series A: Biomedical Sciences and Medical Sciences, 66(11), 1192-1200.
Kukull, W. A., Larson, E. B., Teri, L., Bowen, J., McCormick, W., & Pfanschmidt, M. L. (1994). The Mini-Mental State Examination score and the clinical diagnosis of dementia. Journal of clinical epidemiology, 47(9), 1061-1067.
Kumar, A., & Foster, T. C. (2019). Alteration in NMDA Receptor Mediated Glutamatergic Neurotransmission in the Hippocampus During Senescence. Neurochemical research, 44(1), 38-48.
LaFerla, F. M. (2002). Calcium dyshomeostasis and intracellular signalling in Alzheimer's disease. Nature Reviews Neuroscience, 3(11), 862.
Lakowicz, J. R., Szmacinski, H., Nowaczyk, K., & Johnson, M. L. (1992). Fluorescence lifetime imaging of free and protein-bound NADH. Proceedings of the National Academy of Sciences, 89(4), 1271-1275.

Larsson, S. C., & Markus, H. S. (2017). Branched-chain amino acids and Alzheimer's disease: a Mendelian randomization analysis. Scientific reports, 7(1), 13604.
Lavrovsky, Y., Chatterjee, B., Clark, R. A., & Roy, A. K. (2000). Role of redox-regulated transcription factors in inflammation, aging and age-related diseases. Experimental gerontology, 35(5), 521-532.
Lee, Y., Kim, J., Han, E. S., Chae, S., Ryu, M., Ahn, K. H., & Park, E. J. (2015). Changes in physical activity and cognitive decline in older adults living in the community. Age, 37(2), 20.
Lehninger, A. L., & Greville, G. D. (1953). The enzymic oxidation of d-and l-β-hydroxybutyrate. Biochimica et biophysica acta, 12(1-2), 188-202.
Lewis, C. A., Parker, S. J., Fiske, B. P., McCloskey, D., Gui, D. Y., Green, C. R., ... & Metallo, C. M. (2014). Tracing compartmentalized NADPH metabolism in the cytosol and mitochondria of mammalian cells. Molecular cell, 55(2), 253-263.
Li, H., Ye, D., Xie, W., Hua, F., Yang, Y., Wu, J., ... & Mao, K. (2018). Defect of branched-chain amino acid metabolism promotes the development of Alzheimer's disease by targeting the mTOR signaling. Bioscience reports, 38(4), BSR20180127.
Liang, W. S., Reiman, E. M., Valla, J., Dunckley, T., Beach, T. G., Grover, A., ... & Kukull, W. (2008). Alzheimer's disease is associated with reduced expression of energy metabolism genes in posterior cingulate neurons. Proceedings of the National Academy of Sciences, 105(11), 4441-4446.
Liguori, C., Chiaravalloti, A., Sancesario, G., Stefani, A., Sancesario, G. M., Mercuri, N. B., ... & Pierantozzi, M. (2016). Cerebrospinal fluid lactate levels and brain [18F] FDG PET hypometabolism within the default mode network in Alzheimer's disease. European journal of nuclear medicine and molecular imaging, 43(11), 2040-2049.
Lin, A. P., Shic, F., Enriquez, C., & Ross, B. D. (2003). Reduced glutamate neurotransmission in patients with Alzheimer's disease–an in vivo 13 C magnetic resonance spectroscopy study. Magnetic Resonance Materials in Physics, Biology and Medicine, 16(1), 29-42.
Lin, M. T., & Beal, M. F. (2006). Mitochondrial dysfunction and oxidative stress in neurodegenerative diseases. Nature, 443(7113), 787.
Lipinski, M. M., Zheng, B., Lu, T., Yan, Z., Py, B. F., Ng, A., ... & Yuan, J. (2010). Genome-wide analysis reveals mechanisms modulating autophagy in normal brain aging and in Alzheimer's disease. Proceedings of the National Academy of Sciences, 107(32), 14164-14169.
Liu, D., Pitta, M., Jiang, H., Lee, J. H., Zhang, G., Chen, X., ... & Mattson, M. P. (2013). Nicotinamide forestalls pathology and cognitive decline in Alzheimer mice: evidence for improved neuronal bioenergetics and autophagy procession. Neurobiology of aging, 34(6), 1564-1580.
Liu, Y., Liu, F., Iqbal, K., Grundke-Iqbal, I., & Gong, C. X. (2008). Decreased glucose transporters correlate to abnormal hyperphosphorylation of tau in Alzheimer disease. FEBS letters, 582(2), 359-364.
López-Torres, M., & Barja, G. (2008). Lowered methionine ingestion as responsible for the decrease in rodent mitochondrial oxidative stress in protein and dietary restriction: possible implications for humans. Biochimica et Biophysica Acta (BBA)-General Subjects, 1780(11), 1337-1347.
Lutz, M. W., Sundseth, S. S., Burns, D. K., Saunders, A. M., Hayden, K. M., Burke, J. R., ... & Alzheimer's Disease Neuroimaging Initiative. (2016). A genetics-based biomarker risk algorithm for predicting risk of Alzheimer's disease. Alzheimer's & Dementia: Translational Research & Clinical Interventions, 2(1), 30-44.
Ma, N., Digman, M. A., Malacrida, L., & Gratton, E. (2016). Measurements of absolute concentrations of NADH in cells using the phasor FLIM method. Biomedical optics express, 7(7), 2441-2452.
Maceyka, M., & Spiegel, S. (2014). Sphingolipid metabolites in inflammatory disease. Nature, 510(7503), 58.
Magesh, S., Chen, Y., & Hu, L. (2012). Small Molecule Modulators of K eap1-N rf2-ARE Pathway as Potential Preventive and Therapeutic Agents. Medicinal research reviews, 32(4), 687-726.
Magistretti, P. J., & Allaman, I. (2013). Brain energy metabolism. Neuroscience in the 21st century: From basic to clinical, 1591-1620.
Magistretti, P. J., & Allaman, I. (2018). Lactate in the brain: from metabolic end-product to signalling molecule. Nature Reviews Neuroscience, 19(4), 235.
Mailloux, R. J., Jin, X., & Willmore, W. G. (2014). Redox regulation of mitochondrial function with emphasis on cysteine oxidation reactions. Redox biology, 2, 123-139.
Maki, P. M., & Resnick, S. M. (2000). Longitudinal effects of estrogen replacement therapy on PET cerebral blood flow and cognition. Neurobiology of aging, 21(2), 373-383.

Manavalan, A., Mishra, M., Feng, L., Sze, S. K., Akatsu, H., & Heese, K. (2013). Brain site-specific proteome changes in aging-related dementia. Experimental & molecular medicine, 45(9), e39.
Manczak, M., & Reddy, P. H. (2012). Abnormal interaction between the mitochondrial fission protein Drp1 and hyperphosphorylated tau in Alzheimer's disease neurons: implications for mitochondrial dysfunction and neuronal damage. Human molecular genetics, 21(11), 2538-2547.
Mandal, P. K., Shukla, D., Tripathi, M., & Ersland, L. (2019). Cognitive Improvement with Glutathione Supplement in Alzheimer's Disease: A Way Forward. Journal of Alzheimer's Disease, (Preprint), 1-5.
Mangialasche, F., Solomon, A., Winblad, B., Mecocci, P., & Kivipelto, M. (2010). Alzheimer's disease: clinical trials and drug development. The Lancet Neurology, 9(7), 702-716.
Mapstone, M., Cheema, A. K., Fiandaca, M. S., Zhong, X., Mhyre, T. R., MacArthur, L. H., ... & Nazar, M. D. (2014). Plasma phospholipids identify antecedent memory impairment in older adults. Nature medicine, 20(4), 415.
Mariani, E., Polidori, M. C., Cherubini, A., & Mecocci, P. (2005). Oxidative stress in brain aging, neurodegenerative and vascular diseases: an overview. Journal of Chromatography B, 827(1), 65-75.
Marina, R. J., Sturgill, D., Bailly, M. A., Thenoz, M., Varma, G., Prigge, M. F., ... & Oberdoerffer, S. (2016). TET-catalyzed oxidation of intragenic 5-methylcytosine regulates CTCF-dependent alternative splicing. The EMBO journal, 35(3), 335-355.
Markovic, J., Borrás, C., Ortega, Á., Sastre, J., Viña, J., & Pallardó, F. V. (2007). Glutathione is recruited into the nucleus in early phases of cell proliferation. Journal of Biological Chemistry, 282(28), 20416-20424.
Martens, C. R., Denman, B. A., Mazzo, M. R., Armstrong, M. L., Reisdorph, N., McQueen, M. B., ... & Seals, D. R. (2018). Chronic nicotinamide riboside supplementation is well-tolerated and elevates NAD+ in healthy middle-aged and older adults. Nature communications, 9(1), 1286.
Martin, S. A., DeMuth, T. M., Miller, K. N., Pugh, T. D., Polewski, M. A., Colman, R. J., ... & Anderson, R. M. (2016). Regional metabolic heterogeneity of the hippocampus is nonuniformly impacted by age and caloric restriction. Aging Cell, 15(1), 100-110.
Martins, I. V., Rivers-Auty, J., Allan, S. M., & Lawrence, C. B. (2017). Mitochondrial abnormalities and synaptic loss underlie memory deficits seen in mouse models of obesity and Alzheimer's disease. Journal of Alzheimer's Disease, 55(3), 915-932.
Mastrogiacomo, F., Bergeron, C., & Kish, S. J. (1993). Brain α-Ketoglutarate Dehydrotenase Complex Activity in Alzheimer's Disease. Journal of neurochemistry, 61(6), 2007-2014.
Mattson, M. P., & Arumugam, T. V. (2018). Hallmarks of brain aging: adaptive and pathological modification by metabolic states. Cell metabolism, 27(6), 1176-1199.
Mattsson, N., Andreasson, U., Zetterberg, H., & Blennow, K. (2017). Association of plasma neurofilament light with neurodegeneration in patients with Alzheimer disease. JAMA neurology, 74(5), 557-566.
McEntee, W. J., & Crook, T. H. (1993). Glutamate: its role in learning, memory, and the aging brain. Psychopharmacology, 111(4), 391-401.
McPherson, R. A., & Hardy, G. (2011). Clinical and nutritional benefits of cysteine-enriched protein supplements. Current Opinion in Clinical Nutrition & Metabolic Care, 14(6), 562-568.
Meyerhoff, Dieter J., et al. "Reduced brain N-acetylaspartate suggests neuronal loss in cognitively impaired human immunodeficiency virus-seropositive individuals: in vivo 1H magnetic resonance spectroscopic imaging." Neurology 43.3 Part 1 (1993): 509-509.
Mielke, M. M., Bandaru, V. V. R., McArthur, J. C., Chu, M., & Haughey, N. J. (2010). Disturbance in cerebral spinal fluid sphingolipid content is associated with memory impairment in subjects infected with the human immunodeficiency virus. Journal of neurovirology, 16(6), 445-456.
Miller, J. A., Horvath, S., & Geschwind, D. H. (2010). Divergence of human and mouse brain transcriptome highlights Alzheimer disease pathways. Proceedings of the National Academy of Sciences, 107(28), 12698-12703.
Mokhtari, V., Afsharian, P., Shahhoseini, M., Kalantar, S. M., & Moini, A. (2017). A review on various uses of N-acetyl cysteine. Cell Journal (Yakhteh), 19(1), 11.
Monteiro-Cardoso, V. F., Oliveira, M. M., Melo, T., Domingues, M. R., Moreira, P. I., Ferreiro, E., ... & Videira, R. A. (2015). Cardiolipin profile changes are associated to the early synaptic mitochondrial dysfunction in Alzheimer's disease. Journal of Alzheimer's Disease, 43(4), 1375-1392.
Moreira, P. I., Harris, P. L., Zhu, X., Santos, M. S., Oliveira, C. R., Smith, M. A., & Perry, G. (2007). Lipoic acid and N-acetyl cysteine decrease mitochondrial-related oxidative stress in Alzheimer disease patient fibroblasts. Journal of Alzheimer's Disease, 12(2), 195-206.

Mosconi, L. (2005). Brain glucose metabolism in the early and specific diagnosis of Alzheimer's disease. European journal of nuclear medicine and molecular imaging, 32(4), 486-510.
Mosconi, L., Pupi, A., & De Leon, M. J. (2008). Brain glucose hypometabolism and oxidative stress in preclinical Alzheimer's disease. Annals of the New York Academy of Sciences, 1147(1), 180-195.
Mouchiroud, L., Houtkooper, R. H., Moullan, N., Katsyuba, E., Ryu, D., Cantó, C., ... & Guarente, L. (2013). The NAD+/sirtuin pathway modulates longevity through activation of mitochondrial UPR and FOXO signaling. Cell, 154(2), 430-441.
Müller, W. E., Eckert, A., Kurz, C., Eckert, G. P., & Leuner, K. (2010). Mitochondrial dysfunction: common final pathway in brain aging and Alzheimer's disease—therapeutic aspects. Molecular neurobiology, 41(2-3), 159-171.
Nakagawa, T., Lomb, D. J., Haigis, M. C., & Guarente, L. (2009). SIRT5 Deacetylates carbamoyl phosphate synthetase 1 and regulates the urea cycle. Cell, 137(3), 560-570.
Naudí, A., Caro, P., Jové, M., Gómez, J., Boada, J., Ayala, V., ... & Pamplona, R. (2007). Methionine restriction decreases endogenous oxidative molecular damage and increases mitochondrial biogenesis and uncoupling protein 4 in rat brain. Rejuvenation research, 10(4), 473-484.
Newman, L. A., Korol, D. L., & Gold, P. E. (2011). Lactate produced by glycogenolysis in astrocytes regulates memory processing. PloS one, 6(12), e28427.
Nixon, R. A. (2013). The role of autophagy in neurodegenerative disease. Nature medicine, 19(8), 983.
Oddo, S., Caccamo, A., Shepherd, J. D., Murphy, M. P., Golde, T. E., Kayed, R., ... & LaFerla, F. M. (2003). Triple-transgenic model of Alzheimer's disease with plaques and tangles: intracellular Aβ and synaptic dysfunction. Neuron, 39(3), 409-421.
Ödman, P., Wellborn, W. B., & Bommarius, A. S. (2004). An enzymatic process to α-ketoglutarate from l-glutamate: the coupled system l-glutamate dehydrogenase/NADH oxidase. Tetrahedron: Asymmetry, 15(18), 2933-2937.
Okada, T., Kajimoto, T., Jahangeer, S., & Nakamura, S. I. (2009). Sphingosine kinase/sphingosine 1-phosphate signalling in central nervous system. Cellular signalling, 21(1), 7-13.
Onyango, I. G., Dennis, J., & Khan, S. M. (2016). Mitochondrial dysfunction in Alzheimer's disease and the rationale for bioenergetics based therapies. Aging and disease, 7(2), 201.
Orešič, M., Hyötyläinen, T., Herukka, S. K., Sysi-Aho, M., Mattila, I., Seppänan-Laakso, T., ... & Kivipelto, M. (2011). Metabolome in progression to Alzheimer's disease. Translational psychiatry, 1(12), e57.
Palmer, A. M., & Gershon, S. A. M. U. E. L. (1990). Is the neuronal basis of Alzheimer's disease cholinergic or glutamatergic?. The FASEB Journal, 4(10), 2745-2752.
Pan, X., Nasaruddin, M. B., Elliott, C. T., McGuinness, B., Passmore, A. P., Kehoe, P. G., ... & Green, B. D. (2016). Alzheimer's disease–like pathology has transient effects on the brain and blood metabolome. Neurobiology of aging, 38, 151-163.
Paoli, A., Bosco, G., Camporesi, E. M., & Mangar, D. (2015). Ketosis, ketogenic diet and food intake control: a complex relationship. Frontiers in psychology, 6, 27.
Parihar, M. S., & Brewer, G. J. (2007). Simultaneous age-related depolarization of mitochondrial membrane potential and increased mitochondrial reactive oxygen species production correlate with age-related glutamate excitotoxicity in rat hippocampal neurons. Journal of neuroscience research, 85(5), 1018-1032.
Parihar, M. S., Kunz, E. A., & Brewer, G. J. (2008). Age-related decreases in NAD (P) H and glutathione cause redox declines before ATP loss during glutamate treatment of hippocampal neurons. Journal of neuroscience research, 86(10), 2339-2352.
Patel, J. R., & Brewer, G. J. (2003). Age-related changes in neuronal glucose uptake in response to glutamate and β-amyloid. Journal of neuroscience research, 72(4), 527-536.
Paula-Lima, A. C., Brito-Moreira, J., & Ferreira, S. T. (2013). Deregulation of excitatory neurotransmission underlying synapse failure in Alzheimer's disease. Journal of neurochemistry, 126(2), 191-202.
Payami, H., Zareparsi, S., Montee, K. R., Sexton, G. J., Kaye, J. A., Bird, T. D., ... & Schellenberg, G. D. (1996). Gender difference in apolipoprotein E-associated risk for familial Alzheimer disease: a possible clue to the higher incidence of Alzheimer disease in women. American journal of human genetics, 58(4), 803.
Pedrós, I., Petrov, D., Allgaier, M., Sureda, F., Barroso, E., Beas-Zarate, C., ... & Folch, J. (2014). Early alterations in energy metabolism in the hippocampus of APPswe/PS1dE9 mouse model of Alzheimer's disease. Biochimica et Biophysica Acta (BBA)-Molecular Basis of Disease, 1842(9), 1556-1566.

Peng, S., Zhang, Y., Zhang, J., Wang, H., & Ren, B. (2011). Glutamate receptors and signal transduction in learning and memory. Molecular biology reports, 38(1), 453-460.
Peng, Y., Shapiro, S. L., Banduseela, V. C., Dieterich, I. A., Hewitt, K. J., Bresnick, E. H., ... & Attie, A. D. (2018). Increased transport of acetyl-CoA into the endoplasmic reticulum causes a progeria-like phenotype. Aging cell, 17(5), e12820.
Perez Ortiz, J. M., & Swerdlow, R. H. (2019). Mitochondrial dysfunction in Alzheimer's disease: Role in pathogenesis and novel therapeutic opportunities. British journal of pharmacology.
Petersen, R. C., Aisen, P. S., Beckett, L. A., Donohue, M. C., Gamst, A. C., Harvey, D. J., ... & Trojanowski, J. Q. (2010). Alzheimer's disease neuroimaging initiative (ADNI): clinical characterization. Neurology, 74(3), 201-209.
Pifferi, F., Tremblay, S., Croteau, E., Fortier, M., Tremblay-Mercier, J., Lecomte, R., & Cunnane, S. C. (2011). Mild experimental ketosis increases brain uptake of 11C-acetoacetate and 18F-fluorodeoxyglucose: a dual-tracer PET imaging study in rats. Nutritional neuroscience, 14(2), 51-58.
Pittelli, M., Felici, R., Pitozzi, V., Giovannelli, L., Bigagli, E., Cialdai, F., ... & Chiarugi, A. (2011). Pharmacological effects of exogenous NAD on mitochondrial bioenergetics, DNA repair, and apoptosis. Molecular pharmacology, 80(6), 1136-1146.
Prolla, T. A., & Denu, J. M. (2014). NAD+ deficiency in age-related mitochondrial dysfunction. Cell metabolism, 19(2), 178-180.
Qin, W., Yang, T., Ho, L., Zhao, Z., Wang, J., Chen, L., ... & Puigserver, P. (2006). Neuronal SIRT1 activation as a novel mechanism underlying the prevention of Alzheimer disease amyloid neuropathology by calorie restriction. Journal of Biological Chemistry, 281(31), 21745-21754.
Quansah, E., Peelaerts, W., Langston, J. W., Simon, D. K., Colca, J., & Brundin, P. (2018). Targeting energy metabolism via the mitochondrial pyruvate carrier as a novel approach to attenuate neurodegeneration. Molecular Neurodegeneration, 13(1), 28.
Ralser, M., Wamelink, M. M., Kowald, A., Gerisch, B., Heeren, G., Struys, E. A., ... & Krobitsch, S. (2007). Dynamic rerouting of the carbohydrate flux is key to counteracting oxidative stress. Journal of biology, 6(4), 10.
Rapado-Castro, M., Dodd, S., Bush, A. I., Malhi, G. S., Skvarc, D. R., On, Z. X., ... & Dean, O. M. (2017). Cognitive effects of adjunctive N-acetyl cysteine in psychosis. Psychological medicine, 47(5), 866-876.
Ravaglia, G., Forti, P., Maioli, F., Chiappelli, M., Montesi, F., Tumini, E., ... & Patterson, C. (2007). Blood inflammatory markers and risk of dementia: The Conselice Study of Brain Aging. Neurobiology of aging, 28(12), 1810-1820.
Reddy, P. H. (2007). Mitochondrial dysfunction in aging and Alzheimer's disease: strategies to protect neurons. Antioxidants & redox signaling, 9(10), 1647-1658.
Reddy, P. H., Yin, X., Manczak, M., Kumar, S., Pradeepkiran, J. A., Vijayan, M., & Reddy, A. P. (2018). Mutant APP and amyloid beta-induced defective autophagy, mitophagy, mitochondrial structural and functional changes and synaptic damage in hippocampal neurons from Alzheimer's disease. Human molecular genetics, 27(14), 2502-2516.
Reilly, J. F., Games, D., Rydel, R. E., Freedman, S., Schenk, D., Young, W. G., ... & Bloom, F. E. (2003). Amyloid deposition in the hippocampus and entorhinal cortex: quantitative analysis of a transgenic mouse model. Proceedings of the National Academy of Sciences, 100(8), 4837-4842.
Reiman, E. M., Chen, K., Alexander, G. E., Caselli, R. J., Bandy, D., Osborne, D., ... & Hardy, J. (2004). Functional brain abnormalities in young adults at genetic risk for late-onset Alzheimer's dementia. Proceedings of the National Academy of Sciences, 101(1), 284-289.
Remington, R., Bechtel, C., Larsen, D., Samar, A., Doshanjh, L., Fishman, P., ... & Shea, T. B. (2015). A phase II randomized clinical trial of a nutritional formulation for cognition and mood in Alzheimer's disease. Journal of Alzheimer's Disease, 45(2), 395-405.
Resende, R., Moreira, P. I., Proença, T., Deshpande, A., Busciglio, J., Pereira, C., & Oliveira, C. R. (2008). Brain oxidative stress in a triple-transgenic mouse model of Alzheimer disease. Free Radical Biology and Medicine, 44(12), 2051-2057.
Revollo, J. R., Grimm, A. A., & Imai, S. I. (2004). The NAD biosynthesis pathway mediated by nicotinamide phosphoribosyltransferase regulates Sir2 activity in mammalian cells. Journal of Biological Chemistry, 279(49), 50754-50763.

Rhein, V., & Eckert, A. (2007). Effects of Alzheimer's amyloid-beta and tau protein on mitochondrial function—Role of glucose metabolism and insulin signalling. Archives of physiology and biochemistry, 113(3), 131-141.
Robinson, J. L., Corrada, M. M., Kovacs, G. G., Dominique, M., Caswell, C., Xie, S. X., ... & Trojanowski, J. Q. (2018). Non-Alzheimer's contributions to dementia and cognitive resilience in the 90+ Study. Acta neuropathologica, 136(3), 377-388.
Ronchi, J. A., Francisco, A., Passos, L. A. C., Figueira, T. R., & Castilho, R. F. (2016). The contribution of nicotinamide nucleotide transhydrogenase to peroxide detoxification is dependent on the respiratory state and counterbalanced by other sources of NADPH in liver mitochondria. Journal of Biological Chemistry, 291(38), 20173-20187.
Ross, J. M., Öberg, J., Brené, S., Coppotelli, G., Terzioglu, M., Pernold, K., ... & Larsson, N. G. (2010). High brain lactate is a hallmark of aging and caused by a shift in the lactate dehydrogenase A/B ratio. Proceedings of the National Academy of Sciences, 107(46), 20087-20092.
Sahar, S., Nin, V., Barbosa, M. T., Chini, E. N., & Sassone-Corsi, P. (2011). Altered behavioral and metabolic circadian rhythms in mice with disrupted NAD+ oscillation. Aging (Albany NY), 3(8), 794.
Saitoh, T., Horsburgh, K., & Masliah, E. (1993). Hyperactivation of Signal Transduction Systems in Alzheimer's Disease a. Annals of the New York Academy of Sciences, 695(1), 34-41.
Schiff, M., Bénit, P., Coulibaly, A., Loublier, S., El-Khoury, R., & Rustin, P. (2011). Mitochondrial response to controlled nutrition in health and disease. Nutrition reviews, 69(2), 65-75.
Schubert, D. (2005). Glucose metabolism and Alzheimer's disease. Ageing research reviews, 4(2), 240-257.
Sekhar, R. V., Patel, S. G., Guthikonda, A. P., Reid, M., Balasubramanyam, A., Taffet, G. E., & Jahoor, F. (2011). Deficient synthesis of glutathione underlies oxidative stress in aging and can be corrected by dietary cysteine and glycine supplementation–. The American journal of clinical nutrition, 94(3), 847-853.
Sen, C. K. (1998). Redox signaling and the emerging therapeutic potential of thiol antioxidants. Biochemical pharmacology, 55(11), 1747-1758.
Sepehrmanesh, Z., Heidary, M., Akasheh, N., Akbari, H., & Heidary, M. (2018). Therapeutic effect of adjunctive N-acetyl cysteine (NAC) on symptoms of chronic schizophrenia: a double-blind, randomized clinical trial. Progress in Neuro-Psychopharmacology and Biological Psychiatry, 82, 289-296.
Seshadri, S., Fitzpatrick, A. L., Ikram, M. A., DeStefano, A. L., Gudnason, V., Boada, M., ... & Harold, D. (2010). Genome-wide analysis of genetic loci associated with Alzheimer disease. Jama, 303(18), 1832-1840.
Shaw, L. M., Vanderstichele, H., Knapik-Czajka, M., Clark, C. M., Aisen, P. S., Petersen, R. C., ... & Dean, R. (2009). Cerebrospinal fluid biomarker signature in Alzheimer's disease neuroimaging initiative subjects. Annals of neurology, 65(4), 403-413.
Shea, T. B., & Remington, R. (2015). Nutritional supplementation for Alzheimer's disease?. Current opinion in psychiatry, 28(2), 141-147.
Shetty, P. K., Galeffi, F., & Turner, D. A. (2014). Nicotinamide pre-treatment ameliorates NAD (H) hyperoxidation and improves neuronal function after severe hypoxia. Neurobiology of disease, 62, 469-478.
Shi, Q., Xu, H., Yu, H., Zhang, N., Ye, Y., Estevez, A. G., ... & Gibson, G. E. (2011). Inactivation and reactivation of the mitochondrial α-ketoglutarate dehydrogenase complex. Journal of Biological Chemistry, 286(20), 17640-17648.
Shi, Y., & Holtzman, D. M. (2018). Interplay between innate immunity and Alzheimer disease: APOE and TREM2 in the spotlight. Nature reviews Immunology, 1.
Singh, R., Lemire, J., Mailloux, R. J., & Appanna, V. D. (2008). A novel strategy involved anti-oxidative defense: the conversion of NADH into NADPH by a metabolic network. PLoS One, 3(7), e2682.
Smith, J., Ladi, E., Mayer-Pröschel, M., & Noble, M. (2000). Redox state is a central modulator of the balance between self-renewal and differentiation in a dividing glial precursor cell. Proceedings of the National Academy of Sciences, 97(18), 10032-10037.
Sohal, R. S., & Orr, W. C. (2012). The redox stress hypothesis of aging. Free Radical Biology and Medicine, 52(3), 539-555.
Sokoloff, L. O. U. I. S. (1973). Metabolism of ketone bodies by the brain. Annual review of medicine, 24(1), 271-280.

Sonnino, S., & Prinetti, A. (2016). The role of sphingolipids in neuronal plasticity of the brain. Journal of neurochemistry, 137(4), 485-488.
Soria, F. N., Zabala, A., Pampliega, O., Palomino, A., Miguelez, C., Ugedo, L., ... & Domercq, M. (2016). Cystine/glutamate antiporter blockage induces myelin degeneration. Glia, 64(8), 1381-1395.
Sperling, R. A., Aisen, P. S., Beckett, L. A., Bennett, D. A., Craft, S., Fagan, A. M., ... & Park, D. C. (2011). Toward defining the preclinical stages of Alzheimer's disease: Recommendations from the National Institute on Aging-Alzheimer's Association workgroups on diagnostic guidelines for Alzheimer's disease. Alzheimer's & dementia, 7(3), 280-292.
Sporty, J. L., Kabir, M. M., Turteltaub, K. W., Ognibene, T., Lin, S. J., & Bench, G. (2008). Single sample extraction protocol for the quantification of NAD and NADH redox states in Saccharomyces cerevisiae. Journal of separation science, 31(18), 3202-3211.
Squier, T. C. (2001). Oxidative stress and protein aggregation during biological aging. Experimental gerontology, 36(9), 1539-1550.
St George-Hyslop, P. H. (2000). Molecular genetics of Alzheimer's disease. Biological psychiatry, 47(3), 183-199.
Stein, L. R., & Imai, S. I. (2012). The dynamic regulation of NAD metabolism in mitochondria. Trends in Endocrinology & Metabolism, 23(9), 420-428.
Stolle, S., Ciapaite, J., Reijne, A. C., Talarovicova, A., Wolters, J. C., Aguirre-Gamboa, R., ... & Deelen, P. (2018). Running-wheel activity delays mitochondrial respiratory flux decline in aging mouse muscle via a post-transcriptional mechanism. Aging cell, 17(1), e12700.
Stringari, C., Nourse, J. L., Flanagan, L. A., & Gratton, E. (2012). Phasor fluorescence lifetime microscopy of free and protein-bound NADH reveals neural stem cell differentiation potential. PloS one, 7(11), e48014.
Stringari, C., Wang, H., Geyfman, M., Crosignani, V., Kumar, V., Takahashi, J. S., ... & Gratton, E. (2015). In vivo single-cell detection of metabolic oscillations in stem cells. Cell reports, 10(1), 1-7.
Stutzmann, G. E., Smith, I., Caccamo, A., Oddo, S., LaFerla, F. M., & Parker, I. (2006). Enhanced ryanodine receptor recruitment contributes to Ca2+ disruptions in young, adult, and aged Alzheimer's disease mice. Journal of Neuroscience, 26(19), 5180-5189.
Sullivan, P. G., & Brown, M. R. (2005). Mitochondrial aging and dysfunction in Alzheimer's disease. Progress in Neuro-Psychopharmacology and Biological Psychiatry, 29(3), 407-410.
Sultana, R., & Butterfield, D. A. (2010). Role of oxidative stress in the progression of Alzheimer's disease. Journal of Alzheimer's Disease, 19(1), 341-353.
Suzuki, A., Stern, S. A., Bozdagi, O., Huntley, G. W., Walker, R. H., Magistretti, P. J., & Alberini, C. M. (2011). Astrocyte-neuron lactate transport is required for long-term memory formation. Cell, 144(5), 810-823.
Swerdlow, R. H. (2011). Brain aging, Alzheimer's disease, and mitochondria. Biochimica et Biophysica Acta (BBA)-Molecular Basis of Disease, 1812(12), 1630-1639.
Terry, R. D., Masliah, E., Salmon, D. P., Butters, N., DeTeresa, R., Hill, R., ... & Katzman, R. (1991). Physical basis of cognitive alterations in Alzheimer's disease: synapse loss is the major correlate of cognitive impairment. Annals of Neurology: Official Journal of the American Neurological Association and the Child Neurology Society, 30(4), 572-580.
Teunissen, C. E., Van Boxtel, M. P. J., Bosma, H., Bosmans, E., Delanghe, J., De Bruijn, C., ... & De Vente, J. (2003). Inflammation markers in relation to cognition in a healthy aging population. Journal of neuroimmunology, 134(1-2), 142-150.
Tilton, W. M., Seaman, C., Carriero, D., & Piomelli, S. (1991). Regulation of glycolysis in the erythrocyte: role of the lactate/pyruvate and NAD/NADH ratios. The Journal of laboratory and clinical medicine, 118(2), 146-152.
Tournissac, M., Vandal, M., Tremblay, C., Bourassa, P., Vancassel, S., Emond, V., ... & Calon, F. (2018). Dietary intake of branched-chain amino acids in a mouse model of Alzheimer's disease: Effects on survival, behavior, and neuropathology. Alzheimer's & Dementia: Translational Research & Clinical Interventions, 4, 677-687.
Trushina, E., Dutta, T., Persson, X. M. T., Mielke, M. M., & Petersen, R. C. (2013). Identification of altered metabolic pathways in plasma and CSF in mild cognitive impairment and Alzheimer's disease using metabolomics. PloS one, 8(5), e63644.
Uppal, A., & Gupta, P. K. (2003). Measurement of NADH concentration in normal and malignant human tissues from breast and oral cavity. Biotechnology and applied biochemistry, 37(1), 45-50.

Ushio-Fukai, M. (2009). Compartmentalization of redox signaling through NADPH oxidase–derived ROS. Antioxidants & redox signaling, 11(6), 1289-1299.
Van der Auwera, I., Wera, S., Van Leuven, F., & Henderson, S. T. (2005). A ketogenic diet reduces amyloid beta 40 and 42 in a mouse model of Alzheimer's disease. Nutrition & metabolism, 2(1), 28.
van Munster, E. B., & Gadella, T. W. (2005). Fluorescence lifetime imaging microscopy (FLIM). In Microscopy techniques(pp. 143-175). Springer, Berlin, Heidelberg.
Veech, R. L. (2004). The therapeutic implications of ketone bodies: the effects of ketone bodies in pathological conditions: ketosis, ketogenic diet, redox states, insulin resistance, and mitochondrial metabolism. Prostaglandins, leukotrienes and essential fatty acids, 70(3), 309-319.
Vemuri, P., Wiste, H. J., Weigand, S. D., Shaw, L. M., Trojanowski, J. Q., Weiner, M. W., ... & Jack, C. R. (2009). MRI and CSF biomarkers in normal, MCI, and AD subjects: predicting future clinical change. Neurology, 73(4), 294-301.
Verdin, E. (2015). NAD+ in aging, metabolism, and neurodegeneration. Science, 350(6265), 1208-1213.
Vina, J., & Lloret, A. (2010). Why women have more Alzheimer's disease than men: gender and mitochondrial toxicity of amyloid-β peptide. Journal of Alzheimer's disease, 20(s2), S527-S533.
Voehringer, D. W. (1999). BCL-2 and glutathione: alterations in cellular redox state that regulate apoptosis sensitivity. Free Radical Biology and Medicine, 27(9-10), 945-950.
Waagepetersen, H. S., Sonnewald, U., Larsson, O. M., & Schousboe, A. (1999). Synthesis of vesicular GABA from glutamine involves TCA cycle metabolism in neocortical neurons. Journal of neuroscience research, 57(3), 342-349.
Wakil, S. J. (1956). Studies on the fatty acid oxidizing system of animal tissues IX. Stereospecificity of unsaturated acyl CoA hydrase. Biochimica et biophysica acta, 19, 497-504.
Walker, M. P., LaFerla, F. M., Oddo, S. S., & Brewer, G. J. (2013). Reversible epigenetic histone modifications and Bdnf expression in neurons with aging and from a mouse model of Alzheimer's disease. Age, 35(3), 519-531.
Walsh, D. M., Klyubin, I., Fadeeva, J. V., Cullen, W. K., Anwyl, R., Wolfe, M. S., ... & Selkoe, D. J. (2002). Naturally secreted oligomers of amyloid β protein potently inhibit hippocampal long-term potentiation in vivo. Nature, 416(6880), 535.
Wang, H., Lim, P. J., Karbowski, M., & Monteiro, M. J. (2008). Effects of overexpression of huntingtin proteins on mitochondrial integrity. Human molecular genetics, 18(4), 737-752.
Wang, X., Li, K., Adams, E., & Van Schepdael, A. (2013). Capillary electrophoresis–mass spectrometry in metabolomics: the potential for driving drug discovery and development. Current drug metabolism, 14(7), 807-813.
Wang, X., Zhu, M., Hjorth, E., Cortés-Toro, V., Eyjolfsdottir, H., Graff, C., ... & Fitzgerald, J. M. (2015). Resolution of inflammation is altered in Alzheimer's disease. Alzheimer's & Dementia, 11(1), 40-50.
Ward, A., Tardiff, S., Dye, C., & Arrighi, H. M. (2013). Rate of conversion from prodromal Alzheimer's disease to Alzheimer's dementia: a systematic review of the literature. Dementia and geriatric cognitive disorders extra, 3(1), 320-332.
Ward, M. W., Rego, A. C., Frenguelli, B. G., & Nicholls, D. G. (2000). Mitochondrial membrane potential and glutamate excitotoxicity in cultured cerebellar granule cells. Journal of Neuroscience, 20(19), 7208-7219.
Watson, G. S., & Craft, S. (2003). The role of insulin resistance in the pathogenesis of Alzheimer's disease. CNS drugs, 17(1), 27-45.
Watts, S. D., Torres-Salazar, D., Divito, C. B., & Amara, S. G. (2014). Cysteine transport through excitatory amino acid transporter 3 (EAAT3). PLoS One, 9(10), e109245.
Weiner, M. W., Veitch, D. P., Aisen, P. S., Beckett, L. A., Cairns, N. J., Green, R. C., ... & Petersen, R. C. (2017). Recent publications from the Alzheimer's Disease Neuroimaging Initiative: Reviewing progress toward improved AD clinical trials. Alzheimer's & Dementia, 13(4), e1-e85.
Wicks, S. E., Vandanmagsar, B., Haynie, K. R., Fuller, S. E., Warfel, J. D., Stephens, J. M., ... & Mynatt, R. L. (2015). Impaired mitochondrial fat oxidation induces adaptive remodeling of muscle metabolism. Proceedings of the National Academy of Sciences, 112(25), E3300-E3309.
Wiley, C. D., & Campisi, J. (2016). From ancient pathways to aging cells—connecting metabolism and cellular senescence. Cell Metabolism, 23(6), 1013-1021.
Williamson, D. H., Lund, P., & Krebs, H. A. (1967). The redox state of free nicotinamide-adenine dinucleotide in the cytoplasm and mitochondria of rat liver. Biochemical Journal, 103(2), 514.

Winblad, B., & Poritis, N. (1999). Memantine in severe dementia: results of the 9M-best study (benefit and efficacy in severly demented patients during treatment with memantine). International journal of geriatric psychiatry, 14(2), 135-146.
Winkler, U., & Hirrlinger, J. (2015). Crosstalk of signaling and metabolism mediated by the NAD+/NADH redox state in brain cells. Neurochemical research, 40(12), 2394-2401.
Winston, C. N., Goetzl, E. J., Akers, J. C., Carter, B. S., Rockenstein, E. M., Galasko, D., ... & Rissman, R. A. (2016). Prediction of conversion from mild cognitive impairment to dementia with neuronally derived blood exosome protein profile. Alzheimer's & Dementia: Diagnosis, Assessment & Disease Monitoring, 3, 63-72.
Winterbourn, C. C. (2008). Reconciling the chemistry and biology of reactive oxygen species. Nature chemical biology, 4(5), 278.
Wirth, M., Villeneuve, S., Haase, C. M., Madison, C. M., Oh, H., Landau, S. M., ... & Jagust, W. J. (2013). Associations between Alzheimer disease biomarkers, neurodegeneration, and cognition in cognitively normal older people. JAMA neurology, 70(12), 1512-1519.
Wu, L., Zhang, X., & Zhao, L. (2018). Human ApoE Isoforms Differentially Modulate Brain Glucose and Ketone Body Metabolism: Implications for Alzheimer's Disease Risk Reduction and Early Intervention. Journal of Neuroscience, 38(30), 6665-6681.
Xiao, W., Wang, R. S., Handy, D. E., & Loscalzo, J. (2018). NAD (H) and NADP (H) redox couples and cellular energy metabolism. Antioxidants & redox signaling, 28(3), 251-272.
Xin, L., Ipek, Ö., Beaumont, M., Shevlyakova, M., Christinat, N., Masoodi, M., ... & Cuenoud, B. (2018). Nutritional ketosis increases NAD+/NADH ratio in healthy human brain: an in vivo study by 31P-MRS. Frontiers in nutrition, 5, 62.
Yaffe, K., Weston, A., Graff-Radford, N. R., Satterfield, S., Simonsick, E. M., Younkin, S. G., ... & Harris, T. B. (2011). Association of plasma β-amyloid level and cognitive reserve with subsequent cognitive decline. Jama, 305(3), 261-266.
Yaku, K., Okabe, K., & Nakagawa, T. (2018). NAD metabolism: Implications in aging and longevity. Ageing research reviews.
Yamauchi, T., Kamon, J., Minokoshi, Y. A., Ito, Y., Waki, H., Uchida, S., ... & Eto, K. (2002). Adiponectin stimulates glucose utilization and fatty-acid oxidation by activating AMP-activated protein kinase. Nature medicine, 8(11), 1288.
Yanagisawa, M., Planel, E., Ishiguro, K., & Fujita, S. C. (1999). Starvation induces tau hyperphosphorylation in mouse brain: implications for Alzheimer's disease. FEBS letters, 461(3), 329-333.
Yang, H., Yang, T., Baur, J. A., Perez, E., Matsui, T., Carmona, J. J., ... & de Cabo, R. (2007). Nutrient-sensitive mitochondrial NAD+ levels dictate cell survival. Cell, 130(6), 1095-1107.
Yang, L., Licastro, D., Cava, E., Veronese, N., Spelta, F., Rizza, W., ... & Fontana, L. (2016). Long-term calorie restriction enhances cellular quality-control processes in human skeletal muscle. Cell reports, 14(3), 422-428.
Yang, Y., Quitschke, W., Vostrov, A. A., & Brewer, G. J. (1999). CTCF is essential for up-regulating expression from the amyloid precursor protein promoter during differentiation of primary hippocampal neurons. Journal of neurochemistry, 73(6), 2286-2298.
Yaniv, Y., Juhaszova, M., & Sollott, S. J. (2013). Age-related changes of myocardial ATP supply and demand mechanisms. Trends in Endocrinology & Metabolism, 24(10), 495-505.
Yao, J., Irwin, R. W., Zhao, L., Nilsen, J., Hamilton, R. T., & Brinton, R. D. (2009). Mitochondrial bioenergetic deficit precedes Alzheimer's pathology in female mouse model of Alzheimer's disease. Proceedings of the National Academy of Sciences, 106(34), 14670-14675.
Yao, J., Irwin, R., Chen, S., Hamilton, R., Cadenas, E., & Brinton, R. D. (2012). Ovarian hormone loss induces bioenergetic deficits and mitochondrial β-amyloid. Neurobiology of aging, 33(8), 1507-1521.
Yao, J., Rettberg, J. R., Klosinski, L. P., Cadenas, E., & Brinton, R. D. (2011). Shift in brain metabolism in late onset Alzheimer's disease: implications for biomarkers and therapeutic interventions. Molecular aspects of medicine, 32(4-6), 247-257.
Yin, F., Sancheti, H., Patil, I., & Cadenas, E. (2016). Energy metabolism and inflammation in brain aging and Alzheimer's disease. Free Radical Biology and Medicine, 100, 108-122.
Ying, W. (2008). NAD+/NADH and NADP+/NADPH in cellular functions and cell death: regulation and biological consequences. Antioxidants & redox signaling, 10(2), 179-206.

Yu, Q., & Heikal, A. A. (2009). Two-photon autofluorescence dynamics imaging reveals sensitivity of intracellular NADH concentration and conformation to cell physiology at the single-cell level. Journal of Photochemistry and Photobiology B: Biology, 95(1), 46-57.

Yu, S. W., Wang, H., Poitras, M. F., Coombs, C., Bowers, W. J., Federoff, H. J., ... & Dawson, V. L. (2002). Mediation of poly (ADP-ribose) polymerase-1-dependent cell death by apoptosis-inducing factor. Science, 297(5579), 259-263.

Zhang, L., Trushin, S., Christensen, T. A., Bachmeier, B. V., Gateno, B., Schroeder, A., ... & Gylys, K. H. (2016). Altered brain energetics induces mitochondrial fission arrest in Alzheimer's Disease. Scientific reports, 6, 18725.

Zhao, L., Mao, Z., Woody, S. K., & Brinton, R. D. (2016). Sex differences in metabolic aging of the brain: insights into female susceptibility to Alzheimer's disease. Neurobiology of aging, 42, 69-79.

Zhou, J. S., Zhu, Z., Wu, F., Zhou, Y., Sheng, R., Wu, J. C., & Qin, Z. H. (2018). NADPH ameliorates MPTP-induced dopaminergic neurodegeneration through inhibiting p38MAPK activation. Acta pharmacologica Sinica, 1.

Zhou, Q., Lam, P. Y., Han, D., & Cadenas, E. (2009). Activation of c-Jun-N-terminal kinase and decline of mitochondrial pyruvate dehydrogenase activity during brain aging. FEBS letters, 583(7), 1132-1140.

Zhu, X. H., Lu, M., Lee, B. Y., Ugurbil, K., & Chen, W. (2015). In vivo NAD assay reveals the intracellular NAD contents and redox state in healthy human brain and their age dependences. Proceedings of the National Academy of Sciences, 112(9), 2876-2881.

Zhu, X., Su, B., Wang, X., Smith, M. A., & Perry, G. (2007). Causes of oxidative stress in Alzheimer disease. Cellular and molecular life sciences, 64(17), 2202-2210.

Zierer, J., Menni, C., Kastenmüller, G., & Spector, T. D. (2015). Integration of 'omics' data in aging research: from biomarkers to systems biology. Aging cell, 14(6), 933-944.

Zilberter, M., Ivanov, A., Ziyatdinova, S., Mukhtarov, M., Malkov, A., Alpár, A., ... & Pitkänen, A. (2013). Dietary energy substrates reverse early neuronal hyperactivity in a mouse model of Alzheimer's disease. Journal of neurochemistry, 125(1), 157-171.